University of Stavanger

Faculty of Science and Technology

MASTER'S THESIS

Study program/ Specialization: Petroleum Engineering / Drilling Engineer	Spring semester, 2017 Restricted access
Writer: Trym Wirgenes	…… (Writer'ssignature)

Faculty supervisor: Mohsen Assadi, Homam Nikpey Somehsaraei

External supervisor(s): Eric Cayeux

Thesis title:

Flow-Rate out Measurement from a Well During Drilling

Credits (ECTS): 30

Key words: Compressibility Conservation of momentum Mud retention Transient time periods Innovative flow sensor	Pages: 100 + enclosure: 11 Stavanger, 29/06/2017 Date/year

Front page for master thesis
Faculty of Science and Technology

Master's Thesis

Flow-Rate out Measurement from a Well During Drilling

Trym Wirgenes

Faculty of Science and Technology
University of Stavanger

This dissertation is submitted for the degree of
Master of Science

June 2017

Acknowledgements

First and foremost I would like to thank my external supervisor, Eric Cayeux, for being a great support throughout this thesis. You have provided great guidance, and your enthusiasm for your work is inspiring.

Secondly, I would like to thank my faculty supervisor, Homam Nikpey Somehsaraei, for your guidance and for keeping me on the right track.

Finally, I would like to thank IRIS for letting me work on my thesis at their facilities.

Abstract

Accurate measurements of flow rate out is crucial in order to prevent unnecessary harm to the environment, equipment or personnel. Harmful situations, such as inflows can potentially be detected earlier with a precise measuring tool. The conventional methods to measuring flow rate out are not flawless, therefore this thesis aims to contribute in the development of a new and innovative measuring method.

This thesis will present technical background and theoretical studies that are relevant to the simulation and experimental part. The simulations investigate the challenges linked with measuring and analyzing flow rate out of a well. The challenges include the effects of fluid compressibility and transient time periods. The experimental part of the thesis describes a new type of flow sensor that is developed and tested.

From the simulation studies, among others the results show that:

- Compressibility effects increases with increasing flow rates
- Effects from compressibility increases with increasing bit depth
- A decreasing effect of compressibility is observed when the density increases
- Compressibility effects increase with increasing OWR
- A trend of increasing compressibility effects is observed for more viscous fluids, compared to less viscous fluids
- Compressibility effect increases when drilling in open hole sections will lower diameters

The second objective of the thesis was to investigate and verify the measuring principle of a new flow sensor that is developed at IRIS. The experiments were conducted with water as circulation fluid. The results show a trend that correspond with the expected result, but the measuring principle could not be verified, as the measurements were affected by an excessive amount of noise. Regardless, the testing showed various aspects where the new flow sensor could be improved in order to verify the measuring principle.

Table of contents

List of figures

List of tables

Nomenclature

Greek Symbols

μ	Viscosity
τ	Shear stress

Other Symbols

Δq	Delta flow
q_{bp}	flow-rate from booster pump
q_{in}	flow-rate into well
q_{out}	flow-rate out of well

Acronyms / Abbreviations

GPM	Gallon Per Minute
LPM	Liters Per Minute
ADP	Annular Discharge Pressure
BHA	Bottom Hole Assembly
BHP	Bottom Hole Pressure
DAPC	Dynamic Annular Pressure Control
ECD	Equivalent Circulating Density
FAF	False Alarm Frequency
FAR	False Alarm Rate

HCR Hydraulic Control Remote

HPHT High Pressure High Temperature

IDAPS Influx Detection at Pumps Stop Software

IRIS International Research Institute of Stavanger

MD Measured Depth

MPD Managed Pressure Drilling

NPT No Production Time

OWR Oil Water Ratio

PDM Positive Displacement Motor

PV Plastic Viscosity

QED Quick Event Detection

RCD Rotating Control Device

ROP Rate of Penetration

RPM Revolutions Per Minute

RTOC Real-Time Operations Centers

SPP Stand Pipe Pressure

TVD True Vertical Depth

YP Yield Point

Chapter 1

Introduction

Performing measurements on the flow-rate out of a well during well-construction activities has a pivotal role in determining critical influxes, loss of circulation situations and the amount of cuttings being transported out of the well. These measurements are used to prevent dangerous situations that may cause harm to personnel, reputation, environment or equipment [1]. Detecting a kick- or loss of circulation situation as early as possible is crucial to minimize the impact of the situation, therefore it is important to perform accurate and precise measurements on the flow that exits the well.

There are three different well-construction activities that needs to be considered when detecting hazardous situations:

1. Drilling and circulating
2. Making connections
3. Tripping in or out

These different activities have different kick indicators as stated in table 1.1 that need to be treated differently. It is especially challenging to detect a kick while making pipe connections, because of the transient behavior of the fluid [2].

Table 1.1 Well-construction activities and their kick indicators [2]

Well-construction activities	Kick indicators
Drilling & circulating	flow-rate out > flow-rate in, and pit gain
Making pipe connections	Continued return flow with pumps off and abnormal trip-tank gain
Tripping in or out	Continued return flow and abnormal trip-tank gain

1.1 Background

Historically the kick detection methods have focused on pumps-on operations, but a kick can also occur while the pumps are turned off. This can transpire while making a pipe connection or during flow checks. It happens because the bottom hole pressure (BHP) is reduced when the frictional pressure generated by the flow-rate is reduced or removed. This is known as a reduction of the equivalent circulating density (ECD).

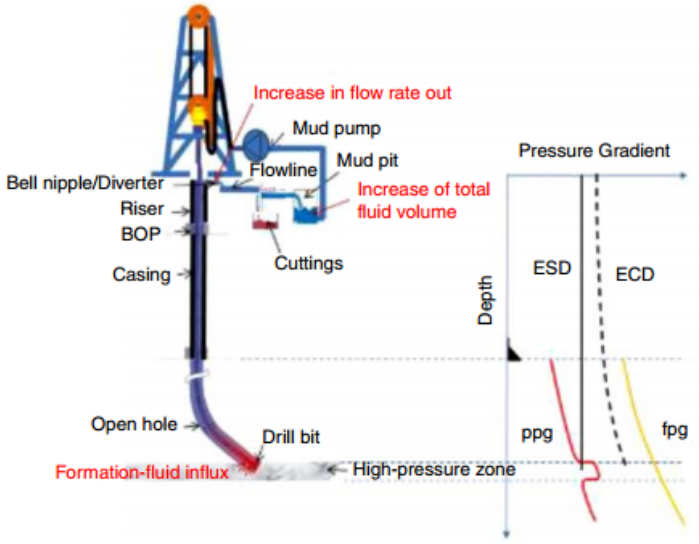

Fig. 1.1 Drilling problem with high-pressure zone while not circulating[3]

Figure 1.1 illustrates that the pressure drop when turning off circulation can cause a kick while drilling through a high-pressure zone. The ECD is reduced to the equivalent static density(ESD), which is beneath the pore pressure and results in an influx. In regards to kicks, high pressure zones are the main cause of concern during conventional drilling. Kick detection during drilling of deep water wells are even more challenging due to a narrower safe drilling window [4].

The conventional method for measuring the flow-rate out of a well is by using a flow paddle or a Coriolis flow-meter, both with their benefits and disadvantages. The flow-paddle is a simple and easy-to-use tool, but it does not allow for accurate and precise measurements. The Coriolis flow-meter is a very precise and accurate tool, but it is very large and can only be used on rigs that has been specifically designed to receive a Coriolis meter [5]. The Coriolis flow meter measurement becomes unstable when there is a substantial amount of gas in the fluid, and connection gas can make it temporarily go out of service [1].

Several attempts have been made to increase the efficiency of the flow-paddle, either by adding extra sensors, complex modelling or SMART alarm systems. Traditionally the data is analyzed and interpreted by a trained driller, but by combining SMART alarm systems with modelling, a software can notify the driller when there is an unwanted situation. While this method can increase the precision of the measurements it requires detailed information of the drill string, the drilling fluid and the wellbore configuration to function [3].

The petroleum industry is always looking to develop new and more cost-effective technology. Previous researchers have had a great deal of focus on developing new measuring methods or new software that accommodates the existing tools. Despite some improvements that have been achieved, these solutions suggest to have a limited achievable precision. The development of a new and more effective tool can set the bar higher.

The International Research Institute of Stavanger (IRIS) is an independent Norwegian research facility that has been developing a new sensor to measure the flow-rate out of a well. The new flow sensor is a type of Coriolis flow meter, but its method of operation is very different from the conventional Coriolis flow meter. The upside of the new flow sensor, is that it is not susceptible to gas, because the flow is exposed to the atmosphere before it reaches the flow sensor. This way, any potential gas can be extracted before the sensor measures the flow. The conventional Coriolis flow meter does not have this option. The new flow sensor is suspected to need low amount of maintenance because it is a rotating flow sensor, any particles or cuttings will experience centrifugal forces that will remove them from the sensor, preventing any accumulation of cuttings. This is explained in detail later.

1.2 Problem Statement

To measure precisely the flow-rate out of a well, a Coriolis-flow meter or a flow-paddle combined with complex modelling, is needed. It is challenging to develop a measuring tool that has all the favorable qualities. Important qualities for a flow-rate measuring tool includes:

- Robust
- Precise
- Low amount of maintenance required
- Relatively small in size

Previous studies have highlighted the limitations of the currently used methods and analysis show that their achievable precision is limited. This thesis introduces a different measuring tool that needs to be tested and analyzed.

1.3 Scope and Objective

The main objective of this thesis is to study the challenges with flow-rate out measurements and verify the measuring principle of the new sensor that is being developed at IRIS. This is accomplished through theoretical- and experimental studies:

The scope of this thesis is formulated as follows:

- Technical background, which includes research on the existing hardware and software that flow-rate measurements are based on
- Review theory, concepts and tools that will be used for analyses later in the thesis
- Investigate challenges with transient time periods linked to flow-rate out measurements through simulations
- The experimental test setup is analyzed to determine the maximum flow-rate the new flow sensor can be tested for
- Introducing the new flow sensor and explaining its measuring principle
- Testing of a small flow-rate sensor prototype. In an attempt to verify the measuring principle and determining the achievable precision of the flow-rate sensor

1.4 Investigation Methodology

To fulfill the thesis' objective, the investigation methodology is divided into two parts:

- Part 1: Flow-rate out simulations
- Part 2: Experimental studies

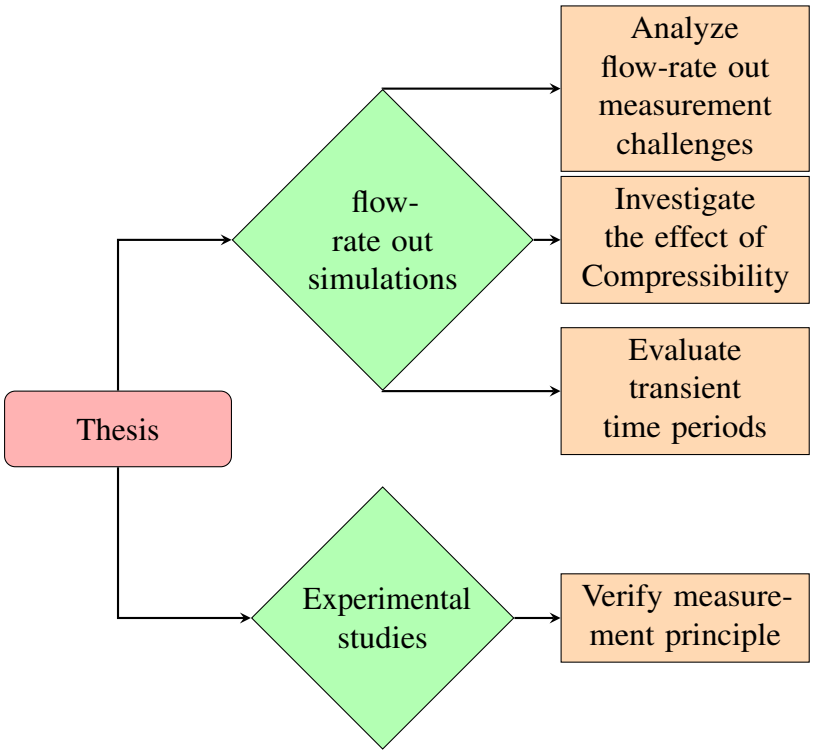

Fig. 1.2 Thesis methodology

flow-rate out simulations are performed to investigate the challenges linked with transient time periods. Analyzing the effect of compressibility and how the effect varies with changes in different parameters such as hole diameter, fluid rheology, flow-rates etc.

After introducing the new flow sensor's method of operation, experimental studies are conducted to test the new flow sensor.

Chapter 2

Technical Background

This chapter will present literature that is associated with measurements performed on the flow out of the well. Methods for optimizing the measuring process is presented and discussed.

The measuring process can be improved through several methods such as:

- Combining software and modeling with existing flow measurement tools
- Developing new measuring tools/methods
- Increasing precision in existing measuring tools

This section will introduce examples to the first two methods.

2.1 Kick Detection History

The most dangerous and potentially expensive drilling situations are kicks. Kicks occur when the pressure in the surrounding formations are larger than the pressure inside the wellbore. This pressure difference will force formation fluid inside the well and this influx must be dealt with in a controlled manner. Uncontrolled kick situations can result in a blowout which can potentially cause damage worth millions of dollars in addition to harm personnel and the environment [6].

Various kick causes with descriptions are listed in table 2.1

Table 2.1 Causes of kicks [6]

Causes of kicks	Description
Insufficient mud weight	This is the main cause of kicks. When the mud weight is insufficient the pressure inside the well is lower than in the surrounding formation and fluids can flow into the wellbore.
Improper hole fill-up when tripping out	While tripping out the mud level decreases as the string is pulled out. If the well is not continuously refilled properly, the hydrostatic pressure from the fluid column is reduced and a kick may occur.
Swabbing	While pulling out the drill string a swab effect can reduce the downhole pressure and result in a kick
Cut mud	Circulation of mud containing gas can cause kick. The gas in the mud expands as it approaches the surface. Resulting in a reduction in effective mud density and reduced downhole pressure.
Lost circulation	Loss of circulation can reduce the fluid column height inside the well and thus reduce the downhole pressure.

It is important to notice a kick as early as possible. To achieve this there are many kick indicators to be aware of. Kick situations can have multiple indications. Table 2.2 shows several indicators and their description.

Table 2.2 Kick indicators with descriptions [7]

Kick indicators	Description
Pit volume	When a kick enters a well the mud inside the wellbore is displaced and an increase in pit volume is seen at the active pit
Increased flow-rate out	During a kick situation the flow-rate out (q_{out}) is equal to the flow-rate in added with the kick in-flow-rate ($q_{in} + q_{kick}$). Thus $q_{out} > q_{in}$
Gas levels	Gas levels in the mud is influenced by kicks and can be measured at the surface
Increased rate of penetration (ROP)	Kick occur in porous formation. When drilling though a porous formation, the driller has to be extra vigilant
Mud density decrease	When a kick occurs the fluid from the kick mixes with the circulated mud resulting in a reduced bulk density and a reduced bottomhole pressure
Annular pressure rise	The mix of circulated mud and the kick fluid generates more friction when circulated and therefore increases the annular pressure

The consensus within the literature is that flow-rate measurements have the potential to give the rapidest detection time for kicks. Challenges with using flow-rate measurements includes high levels of noise in the measurements. Different flow sensors are affected by different types of noise. Flow paddles are for instance more susceptible to noise from several more sources than a Coriolis flow meter. Parameters that cause noise are for instance rig heave, cutting bed accumulation in the return line, etc [7]. Measurements and measuring tools are analyzed further in the theory section of the thesis.

2.2 Importance of Early Kick Detection

Hargreaves Hargreaves, Jardine & Jeffrys explained two scenarios where it is important to detect kicks earlier when drilling [7].

- Deepwater drilling
- Slim hole drilling

When drilling in deep water a larger percentage of the total drilling mud volume is located in the riser. The mud volume in the riser is beyond the BOP in the circulation system and thus the desire to detect the kick earlier is increased. In a case study the kick tolerance was found to be reduced from 180 bbl for a well in 1000 ft of water to less than 10 bbl for a well in 3000 ft of water. In even larger water depths the kick tolerance can be around 1 bbl [7].

Drilling in slim holes were investigated as well. The small cross sectional area has a low volume capacity, hence a kick will propagate upwards faster in a slim hole than in a larger hole. A case study of a 5000 ft conventional hole was analyzed, and the kick tolerance was calculated to be 7.5 bbl which was estimated to be approximately 9 minutes after the influx started. If the hole had been a slim hole the kick tolerance would be reduced to 1.5 bbl and it would require a detection time of 2-3 minutes[7]. The detection time for slim hole drilling can be less than $\frac{1}{3}$ compared to when drilling a conventional hole.

2.3 Combining Software and Modeling with Existing Flow Measurement Tools

Adding software to the measurement process of flow-rate out of the well has shown to reduce the kick detection time in many cases. In this section four software systems are presented.

A study performed by Hargreaves et. al in 2001 highlighted two limitations to earlier used alarm systems, such as thresholds, CUSUM or predictive systems [7]:

1. It was common to use a simple threshold in raw data to detect unwanted events, an alarm was triggered when the threshold was exceeded. This method was susceptible to noise, because it could trigger false alarms. To increase the noise tolerance The CUSUM (cumulative sum) method, was later introduced. However,the CUSUM method is best utilized to detect step changes in the mean of noisy data, whereas a kick is commonly seen as a ramp. Constant operator attention is required to use this method.
2. Predictive systems uses a model to predict the measured values. Deviations between predicted and measured values are interpreted as unwanted events; which triggers the alarm. These systems are dependent on the accuracy of the measuring tools and the precision and completeness of the model that is being used.

2.3.1 Bayesian Kick Detector

The Bayesian method was first introduced in a paper written by Hargreaves et. al in 2001 [7]. The Bayesian method compensates for the noise in measurements, which can be critical in some wells.

The Bayesian kick detector is divided into two components. The first component is the *model set*, and the second component is a probabilistic model matching framework (Bayesian). With the measurements provided from rig equipment the models can recognize and differentiate various scenarios. By analyzing information from both normal and abnormal drilling events the Bayesian framework decides which of these models most likely matches the measured data by using a statistical approach. If the data resemble a kick event, the probability of a kick is estimated, and an alarm is triggered if the probability is relatively high.

In figure 2.1 the detection time for two different detection systems is investigated on a case where a kick situation occurs shortly after 40 minutes. With the CUSUM method the kick was detected at approximately 59 minutes while the Bayesian method detected the kick at 46 minutes, which is approximately $\frac{1}{3}$ of the time.

2.3.2 Quick Event Detection

In a paper published in 2008 [8] a Quick event detection (QED) system is described. The system was developed to minimize the no production time (NPT) due to unplanned events

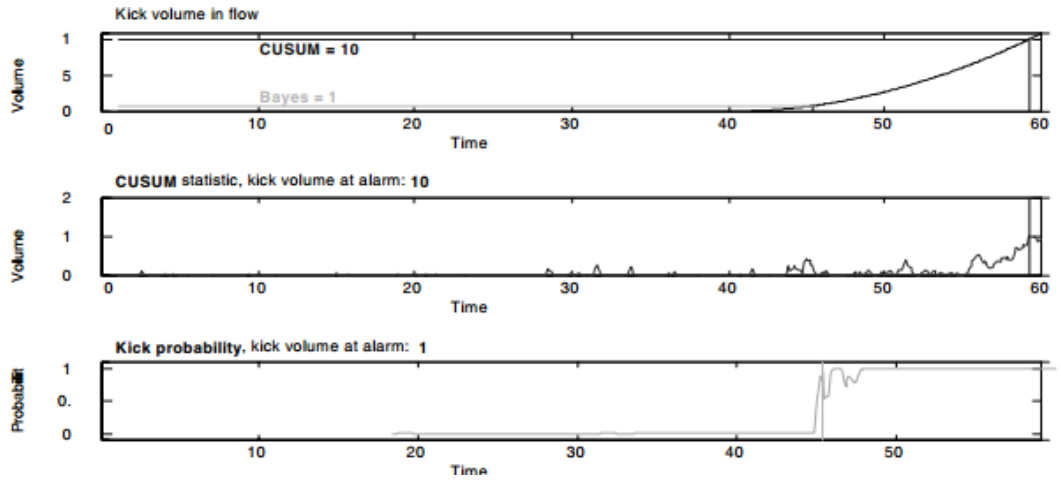

Fig. 2.1 Comparison of the Bayesian- and CUSUM-method [7]

such as kicks, loss of circulation and drillstring washouts. The QED software uses a probabilistic approach to determine if there is an unplanned event occurring. The main output from the QED system is a continuously estimated value of the probability that an event is occurring. An alarm is triggered if the probability reaches a specified threshold. The intention of the QED system is to help the drilling team in making timely and informed decisions in real time [8].

The QED systems uses the Bayesian method for kick detection to avoid problems with thresholds, CUSUM and predictive methods [8].

The QED system is inactive for a short period during pump start or stop to not trigger false alarms, and while the pumps are off the loss of circulation alarm is turned off. During gain or loss situations the active pit volume is not as sensitive as analyzing the delta flow ($\Delta q = q_{out} - q_{in}$) [8].

2.3.3 SMART Kick Detection

In 2015, a paper entitled "SMART Kick Detection: First Step on the Well-Control Automation Journey" was published. This paper introduced a SMART kick detection software which aims to reduce kick detection time and thus reduce the time to shut-in the well. The software automatically detects kicks by analyzing and interpreting well data [2].

This system is intended to work during all well-construction activities. It is able to identify which kick detection methods it uses depending on which well-constructing activity that is going on. During operation the program uses a reference point which is set manually or

automatically, and the software alarms the driller when the measured data deviates from the reference point. The software also gives the driller an option to compare the current situation with the last 5 scenarios of similar type e.g. comparing the present connection period with the last 5 connection periods [2].

During early analysis in this study it was found that the greatest improvement to kick detection and shut-in performance was gained by changing the previously used sensors with higher precision sensors, and to use them in duplicate sets to reduce the uncertainty of the measurements. Having duplicate sets means to have two or more sensors analyzing the same parameter, ideally the two different sensors are based on different measuring principles [2].

Comparing the SMART alarm system to the QED; the former includes various transient periods, but it has a relatively large false alarm frequency (FAF) during these periods. Table 2.3 shows the FAF for various kick- and loss indicators. The results show that the software is operating with relatively high degree of uncertainty during transient periods. The kick indicator "Active pit-volume gain" was triggered during connections, and the two loss indicators "Return-flow decrease" and "Active pit-volume loss" showed false alarms when the rig pumps were stopped or started.

Alarm Variable	False-Alarm Frequency (%)
Kick Indicators	
—Return-flow increase (drilling)	0
—Return flow with zero SPM (connection)	2
—Active pit-volume gain (drilling or connection)	31
—Trip-tank volume-difference gain (tripping)	2
Total % Kick Alarms	35
Loss Indicators	
—Return-flow decrease (drilling)	36
—Active pit-volume loss (drilling or connection)	28
—Trip-tank volume-difference loss (tripping)	1
Total % Loss Alarms	65

Table 2.3 False alarm frequency of the SMART kick-detection system [2]

2.3.4 Influx Detection at Pumps Stop (IDAPS) Software

The influx detection at pumps stop (IDAPS) software has been used at real-time operations centers (RTOC) since 2014. This software's objective is to tackle the challenge of detecting influxes during during pump stops for instance while making connections or flow checks [9].

The IDAPS software uses flow-in, flow-out, pit volume, bit- and hole depth real-time data as input. The measurements in combination with a machine-learning algorithm can recognize patterns or trends from previous data to set thresholds for the real time data; thus recognizing influxes as anomalies [9].

Tested on historical pumps-off events the IDAPS system had a false alarm rate (FAR) of 1 per 195(0.51%) connections and it detected 4/4 verified kicks, resulting in a 100% influx-detection rate [9].

The IDAPS system is dependent on real-time data, and has experienced difficulties with data losses and connectivity issues. Testing showed that 71% of all pump-stops had at least one data pattern that could confound the influx detection process, where the three most frequent confounding patterns were pipe movement, flow-out pulses and flow-out variance. Data-validity was a severe issue in 30% of the pumps-off events [9]. Programs using patterns recognizing can trigger false alarms when they lack data to make a reference point. E.g. during an abnormally long pump stop during connection, when using a new drilling fluid or a new pump rate.

2.4 Developing New Measuring Methods

To achieve a safer drilling operation and to detect kicks earlier the development of new measuring tools and methods are important. This section shows a case study where a Coriolis flow meter is compared to a flow paddle and pit gain. The Coriolis flow meter is explained in more detail in the theory section. A new flow measuring principle by analyzing the annular discharge pressure (ADP) and stand pipe pressure (SPP) is also introduced.

2.4.1 The Benefit of Precise Measuring Tools

In a paper written by Blay et. al the need for a precise measurement tool is proven in a case study of a ultradeepwater well. The paper presents a comparison of the results from three different detection methods; a flow-paddle, monitoring pit gain and a Coriolis flow meter [10]. Figure 2.2 shows that the mud weight window narrows with increasing water depth. The needed precision in the measurements is increased when drilling high pressure high temperature (HPHT) wells, in order to stay within the safe operational window.

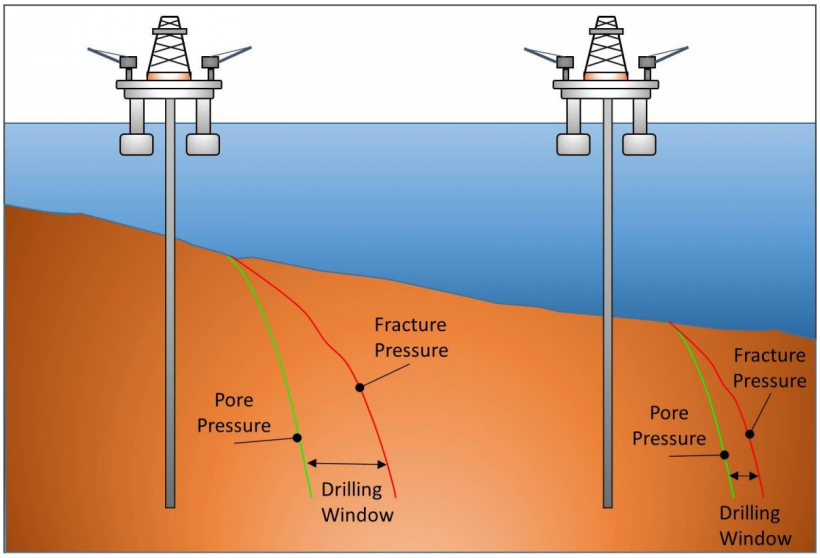

Fig. 2.2 Effects of increasing water depth on the drilling window [4]

The importance of accurate measurements are illustrated by comparing flow paddle measurements to Coriolis flow meter measurements in the case study. This is illustrated in figure 2.3 where the upper diagram shows the flow paddle measurements and the lower diagram shows the differential flow out which is determined from the Coriolis flow meter measurements. The differential flow clearly shows an influx at around 18:58 while no conclusions can be drawn from the flow paddle measurements, thus rendering the flow paddle insufficient to reliably detect kicks in real-time[10]. The drawback of the Coriolis flow meter is the size of the apparatus. To avoid a large pressure drop across the flow meter the system may become quite large. The flow meters footprint can present a challenge, as deck space on offshore installations is very limited.

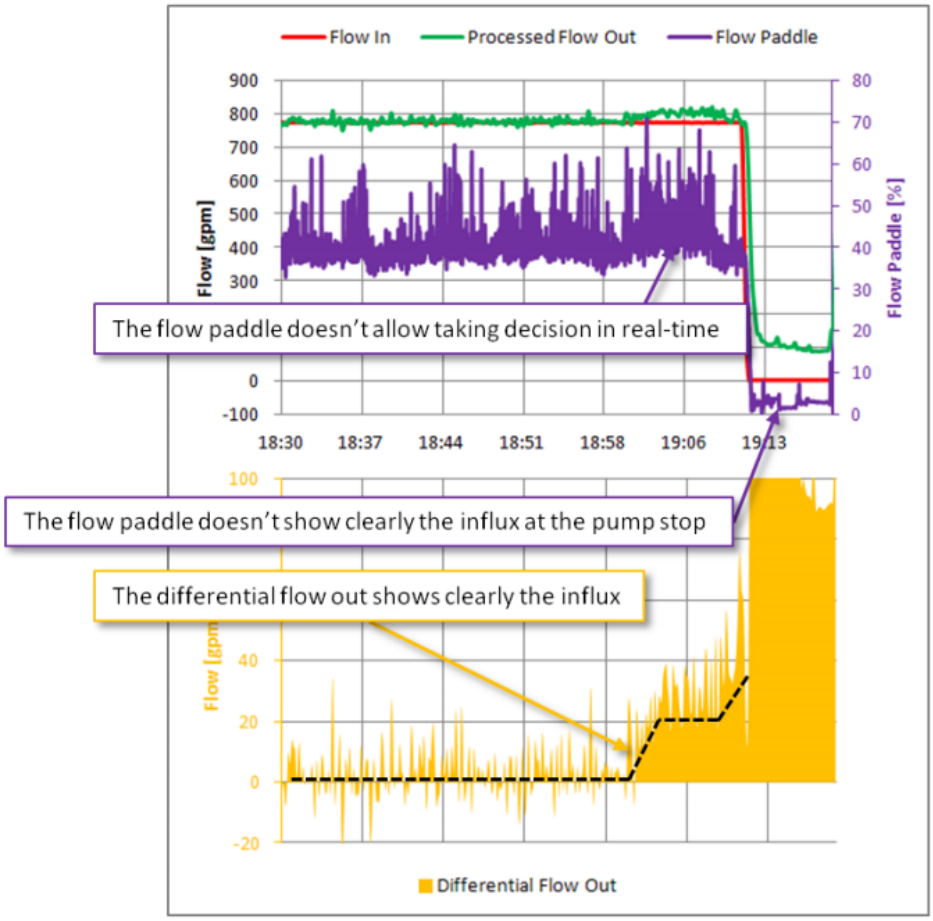

Fig. 2.3 Comparison of a flow paddle and a Coriolis flow meter [10]

The next comparison is between a Coriolis flow meter and monitoring the pit gain. Response time to detect a kick by using a Coriolis flow meter was compared to monitoring the pit gain. Figure 2.4 shows that it is possible to detect a kick 5 minutes earlier by using the differential flow out method. Note that this is a HPHT well, which amplifies the time difference.

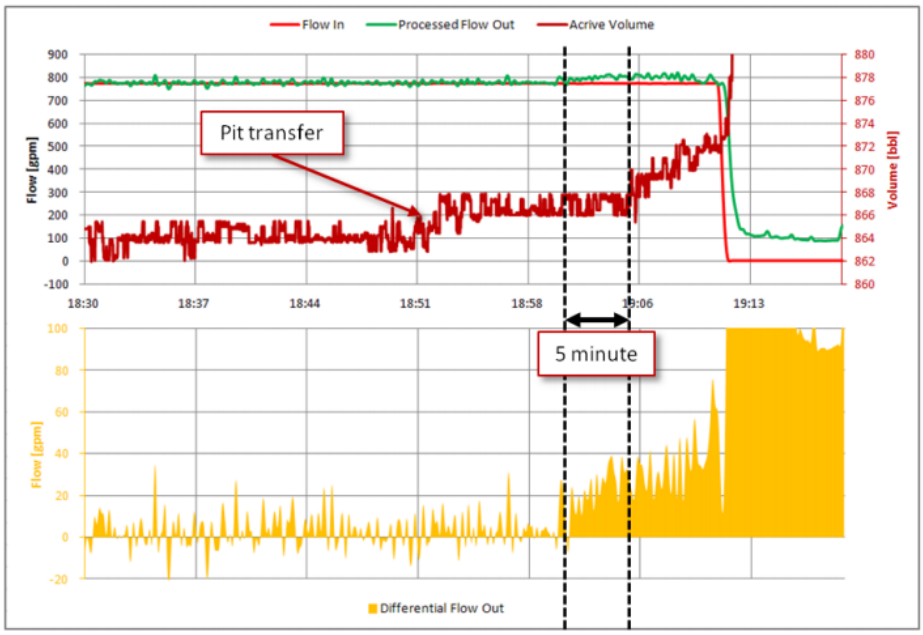

Fig. 2.4 Comparison of a pit gain and differential flow out[10]

2.4.2 Analyzing ADP and SPP to Measure Flow

Don Reitsma has worked on a new way to detect kicks which he states is competitive with the Coriolis flow meter. This method does not monitor the flow-rates in and out, but analyzes the SPP and the ADP [1].

During managed pressure drilling (MPD) a Coriolis flow meter has commonly been used because the flow loop is a closed loop during MPD. A closed loop eliminates the possibility to use a flow paddle or to perform flow checks. Don Reitsma states that during MPD operations the Coriolis flow meter can be replaced by an ADP measuring tool combined with a Dynamic Annular Pressure Control (DAPC) system. The DAPC system uses the ADP measurement to estimate the BHP. Furthermore an automated choke valve controls the ADP by regulating the choke valve opening to achieve the desired BHP. This is done during drilling, making connections and while tripping [1].

The choke valve opening is used as the kick indicator during drilling, as it controls the ADP which again feeds back to the SPP. Kick situations are detected by an increase in choke valve opening and a loss of circulation is recognized as a decrease in choke valve opening. When a kick is detected the DAPC system automatically increases the ADP until the influx stops. This method can only be applied while ADP is constant [1].

Analysis of ADP and SPP requires a very precise sensor to measure the ADP which costs approximately 10 - 20 % of what a Coriolis flow meter costs. The sensor must be located where there is a change in pressure/fluid head. For conventional drilling it is commonly placed upstream of the hydraulic control remote (HCR) valve or in the flow line to measure change in fluid height. For deepwater rigs it can be installed along the discharge pipe, on the riser or at the subsea BOP. The method is not sensitive to gas, requires no deck space and it is less complex than the Coriolis flow meter [11].

A separate study done by Cayeux and Daireaux (2016) included an analysis of a transient period while reaming. This analysis concluded that the methods that are based on measuring ADP and SPP would be valid for less than 3 minutes out of the 12 minutes it took to ream down one stand; because of how starting and stopping the pump affected the SPP and the ADP. This is highlighted in figure 2.5 where it took 5 minutes for the SPP to stabilize after pump start and 1 minute to stabilize after pump stop, and the SPP was stable for less than 3 minutes. Pump-rate changes would have similar effects on the SPP, and can be mistaken for influxes or effluxes [3].

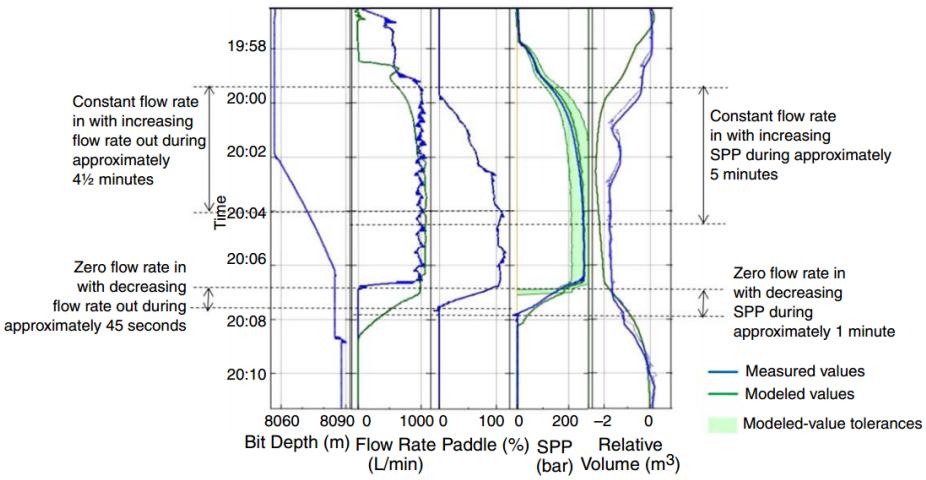

Fig. 2.5 Case study on transient periods [3]

2.5 Summary of the Technical Background

Combining flow-paddle measurements with software and modeling can reduce the FAR, which can lead to a safer operation. This method might require complex models that requires a lot of additional data. This method has difficulties with transient periods, as the FAR is higher than desired. Combining modeling and software to the already imprecise measurements such

as the flow-paddle measurements is sometimes insufficient to achieve the required FAR to have a safe operation.

Different wells requires different measuring tools as the required precision is not always equal. The flow paddle has sufficient reliability for simple wells during steady-state drilling, but because the flow-paddle is imprecise the flow-paddle is highly unreliable when used in complex wells. Wells that are complex and have small safety margins requires precise measuring tools such as the Coriolis flow meter.

The Coriolis flow meter is a very accurate measuring tool, however it requires a large amount of deck space. Rigs have to be specifically designed to receive a Coriolis flow meter during the rig's construction phase. This describes the foundation of the thesis and the desire to have a flow measuring tool that has a smaller footprint than the Coriolis meter and ideally with equal precision.

Chapter 3

Theory and Methods

This chapter will include relevant theory that is associated with measuring the flow-rate out of a well. Theory that is relevant to the experimental part of the thesis is also included.

This chapter is organized into three sections:

1. Theory regarding the measurement process
2. Parameters affecting flow-rate out measurements
3. Theoretical remarks on the experimental study

3.1 Theory Regarding the Measurement Process

This section will present methods for detecting fluid loss or gain situations and discuss different measuring methods and equipment.

3.1.1 Steady Flow Versus Transient Flow

To understand the challenges behind the measuring process, it is important to be familiar with steady flow and transient flow. Transient flow contributes to a large part of the challenges when interpreting measurements.

Steady flow implies no changes in the fluid flow or fluid properties. Parameters such as velocity, pressure, temperature, rheology, etc. is not changing with time [12]. When steady state is the reality, the measuring process is relatively simple.

In fluid dynamics the term transient flow is typically used for developing flows. Transient periods are distinguished as when changes are happening to the fluid flow or the fluid properties. For instance during drilling the starting or stopping of the pump is characterized as transient periods [12]. Whenever the pumps are started or stopped it takes time before the flow-rate out is at the same level as flow-rate in. The SPP also takes time to stabilize. A case study of this was presented by Cayeux and Daireaux where it took approximately 4.5 minutes for flow out to be equal to flow in, and 5 minutes before the SPP stabilized. [3] This time discrepancy is dependent on several factors such as the fluid volume, fluid rheology, etc. This is investigated further in chapter 4.

3.1.2 Fingerprinting Technique

The fingerprinting technique is a method to evaluate measured data. When evaluating previously measured data from earlier pump- starts and stops, the driller can recognize a trend in the data and use this to determine if the new measured data is normal or abnormal. This technique compensates for slight variations in the measured data. It simplifies the process where the driller has to determines if there is a kick situation or not. Fingerprinting is used by many of the new software systems (i.e. SMART alarm system or IDAPS).

This technique gives good results for steady-state conditions, but during transient conditions with abnormally large variations, a false alarm can be triggered.

3.1.3 Methods for Detecting Fluid Loss or Gain

There are mainly four different methods for detecting fluid gain or loss during drilling operations. This section will introduce them and discuss their strengths and weaknesses.

3.1.3.1 Abnormal Variations of Active Volume

Abnormal variations in the active pit volume indicates that a gain or loss situation is occurring. If the well experiences an influx, the mud level inside the active tank will increase, and during loss of circulation the mud level inside the active tank will decrease [3].

When tripping in or out of the hole a trip-tank is used and it allows for more precise measurements than the mud pit. The trip tank is smaller; rendering it easier to monitor. While tripping in, the trip-tank receives the excess volume of drilling fluid that is displaced, and while tripping out, the trip-tank provides the well with necessary mud to keep it filled. During

this operation the measured data from the trip-tank are compared with the theoretically estimated volume gain; thus any variation is easily detected [3].

Measuring variations in active volume is not sufficient during drilling operations. There are too many factors that influences the active volume, which can trigger false alarms. The active volume varies with pump rate, mud retention and with the compressibility of the fluid. The conventional way of dealing with these variations is by the use of the fingerprinting technique. However, this technique requires a sample to compare data to and if the pump rate has been changed or the starting and stopping of the pump do not follow the same trend as before, it can be difficult to detect a gain-loss problem [3].

3.1.3.2 Difference Between In and Out Flow: Delta Flow

The difference in volume rate from the inlet and outlet is called the delta flow ($\Delta q = q_{out} - q_{in}$). Comparing these two values can give us a direct and quick indication of a gain or loss situation.

This method is only accurate during steady-state hydraulic conditions as it does not include dynamic hydraulic processes that exist in the well. Measuring tools of high accuracy are needed to optimize this method, which is why a Coriolis flow-meter or a flow paddle with a complex model is recommended to use for complex wells [3]. Note that the required precision varies with different wells.

Transient periods presents a challenge for this method. False alarms can be triggered by natural discrepancies as well, for instance when the drillstring are moved axially or the mud pump is started/stopped [1].

3.1.3.3 Variations in Standpipe and Annular Discharge Pressure

The third method for detecting a gain/loss situation is by evaluating the SPP and the ADP. This method is explained in details in chapter 2. The SPP is the pressure at the inlet of the circulation system and the ADP is the pressure at the outlet of the well. This method allows us to detect and differentiate between a kick situation and a stuck drillstring/annulus bridging. Kick situations are distinguished by an increase in both the SPP and ADP, while a plugged drillstring or sealed annulus due to bridge-off or packing is characterized by an increase in SPP and a decrease in ADP. Figure 3.1 shows how various changes in SPP and ADP as a function of time (T) correlates to different well problems.

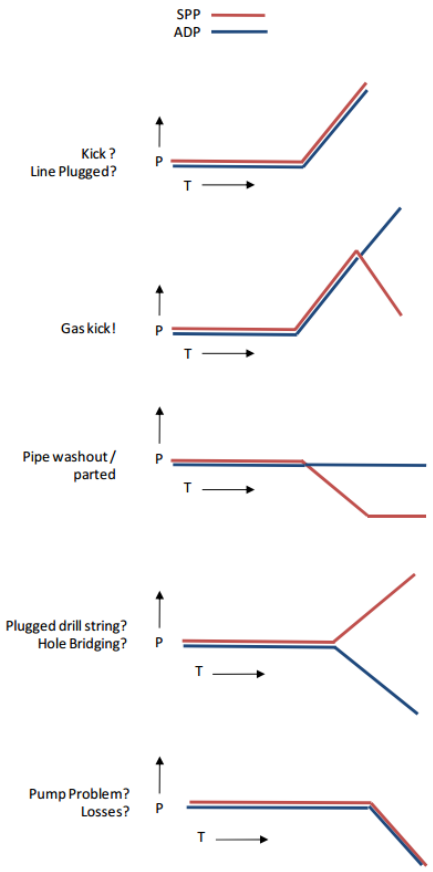

Fig. 3.1 SPP and ADP trending signatures [1]

This method requires a precise measurement of the ADP, and that is done differently during conventional drilling and MPD. During conventional drilling an additional sensor needs to be added upstream of an element that is creating a sufficient pressure drop so that the sensor can detect pressure variations caused by the flow-rate out. In a backpressure MPD situation the measuring process is more convenient as the annulus is already sealed by a rotating control device (RCD) and any pressure variations is reflected on the upstream pressure from the MPD choke valve.

Note that analyzing and interpreting the variations of the SPP and ADP is equivalent to analyzing the delta flow. Instead of directly looking at the difference in flow-rate, it looks at the pressure drop, which is a result of the difference in flow-rate. This means that this method has the same limitations as the delta flow method [3].

3.1.3.4 Processed Differential Flow Out

The previous methods are relatively simple and their challenges and limitations are related to transient time periods. When processing the measured data it is possible to include all flow conditions. This process combines measurements with an advance hydraulic model. The accuracy of this method relies on how advance and accurate the model is. The model requires a lot of well data to achieve great precision. It requires detailed description about the drillstring, drilling fluid, and wellbore geometry to operate. When implementing this method the difference between measured data and estimated data is reduced, resulting in a better FAR [3].

To acquire all this data, this method might require additional sensors and continuous monitoring of the drilling fluid's rheology.

3.1.4 Measuring Process

This section explains how the measurements that are used for detecting fluid losses or gains are achieved, and discusses their reliability.

3.1.4.1 Pit Volume

The fluid level in the pit is normally measured by a float level instrument or a ultrasonic level sensor. The floater uses a magnetostrictive linear position sensor and its readings is affected by the rig movements and it is sensitive to solids deposits up on the surface of the instrument [5].

There are two different tanks with mud on the rig; the active pit and the trip tank. Often there are no signals that differentiates which one is being used. The trip tank is much closer to the wellhead than the active pit and thus the amount of buffered fluid in the return line and the time delay is different for the two tanks. During mud displacement, there needs to be two tanks, one that fills the well and one that receives the previously used mud from the well, again there is no signals of which one is used. Similarly, the mud is circulated from a different tank when a pill is circulated into the well [5].

3.1.4.2 Flow-Rate Into the Well

The flow-rate into the well can be directly derived by the pump rate multiplied with the pump stroke frequency, the stroke volume and the mud pump efficiency. The time between the mud pump strokes are usually measured between two consecutive strokes, but this leaves room for inaccuracy during low flow-rates as it can take quite some time between the strokes [5].

3.1.4.3 Flow-Rate Out of the Well

The conventional methods for measuring the flow-rate out of a well are by either using a flow-paddle or a Coriolis Flow-Meter [9].

3.1.4.3.1 Flow-Paddle

The flow paddle is a tool used to measure the flow-rate out of the well. It is positioned top-side in the return flow channel, where it measures the height of the drilling mud in the return channel which is used as an indirect measurement of the flow-rate. The height of drilling mud in the return channel is a function of several parameters, which is why this is an indicative measurement of the flow-rate. The measured height also varies with the following parameters:

- Fluid viscosity
- Density of the fluid
- Shape of the return channel's cross-sectional area
- Roughness of the flow-line walls

Cutting can accumulate at the bottom of the return channel, which can affect the cross-sectional area of the return channel, as well as the roughness of the pipe. Very often the flow paddle measures a filling percent of the return channel and in those cases even more parameters affect the measurements. Angular rig movements on floaters can induce a difference in the filling percent [3].

3.1.4.3.2 Coriolis Flow Meter

The Coriolis flow meter measures directly the mass flow-rate out of the well. The Coriolis flow meter has two tubes through it and these tubes are set to vibrate. The vibration is influenced by how a drilling fluid is flowing through the tubes, and this is the principle that the Coriolis meter operates on. When there is no flow in the tubes, the two tubes will oscillate

uniformly and symmetrically. While if there is a flow-rate through the tubes, the oscillations deform proportionally to the mass flow-rate. The tubes have sensors on each end which measures the phase shift between the the sensors [13]. In figure 3.2 these sensors and the phase shift is illustrated.

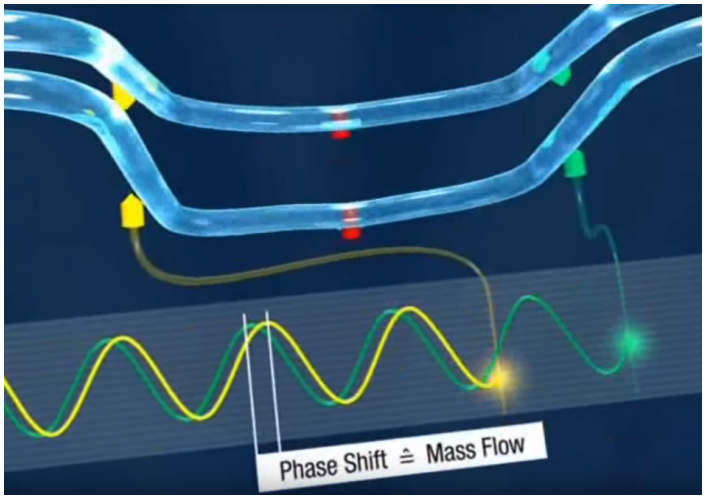

Fig. 3.2 Phase shift in Coriolis flow meter [13]

The mass flow-rate is derived from this phase shift. Furthermore, the density is derived by analyzing the frequency of the oscillations. When the mass flow-rate and density is known, the volume rate can be calculated:

$$\dot{V} = \frac{\dot{m}}{\rho} \tag{3.1}$$

The Coriolis flow meter can have unstable measurements if the flow contains relatively high amounts of gas. This is prone to happen during connections and it is called connection gas. Connection gas is the gas that enters the well during a pipe connection and this gas can make the Coriolis flow meter temporarily go out of service. The Coriolis flow meter can also show false readings on offshore platforms due to vibration from compressors and motors, which affects the vibrations of the two tubes inside the Coriolis flow meter. The flow meter requires some maintenance and it is important to flush out the drilling fluids when it is not being used to avoid plugging [1].

3.1.4.4 Ultrasonic flow-Rate Sensor for Kick Detection

When using an ultrasonic flow-out sensor, it is ideally installed 1m to 3m upstream from the bell nipple. This sensor measures the height of the fluid and is used in combination with a ultrasonic Doppler probe that measures the flow velocity locally in the return line. These

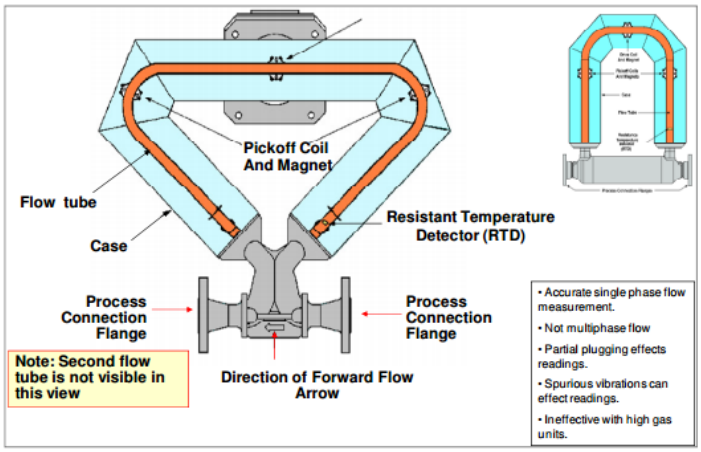

Fig. 3.3 Coriolis flow meter [1]

measurements are processed by a computer that takes into account the pipe geometry and calculates the cross sectional area that the mud fills [14].

This sensor is installed by using two flanges welded onto the return line. This method is not susceptible to plugging because of accumulating sediments or high amounts of gas. The drawback of this method is that it needs an additional temperature measurement to correct the measured height of the fluid in the return line. Maintenance has to be carried out on the velocity probe to make sure it is not buried in sediments [14].

3.2 Parameters Affecting Flow-Rate Out Measurements

This section discuss about parameters that affect the flow measurements. The main parameters are as following:

- Rheology
- Flow regimes
- Pressure drop from circulation
- Natural parameters affecting flow-rate out
- Drilling methods affecting the flow-rate out

This section is the main basis for the next chapter in which the effects of these parameters on flow-rate measurements will be presented.

3.2.1 Rheology

Rheology describes the deformation and flow of matter. The rheological properties of the mud is very important for [15]:

- Removing cuttings from the wellbore
- Establishing sufficient gel strength to hold the cuttings during circulation stop
- Generating the least amount of friction during pumping
- Not harming the well formations

The friction generated from circulating fluids is dependent on the fluid's rheology. The downhole pressure is a function of the friction generated by circulation.

3.2.1.1 Fluid Properties

Fluid rheology is characterized by several fluid properties. This section will explain about fluid properties that are relevant for this thesis.

3.2.1.1.1 Viscosity

Viscosity is a fluid's resistance to deformation. This resistance originates from the internal friction forces between particles/fluid layers in the fluid, and the attracting forces between electrically charged particles or ions in the fluid. Viscosity determines the magnitude of this internal resistance and it is a function of temperature, pressure, shear rate, time and chemical composition. Relevant mud characteristics to the viscosity are: [15]:

- Plastic viscosity (PV)
- Yield point(YP)
- Gel strength
- Apparent viscosity

Figure 3.4 shows how the rate of deformation varies linearly with increasing shear stress for oil, water and air. Equation 3.2 explains this mathematically where the viscosity μ is the slope. This linear relationship is only for Newtonian fluids [12].

$$\tau = \mu * \frac{du}{dy} \tag{3.2}$$

For non-Newtonian fluids the viscosity can either increase or decrease with rate of deformation. Viscosity increases with rate of deformation for dilatant or shear thickening fluids, and

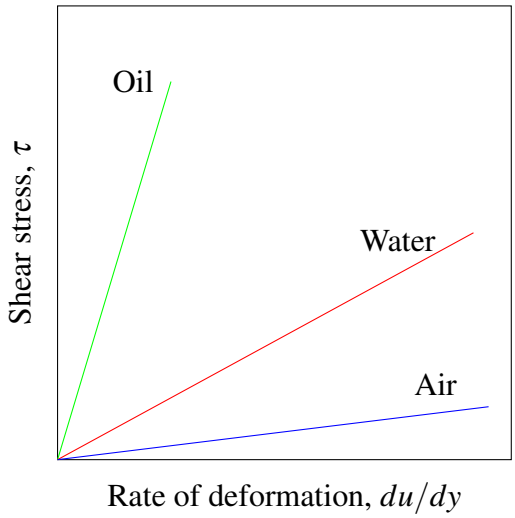

Fig. 3.4 Rate of deformation of a Newtonian fluid is proportional to shear stress

decreases in pseudoplastic or shear thinning fluids as shown in figure 3.5. The slope of the curves are changing and the viscosity is referred to here as apparent viscosity [12].

Viscosity is dependent on temperature, and for liquids it decreases with increasing temperature and decreases with increasing temperature. Viscosity is also dependent on pressure in a lesser degree. Viscosity is an important parameter in flow loops because it is directly connected to the friction generated which again is linked to pump pressure needed for circulation [12].

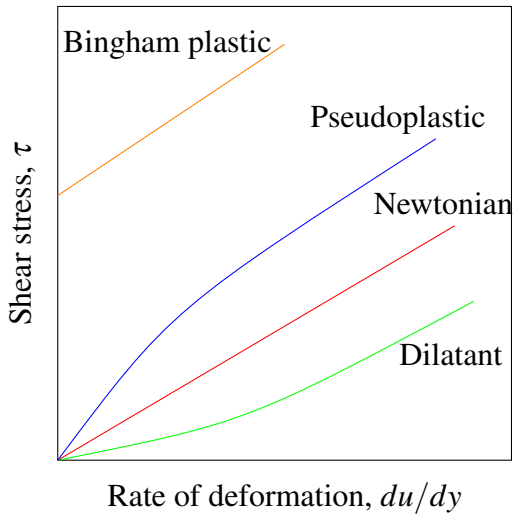

Fig. 3.5 Shear stress vs rate of deformation for Newtonian and non-Newtonian fluids

3.2.1.1.2 Gel Strength

The fluid's gel strength describes the fluids thixotropic properties. This property allows for the fluids viscosity to increase with time during pump stops and the fluid forms a gel structure. How gel strength increases with time is illustrated in figure 3.6 [16].

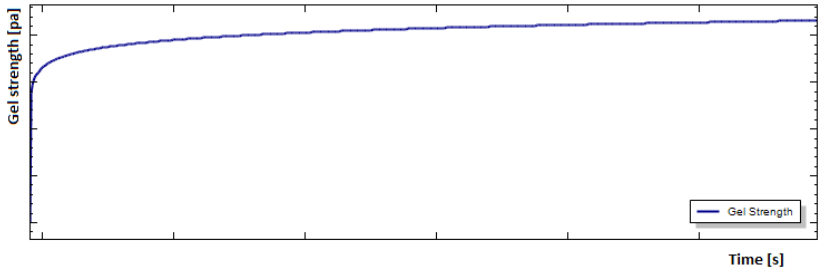

Fig. 3.6 Gel strength versus time

Gel strength is an important mud quality as it holds the cuttings in suspension during circulation stops. Gel strength also influences the flow-rate during pump start after a pump stop [16].

3.2.2 Flow Regimes

During circulation of mud in a well the fluid behaviour is characterized by being laminar, transitional or turbulent. Reynolds number is used to distinguish between the flow states, given by equation 3.3 [12].

$$Re = \frac{\rho V_{avg} D}{\mu} \tag{3.3}$$

Where ρ $[kg/m^3]$ is the fluid density, D $[m]$ is the diameter of the pipe, V $[m/s]$ is the mean fluid velocity and $\mu[Pa \cdot s]$ is the dynamic viscosity of the fluid [12].

Laminar flow is characterized by smooth streamlines and highly ordered motion. The velocity profile is illustrated in figure 3.7. Reynolds number is less than 2300 for laminar flows inside pipes [12].

There is no sudden transition between laminar and turbulent flow. In the transitional phase between the two, the flow is called a transitional flow. In the transitional phase the flow has burst of fluctuations. Reynolds number is between 2300 and 4000 for transitional flow [12].

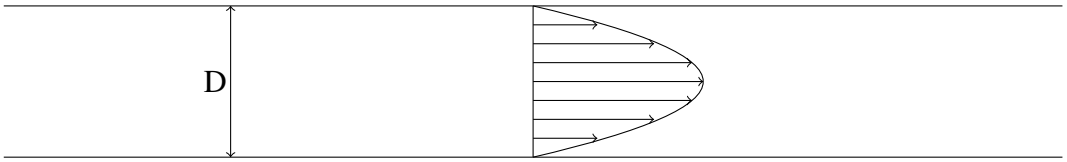

Fig. 3.7 Laminar flow

Turbulent flow is when the flow zigzags rapidly and disorderly. Turbulent flow generates a larger friction force on the fluid and thus requires a larger pump pressure to maintain flow-rate. The velocity profile is illustrated in figure 3.8 [12].

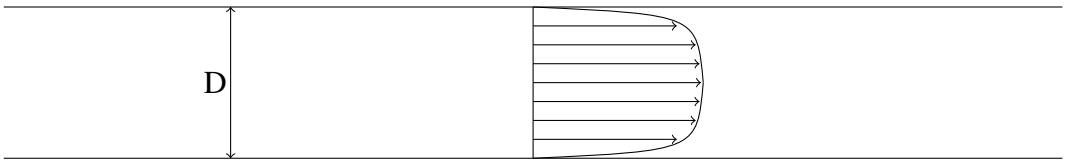

Fig. 3.8 Velocity profile of turbulent flow

3.2.3 Pressure Drop From Circulation

The pressure drop through a flow system is dependent on whether the flow is laminar, transitional or turbulent. The pressure drop is also reliant on bends in the pipes, valves, flow sensors, or any piece of equipment that adds an additional pressure drop.

3.2.3.1 Fanning or Darcy Friction Factor

There are several ways to describe the relationship of the friction between the fluid and the pipe walls. The most common way to describe this is by using a friction factor.

When performing calculations with a friction factor it is important to specify which friction factor that is used. There are two common friction factors that may be used interchangeably, namely Fanning and Darcy. The relationship between the Fanning friction factor and the Darcy friction factor is:

$$f = 4f_F$$

The Darcy friction factor f will be used further in this thesis unless otherwise specified.

3.2.3.2 Pressure Drop in Straight Pipe

The general equation for pressure drop across a cylindrical pipe is equal to [12]:

$$\Delta P_L = f\frac{L}{D}\frac{\rho V_{avg}^2}{2} \tag{3.4}$$

where f is the Darcy friction factor and changes with different flow regimes, L [m] is the length of pipe, D [m] is the diameter of the pipe, ρ [kg/m^3] is the fluid density and V_{avg} [m/s] is the average fluid velocity.

3.2.3.3 Detemining the Friction Factor

The friction factor can be determined by using the Moody Chart or by using the appropriate friction factor equation [17].

The Moody chart is a graphical way to determine the friction factor. The relative roughness and the Reynolds number are used to specify the friction factor. The moody chart is shown in figure 3.9.

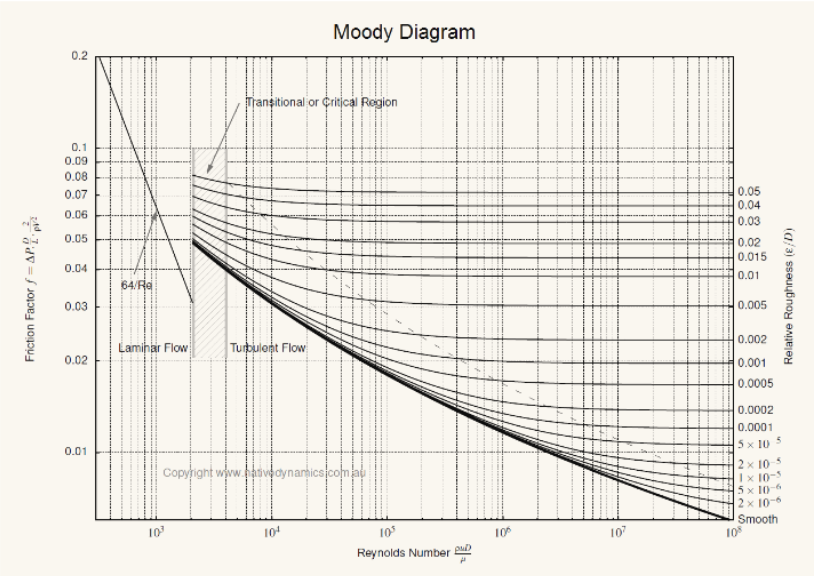

Fig. 3.9 The Moody chart [17]

The relative roughness is defined as $\frac{\varepsilon}{D}$, where ε [m] is the surface roughness and D [m] is the diameter of the pipe. Examples for surface roughness is found in table 3.1.

Table 3.1 Surface Roughness

Material	Roughness
Drawn Tubing, Glass, Plastic	0.0015 - 0.01
Flexible Rubber Tubing - Smooth	0.006 - 0.07
Flexible Rubber Tubing - Wire Reinforced	0.4 - 4
Stainless Steel	0.03
Carbon Steel (NEW)	0.02 - 0.05

To calculate the friction factor with an equation the flow regime has to be known in order to choose the appropriate equation.

The friction factor f for laminar flow is given by:

$$f = \frac{64\mu}{\rho D V_{avg}} = \frac{64}{Re} \tag{3.5}$$

During the transitional phase the flow patterns are unpredictable, hence it is impossible to to find a proper fiction factor.

For turbulent flow several relationships can be utilized. First is the widely accepted Colebrook equation:

$$\frac{1}{\sqrt{f}} = -2.0log(\frac{\varepsilon/D}{3.7} + \frac{2.51}{Re\sqrt{f}}) \tag{3.6}$$

The drawback of the Colebrook equation is that it requires iterations to solve. Several explicit approximations to the Colebrook equation exists. For instance the Haaland equation as shwon below:

$$\frac{1}{\sqrt{f}} \cong -1.8log[\frac{6.9}{Re} + (\frac{\varepsilon/D}{3.7})^{1.11}] \tag{3.7}$$

3.2.4 Natural Parameters Affecting Flow-Rate Out

3.2.4.1 Variation in Drilling Fluid Density

Drilling fluid density changes throughout the well. These changes can be a challenge because it will affect the flow-rate out of the well. The fluid density varies with both:

- Fluid compressibility
- Thermal expansion

3.2.4.1.1 Fluid Compressibility

The drilling fluid's density is influenced by how compressible the fluid is. When subjected to large pressures the fluid will compress and and the density will increase. Oil based mud (OBM) is more compressible than water based mud(WBM). One effect of the increased density is that the drilling fluid volume on topside is not equivalent to the volume of fluid to fill the well. Pressure variations in the well causes changes in the active pit volume [3].

During operations, there are many factors that influences the pressure drop inside the well. These pressure drops affects the pit volume and it can be difficult to differentiate these natural anomalies from kicks or losses. When the mud pumps start the fluid in the well will become more compressed due to the increased pressure from the friction and the pit volume will decrease, vice versa for pump stops. Same principle is true for any change in pump rate. The compressibility effect is more critical when drilling smaller diameter wells, because the pressure drop in the annulus is larger, resulting in a more compressed fluid and a larger BHP [3].

Mathematically the compressibility factor κ can be expressed as

$$\kappa = \frac{d\rho}{dp} \tag{3.8}$$

Consider that total volume inside a well is unchanged while the pumps start and the pit level is reduced, a mass balance then suggests that the mud density must have increased in order to fit additional mud into the well. The amount of additional mud taken by the well is dependent on the frictional pressure along the wall, volume of the well, rheology of the mud and the compressibility of the mud [3].

A different way to view this is by considering the equations for mass and momentum conservation for flow inside a wellbore. For a single phase flow the equations can be written as:

$$\frac{\partial}{\partial t}(A\rho) + \frac{\partial}{s}(A\rho v) = \dot{m} \tag{3.9}$$

$$\frac{\partial}{\partial t}(A\rho v) + \frac{\partial}{\partial s}A\rho v^2 + A\frac{\partial p}{\partial s} = A\rho f + K(v) + \dot{m}v_m \tag{3.10}$$

where t and s are the time and space dimensions, A, ρ, v, p are the cross-sectional area, density, velocity and pressure, f is axial component of the body forces per unit mass and $K(v)$ is a positive function of the velocity[3].

During a change in pump rate, both the compressibility and the conservation of momentum affects the transient time period. The simplest measuring methods that analyses only the delta flow will only work under circumstances where the fluid has a small momentum and where compressibility has a small impact [3].

3.2.4.1.2 Thermal Expansion

The second parameter that is important for the fluid's density is the thermal expansion. The fluid experiences different temperature through the well and its density increases with decreasing temperature and decreases with increasing temperatures. The temperature at the inlet and outlet can be different, and the fluid is continuously exposed to temperature from other fluids and the formation.

3.2.4.2 Mud Retention

Mud retention is the amount of mud that accumulates in the return flowline, shale shakers, sand trap, degasser and other mud treatment equipment on the rig between the outlet of the well and the tank. Mud retention in the return flow line influences the pit volume, as the volume of mud that accumulates here corresponds to the decrease of volume in the tank [3].

The flow velocity through the topside flowlines and equipment depends on the fluids rheology, density and the surface roughness of the pipes and channels. Changing the flow-rate causes transient periods in the pit volume, as the height of mud will increase with increasing flow-rates which results in increased mud retention. If the mud has insufficient viscosity to transport the cuttings in the flowlines, a cuttings bed may accumulate at the bottom of the flow line. The cuttings bed changes the surface roughness of the pipe and thus increasing mud retention [3].

Figure 3.10 shows the pit volume change in two different connection scenarios. One scenario is in a 17.5" hole section while the other is in a 6" hole section. In the 17.5" hole section the active volume change is 60% due to mud retention and 40% due to compressibility effects. While in the 6" hole section the active volume change is 10% due to mud retention and 90% due to compressibility effects.

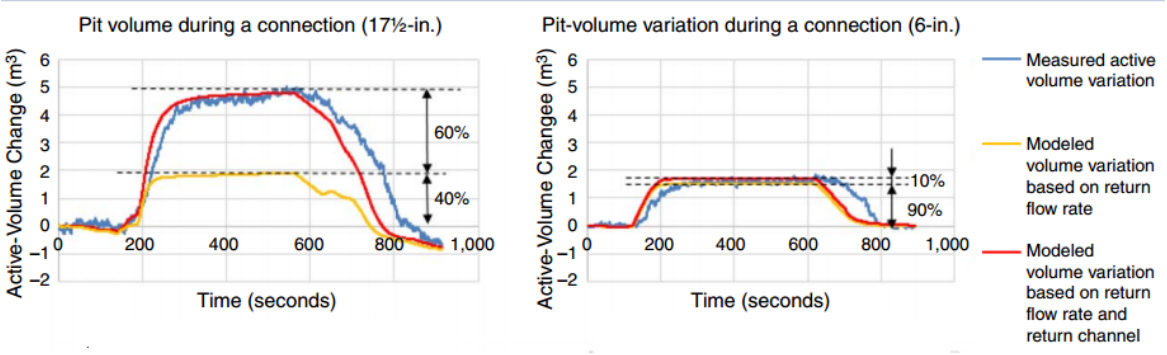

Fig. 3.10 Comparing mud retention and compressibility effect for various hole sizes [3]

3.2.5 Effects of Drilling Methods on Flow-Rate Out

To develop a model that can predict the flow-rate out of the well during steady state- and transient conditions one must understand the parameters that affect the flow-rate out of the well. A complete model needs to account for the flow from the inlet to the outlet [5]. Any instrument or method which affects the pressure drop through the well will have an impact on the flow-rate calculation.

3.2.5.1 Wellbore Geometry

Conventionally, the diameter of the open hole is determined by the bit size used during drilling. Hole openers and under-reamers make it possible to enlarge a hole, section-wise, after the hole is drilled. Flow diverters are used to clean the under-reamer or hole opener. These diverters along with the changes in wellbore diameter influences the pressure drop in the well. This has to be accounted for when detecting kicks or losses with any method that monitors the pressure difference between the inlet and outlet [5].

3.2.5.2 Downhole Motors

A positive displacement motor (PDM) is a downhole motor that transform hydraulic power to mechanical power. It uses hydraulic power from the drilling fluid and converts it to torque on the bit. Bit torque changes results in a change in the pressure drop in the system. The PDM uses flow diversion to lubricate the bearings of the motor, causing some of the flow inside the drillpipe to be diverted to the annulus. The pressure drop in the system depends on how much of the flow that goes through the bit. All methods that uses inlet and outlet pressure needs to consider the influence from downhole motors [5].

3.2.5.3 Float Valve

The drillstring is equipped with a float valve, usually in the BHA, that prevents fluids and cuttings from entering the drill string. The valve is open if the pressure inside the drill pipe is larger than the pressure below the tool, and is closed if the pressure inside the drill pipe is less than the pressure below the tool. The float valve prevents the nozzles being blocked by cuttings [5].

Because of the nature of the float valve it closes during tripping into the well. Because no fluid enters the drill string from the bottom, the fluid level inside the drillstring decreases. The drillstring is filled periodically to avoid unnecessary large hook loads and to minimize the pressure difference between the inside and the outside of the drillstring. Drilling fluid calculations while running into or out from the well needs to account for this displacement of mud. When running into hole the volume is based on the volume of the drillstring including the volume inside, and while running out of hole the displaced volume is equal to only the volume of the drill string [5].

3.2.5.4 Circulation Sub

Whenever a circulation sub is used, all of the flow inside the drillstring is diverted into the annulus. This causes an immediate effect on the pressure loss both on the inside and the outside of the drillstring. This impacts the gain and loss detection methods based on differential pressure between the inlet and the outlet [5].

3.2.5.5 Conventional Drilling

Because of the large diameter in the riser, it can be challenging to achieve a sufficient fluid velocity to transport the cuttings to the surface when drilling a section with a small bit. It is common to have a relatively low flow-rate when drilling in small diameter hole sections. To deal with this problem it is normal to add an additional inflow to the riser, through the kill line of the sub-sea BOP or through the booster line on some marine risers [5].

The delta flow method needs to account for the inflow from the booster pump into the well. Flow out should be equal to flow in from the main pump and the booster pump ($q_{out} = q_{in} + q_{bp}$). Methods that measures inlet and outlet pressures need to consider the additional pressure drop to the ADP measurement from the booster pump. Pit gain is also influenced because there is an additional amount of mud buffered in the return flow lines [5].

3.2.5.6 Pressurized MPD

During MPD drilling that uses back-pressure the back-pressure is caused by a choke that creates a pressure drop when fluids circulate through it. If the circulation through the choke is too low to create the needed back pressure a separate pump is used to create a sufficient pressure drop over the choke valve. Pressurized MPD affects the ADP/SPP- and delta flow method [5].

3.3 Theoretical Remarks on the Experimental Study

In this section the theory that is specifically used in the experimental part of the thesis is presented. Additional theory on pressure differences that is used in chapter 5 to estimate the pressure drop in the circulation loop, that is used for testing the new flow sensor, is included. The Coriolis force is a crucial aspect of the new flow sensor and control theory is included to explain the controller used to control the desired flow-rate in the new flow sensor.

3.4 Pressure Difference From Gravity or Vertical Elevation

The pressure difference in piping systems caused by vertical elevation is given by equation:

$$\Delta P = \rho g \Delta H \tag{3.11}$$

where ΔP [Pa] is the pressure drop due to elevation, ρ [kg/m^3] is the density of the fluid, g [m/s^2] is the acceleration of gravity and ΔH [m] is the vertical elevation or drop.

3.4.1 Pressure Drop in Bends

When a fluid flows through a bend the fluids experiences a radial pressure gradient created by a centrifugal force. This centrifugal force can create a different flow pattern that can result in an increase in pressure loss. The pressure loss in a bend is caused by both friction and change in momentum from the change in flow direction. This thesis estimates the pressure loss from bends by utilizing a bend-loss coefficient [18]:

The bend-loss coefficient can also be used to determine pressure drop through a bend. The equation for calculating pressure drop in a hose with bends by using the bend-loss coefficient is [18]:

$$\Delta P = \frac{1}{2} f_s \rho u^2 \frac{\pi R_b}{D} \frac{\theta}{180^\circ} + \frac{1}{2} k_b \rho u^2 \tag{3.12}$$

where f_s is the Moody friction factor, ρ [kg/m^3] is the density, u [m/s] is the average flow velocity, R_b [m] is the bend radius, D [m] is the tube diameter, θ is the bend angle, k_b is the loss coefficient. The loss coefficient are determined by using figure 3.11 where the angle of bend and $\frac{\text{Centerline Radius of Bend}}{\text{Internal Diameter of Pipe}}$ is used as input. Note that the equation is only valid for one-phase flow.

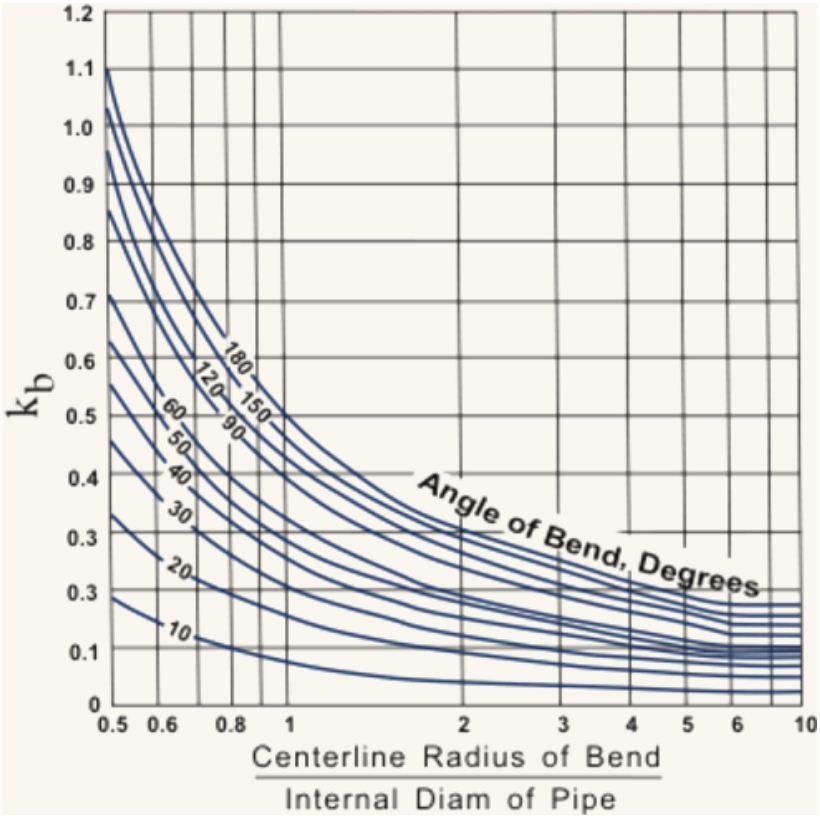

Fig. 3.11 Bend loss coefficient for a pipe [18]

3.4.2 Coriolis Force

The Coriolis force is a fictitious force that acts on objects that are in motion relative to a rotating reference frame. This force causes moving bodies to change direction or deflect

from their path [19]. The Coriolis force is utilized in the Coriolis flow meter and the new flow meter being developed at IRIS.

3.4.2.1 Mathematical Derivation

One way to derive the "Coriolis acceleration" is by a coordinate transformation. By comparing a vector in two separate reference system and analyzing the relationship between the acceleration of a vector B in a coordinate system fixed to the stars(f) relative to a system with an angular velocity of ω. The relationship between the two systems is [19]:

$$(\frac{dB}{dt})_f = (\frac{dB}{dt})_r + \omega \times B \tag{3.13}$$

The absolute acceleration is then derived by first using equation 3.13 with the position vector r, and then with the velocity v to get the relative velocity v_r. Combining these two equations gives:

$$a = a_r + 2\omega \times v_r + \omega \times (\omega \times r) \tag{3.14}$$

Where a_r is the observed acceleration, $\underline{2\omega \times v_r}$ is the Coriolis acceleration and $\omega \times (\omega \times r)$ is the centrifugal acceleration. Note that the Coriolis acceleration is only dependent on the velocity. The Coriolis force is a cross product of the rotational axis and the relative velocity. This means that any motions that are parallel to the rotational axis will not experience a Coriolis force, and velocities that are perpendicular to the rotational axis experiences the maximum Coriolis force [19]. By nature of cross products its possible to determine that the Coriolis force is perpendicular to both the rotational axis and the relative velocity [20].

The Coriolis force (F_c) is often written as [20]:

$$F_c = -2m\omega \times v_r \tag{3.15}$$

3.4.3 Control Theory

This section is explaining control theory by introducing feedback controllers and explaining PID controllers. Automatic control is widely used in engineering and sciences, and most engineers and scientists are familiar with basic control theory [21].

3.4.3.1 Feedback Control

In a feedback control system the objective is to control a parameter e.g. flow-rate, pressure, temperature, etc. An example of this is shown in figure 3.12. The temperature of the discharged water varies with how open the gas fuel valve is. The valve is controlled by a controller. This loop is called a feedback system. The transmitter feeds information about the water temperature from the outlet back to the controller, which adjust the control valve accordingly [22].

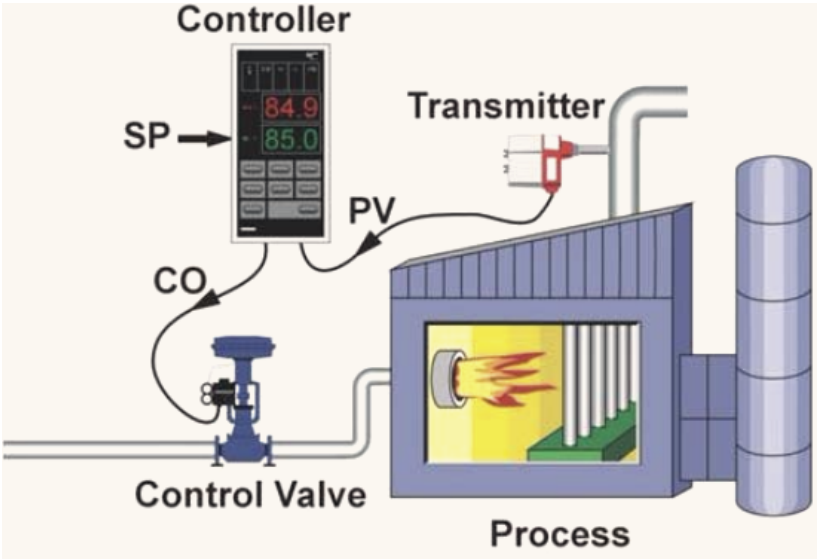

Fig. 3.12 PID controller example [22]

The desired temperature is given to the system and is called the set point (SP). The value that is measured and sent to the controller by the transmitter is called the process value (PV). The controller compares this to the desired set point by calculating the difference which is called the error ($e = SP - PV$), the controller then ensures that the appropriate action is carried out [22]. The feedback control aims to reduce the error to zero.

A simple feedback mechanism for an on-off control can be described as [23]:

$$u = \begin{cases} u_{max} & \text{if } e > 0 \\ u_{min} & \text{if } e < 0 \end{cases} \tag{3.16}$$

The advantage of such an on-off controller is that it is very simple. On the down-side the control equation 3.16 suggests that the maximum corrective action is always used. This often

results in an oscillating control variable. If the oscillating control variable is not acceptable, a more complex controller is used.

3.4.3.2 PID-Controllers

PID-controllers are used in more than 95% of all industrial control systems, to automate processes and control applications [23]. PID-controllers can be applied for controlling pressure, temperature, flow, level in a tank etc.

A PID-controller consists of three elements.

- **P** - Proportional Control
- **I** - Integral Control
- **D** - Derivative Control

The different terms can be used in various combinations e.g. P-controller, PI-controller, PD-controller or PID-controller.

The general equation for PID-controllers is:

$$u(t) = k_p e(t) + k_i \int_0^t e(\tau) d\tau + k_d \frac{de}{dt} \tag{3.17}$$

The terms are explained in more detail in the following subsections.

3.4.3.2.1 Proportional (P) Controller

The on-off system described in section 3.4.3.1 is susceptible to oscillation as it overreact to small changes in the error. To compensate better for the error the proportional controller is introduced. When using a P-controller the change in the actuator is proportional to the control error as highlighted in equation 3.18 [23].

Controller output is proportional to the error signal

$$u = \begin{cases} u_{max} & \text{if } e \geq e_{max} \\ k_p e & \text{if } e_{min} < e < e_{max} \\ u_{min} & \text{if } e \leq e_{min} \end{cases} \tag{3.18}$$

where k_p is the proportional controller gain, $e_{min} = u_{min}/k_p$ and $e_{max} = u_{max}/k_p$.The interval between (e_{min},e_{max}) is called the proportional band as the controller behaves linearly here:

$$u = k_p(SP - PV) = k_p e \quad \text{if } e_{min} \leq e \leq e_{max} \tag{3.19}$$

The P-controller still has limitations. One limitation is that it struggles with completely diminishing the offset. This can lead to the process variable often deviates from the set point [23].

3.4.3.2.2 Proportional Integral (PI) Controller

The PI-controller introduces an integral control action that is proportional to the integral of the error. The objective is to eliminate the offset that the P-controller struggles with.

$$u(t) = k_i \int_0^t e(\tau) d\tau \tag{3.20}$$

where k_i is the integral gain. The integral term causes the manipulated input to keep changing until $e \neq 0$. In contrast to the P-controller the error (e(t)) can be equal to zero, while the term expressed in equation 3.20 is different from zero. PI-controllers may not be steady if the controlled system is oscillating [23].

3.4.3.2.3 Proportional Integral Derivative (PID) Controller

When controlling a system that is oscillating the controller needs to predict the error. A linear extrapolation is given by [23]:

$$e(t + T_d) \approx e(t) + T_d \frac{de(t)}{dt} \tag{3.21}$$

where the error is predicted a time (T_D) ahead.

By combining the term from the proportional, integral and derivative control we get an equation for a PID-controller that when expressed mathematically can be written as in equation 3.17

When deciding which controller to use, the need is dependent on the system. A PID-controller may dampen oscillations compared to a PI-controller, but it is also a more complex controller which is more difficult to tune and it can amplify potential noise in the system [23].

How a PID-controller operates in a feedback loop is illustrated in figure 3.13

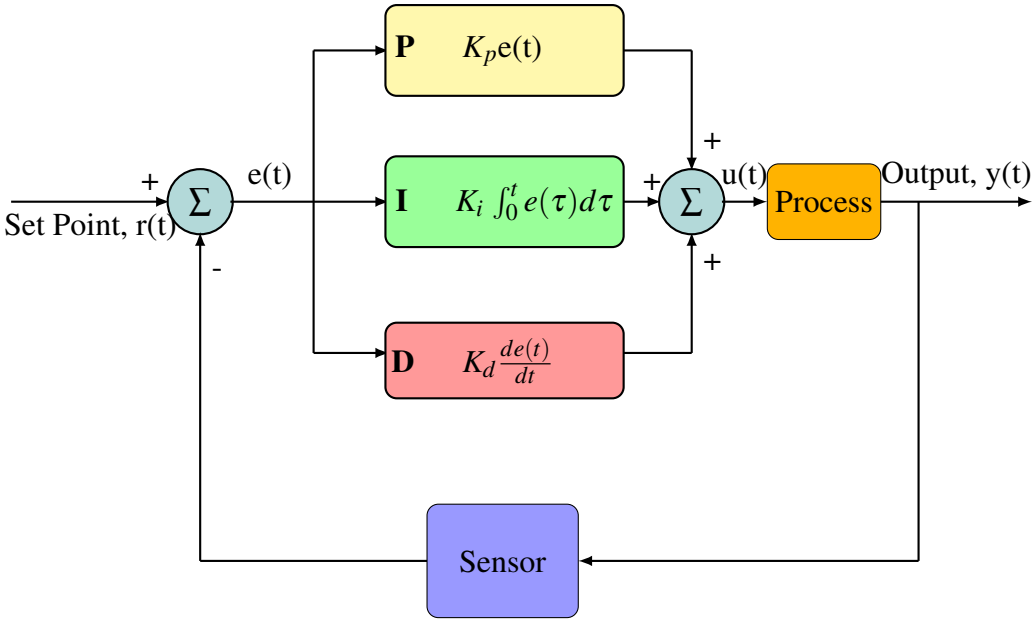

Fig. 3.13 PID-Controller Flow Diagram

Chapter 4

Flow-Rate Out Simulations

In this chapter a case study is investigated to understand how the flow-rate out of the well varies with different parameters. Simulations are conducted in "Drilling Calculator", which is a simulation software developed at IRIS. The results are analyzed and interpreted. This chapter is mainly based on theory provided in section 3.2.

4.1 Introducing the Well

To interpret the results from the simulations, it is important to understand the base case of the study. This includes the size of the well, the well trajectory and the drilling fluid's rheology. The base case for the study is introduced in this section, and then changes to various parameters are analyzed one at a time.

The base case analyzed has 8503 m measured depth (MD) and 4196 m true vertical depth (TVD). The trajectory is visualized in figure 4.1.

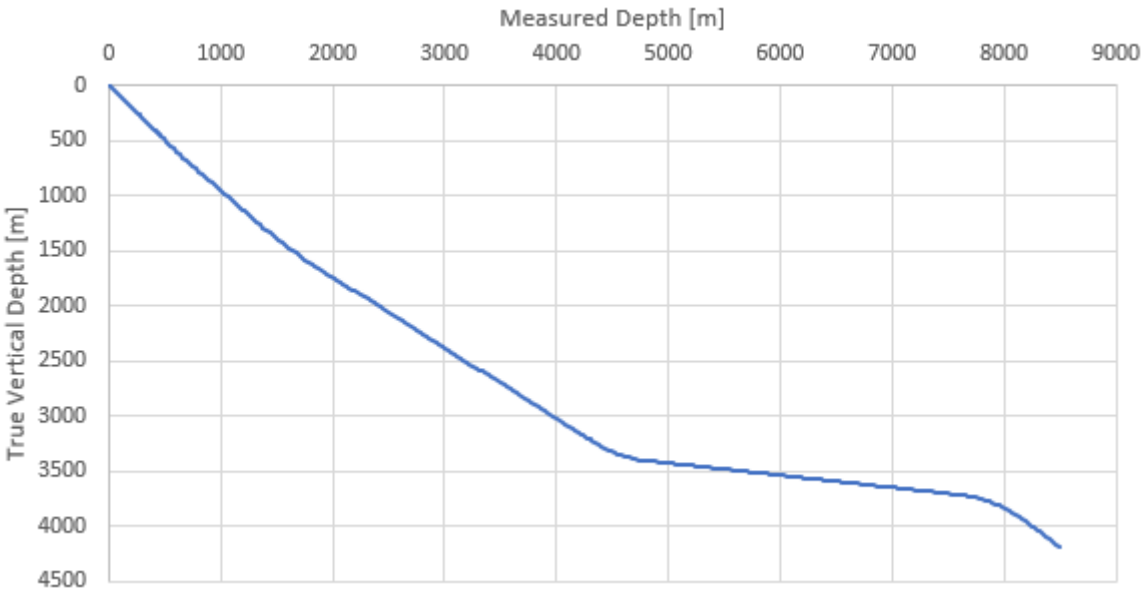

Fig. 4.1 Base case trajectory

The drilling fluid used in the base case is a OBM with a density of 1.680 sg and a oil water ratio (OWR) of 5.250. The rheology of the drilling fluid is presented in figure 4.2. The fluid has a gel strength (10 s) of 1.5 Pa and gel strength (10 min) of 2.0 Pa.

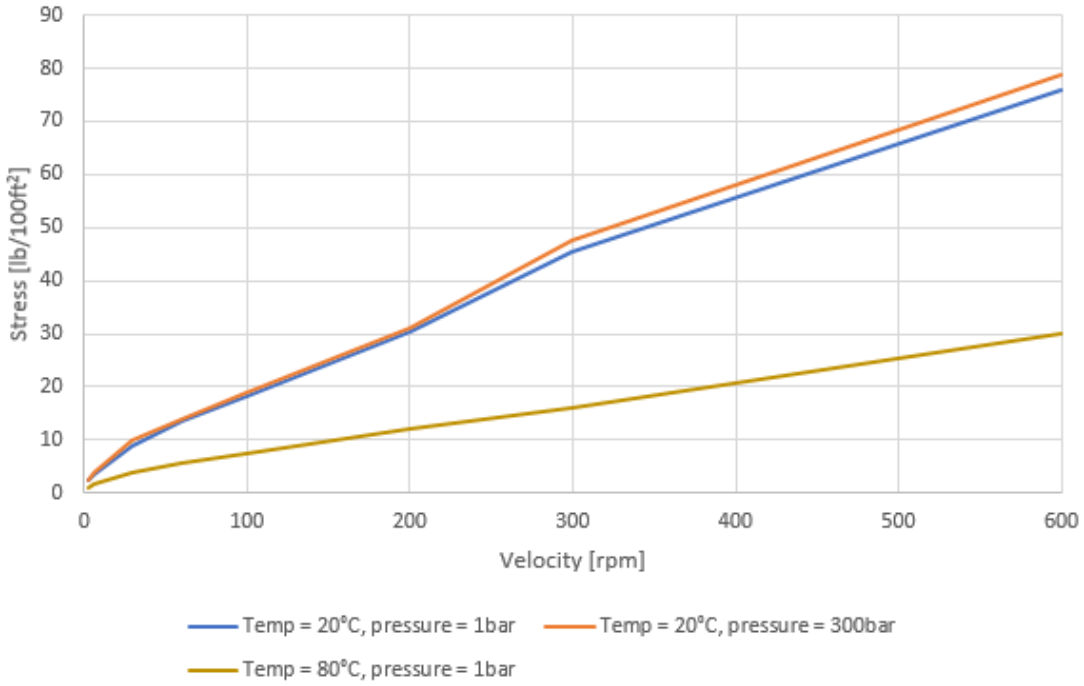

Fig. 4.2 Base case rheology

4.2 Compressibility Effects

Compressibility causes the well to take an additional volume of mud during circulation. In this section the additional volume of mud is estimated, as various parameters change, to investigate how the compressibility effects are influenced by the changes. The standard flow-rate in (q_{in}) used for the simulations is 2000 lpm unless otherwise is specified. At pump start a lower flow-rate of 200 lpm is used to break the gel structure, before the pump rate is increased to 2000 lpm. This is done to avoid unnecessary noise in the simulations, and to isolate the effect of varying one parameter.

To estimate the additional mud inside the well, the flow-rate out (q_{out}) and flow-rate in (q_{in}) is analyzed. When q_{out} and q_{in} are plotted as a function of time, the area difference between the two graphs are equivalent to the additional mud inside the well. Note that when the additional volume is not increasing after a certain amount of time, flow-rate in is equal to flow-rate out ($q_{in} = q_{out}$).

During the time period when $q_{out} \neq q_{in}$ are transient periods. This time period is a result of both compressibility effects and conservation of momentum. The fluid inside the well has an enormous momentum that either takes time to move or stop. These periods are characterized as an increase or decrease in the graphs concerning additional mud. The transient periods are plotted as well, for both pump start and pump stop.

4.2.1 Flow-Rate Variation

The effect of flow-rate variation is illustrated in figure 4.3. The graph shows the amount of additional mud, in liters, the well can contain as the flow-rate varies from 500 lpm to 3000 lpm as a function of time. Pump start is simulated at 171 seconds and pump stop is simulated at 701 seconds.

The increasing amount of additional mud is a result of the mud inside the well being compressed by the additional frictional pressure from the increased flow-rate. Due to the compression of drilling fluid and the increase in momentum when increasing the flow rate, an additional amount of mud is allowed to enter the well.

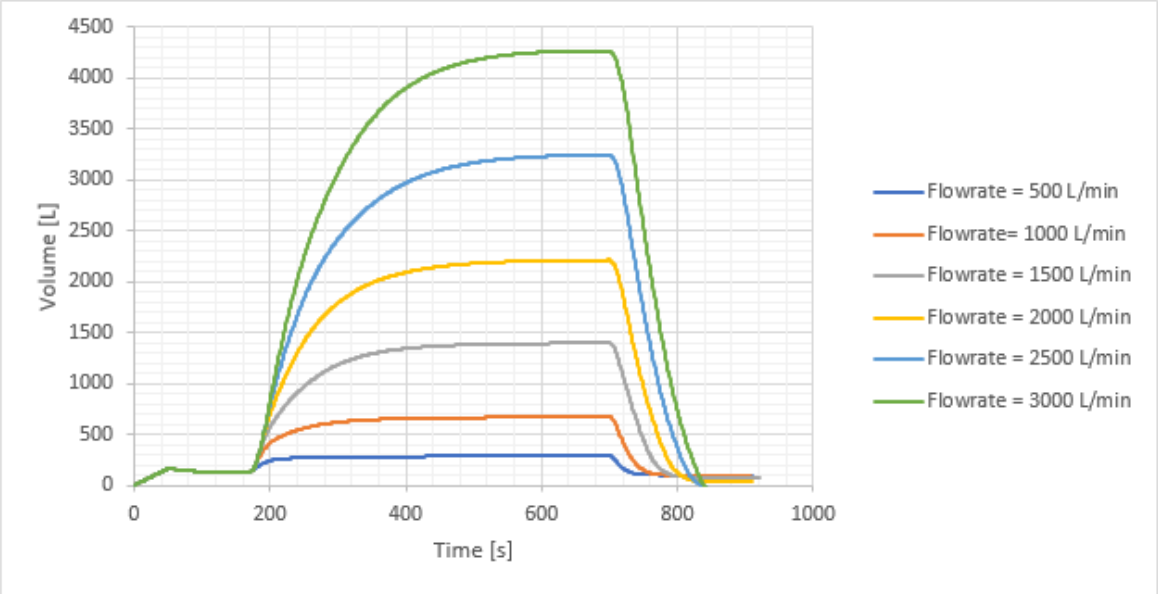

Fig. 4.3 Compressibility from flow-rate variation

Figure 4.4 shows how the bottomhole ECD increases with flow-rate. Note that the ECD is a function of both flow-rate and the density of the mud column in the well, which both are increasing in this scenario.

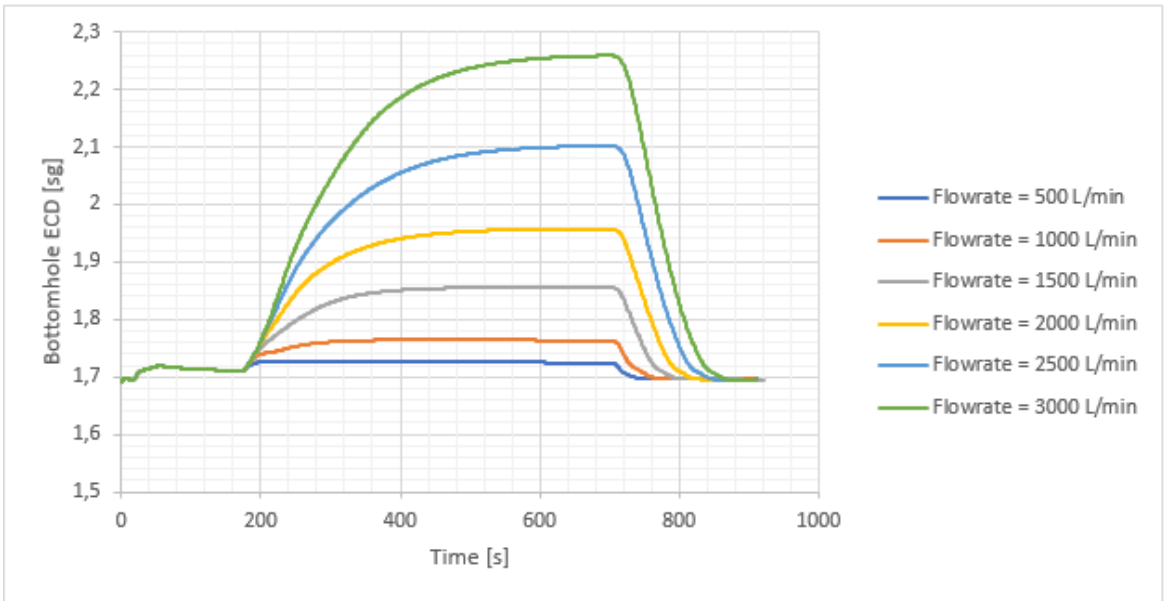

Fig. 4.4 Bottomhole ECD varies with flow-rate

The transient period at pump start and pump stop is shown in figure 4.5. The transient periods increase with higher flow-rates for both pump start and pump stop.

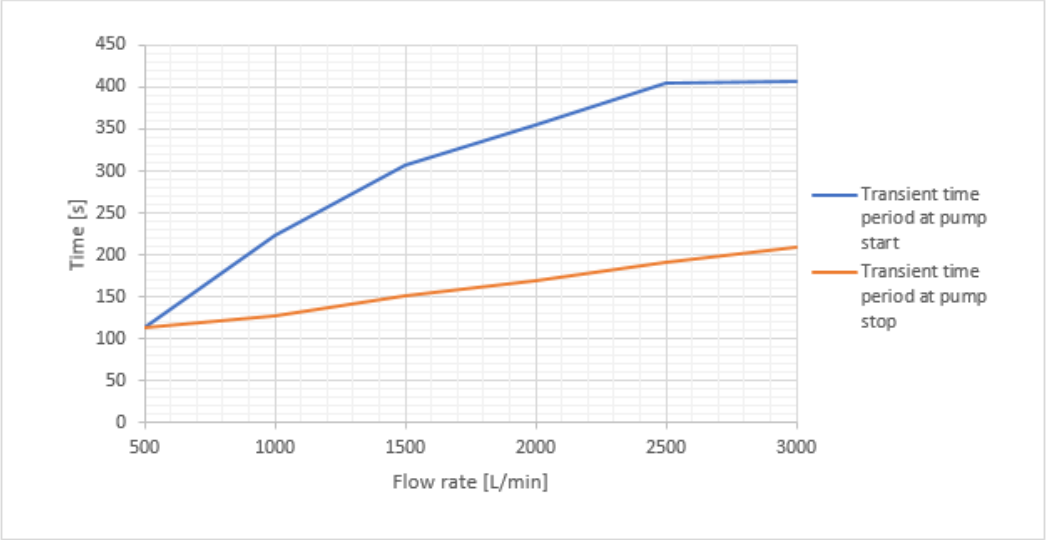

Fig. 4.5 Transient time period as a function of flow-rate

4.2.2 Bit Depth Variation

Increasing bit depth as a hole section is being drilled allows for additional mud volumes due to compressibility effects as showed in figure 4.6. The fluid's momentum is also increased with the volume of fluid.

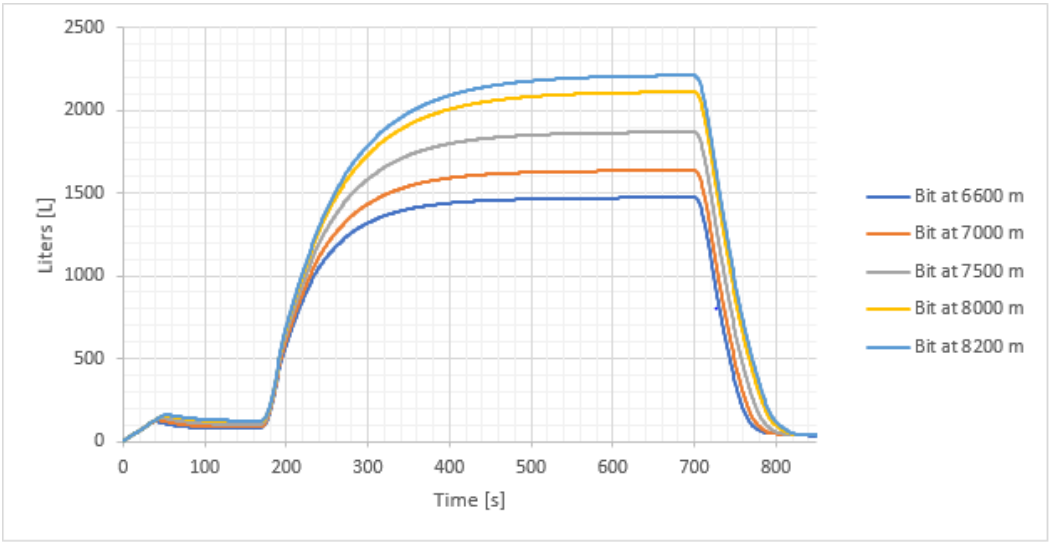

Fig. 4.6 Compressibility from bit depth variation

Compressibility effect are proportional to the volume that is being compressed. When the bit depth is increased, there is an increasing volume of drilling fluid that is available to be compressed, causing the compressibility effect to increase.

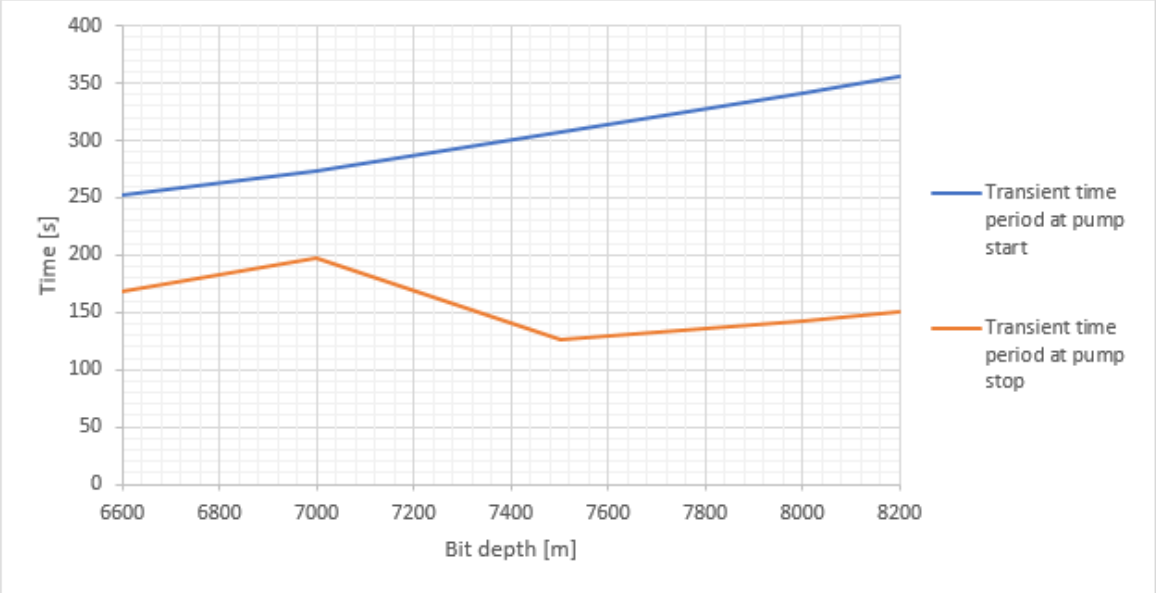

Fig. 4.7 Transient time period as a function of bit depth

The transient time for various bit depths are shown in figure 4.7. The transient time is increasing at pump start with bit depth. The simulation data from the pump stops does not yield a definite conclusion.

4.2.3 Density Variation

The additional volume of drilling mud required to fill the well during circulation reduces with increasing density as shown in figure 4.8.

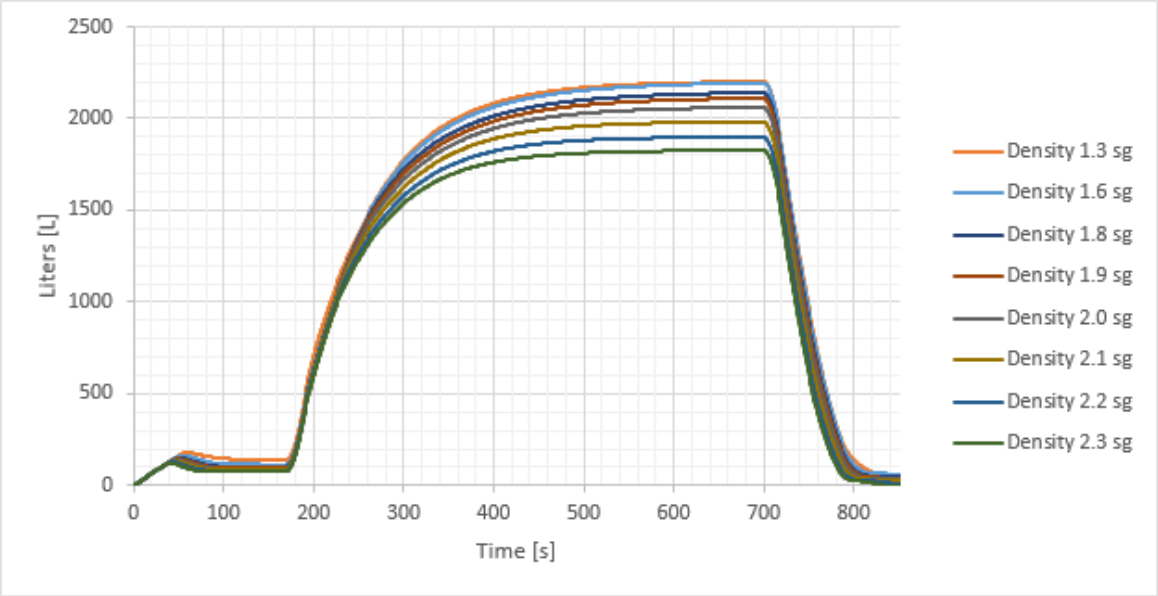

Fig. 4.8 Compressibility from density variation

Fluids with high density have a higher percentage of solids than low density fluids, hence a high density fluid has a lower percentage of fluid. This results in a smaller compressibility effect in high density fluid, because the percentage of fluid is reduced. The momentum of the fluid is also increased by the higher density.

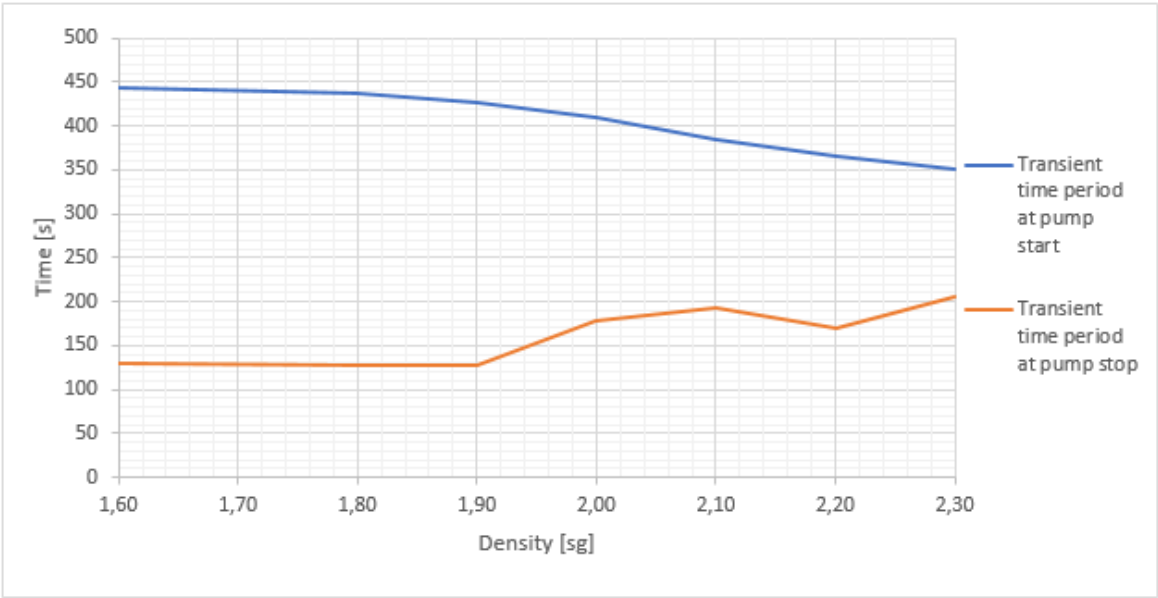

Fig. 4.9 Transient time period as a function of bit fluid density

In figure 4.9 the transient period are shown for pump start and pump stop. The simulation data from the transient time period at pump start shows a decrease in the transient period when the density increases. The data from the pump stop suggests that the transient period is diminished as density is increased.

4.2.4 Oil Water Ratio Variation

The effect from compressibility decreases with increasing OWR as illustrated in figure 4.10.

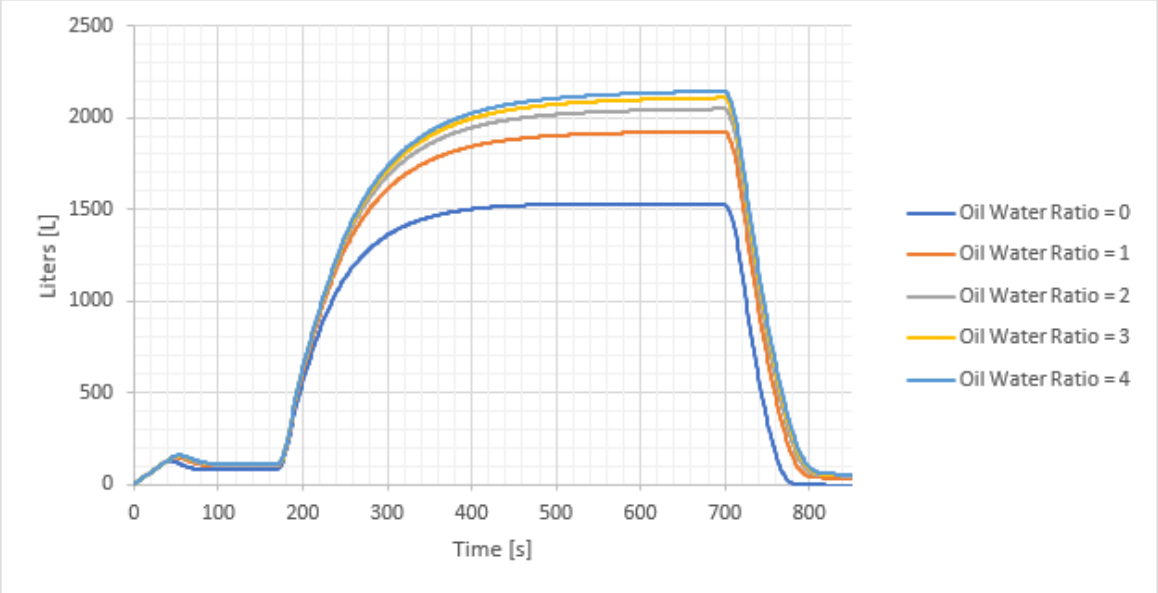

Fig. 4.10 Compressibility from oil water ratio variation

The compressibility effect increases as OWR increases. This is an effect of oil being more compressible than water.

Figure 4.11 shows how the transient time period varies with increasing OWR for both pump start and pump stop. The transient time period increases with increasing OWR for pump start scenarios, while for pump stops the transient period suggests no change in the transient time period.

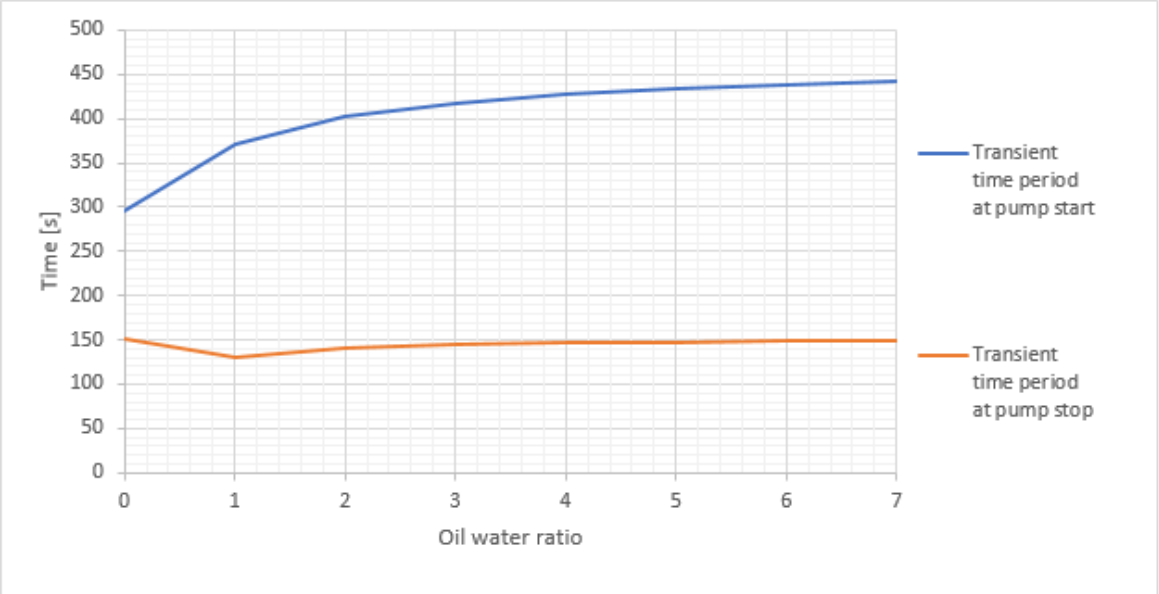

Fig. 4.11 Transient time period as a function of OWR

4.2.5 Rheology Variation

To investigate the effect of rheology variation on compressibility effect, the simulation was performed with 5 different fluids. The fluids have different rheological behaviours as shown in figure 4.12

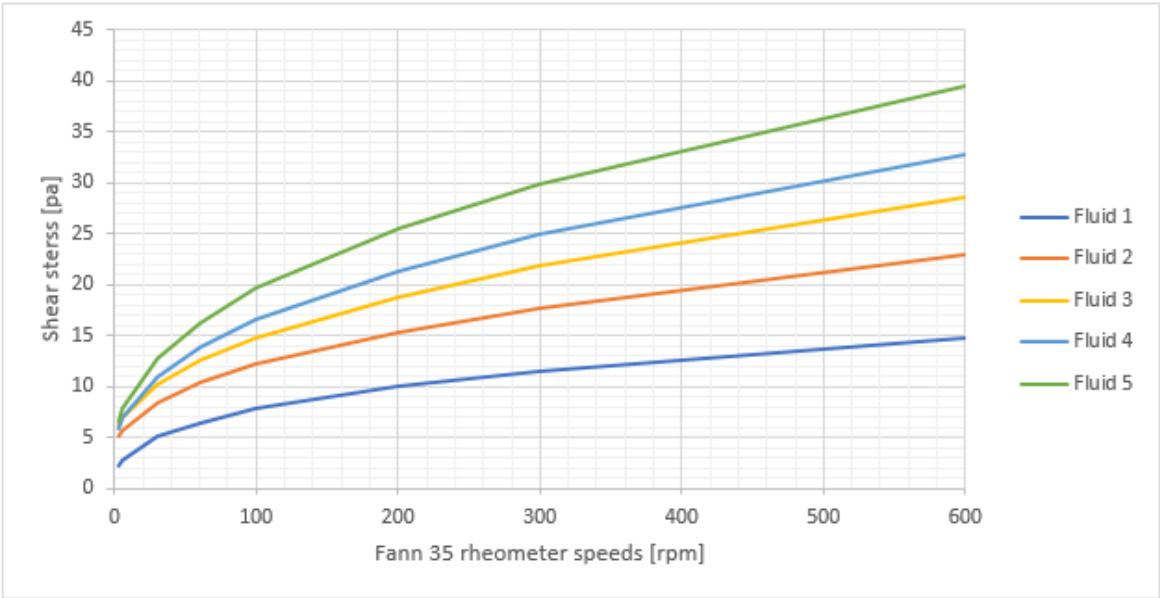

Fig. 4.12 Rheological behaviour of the selected fluids

The selected fluids were then used to analyze the variation in compressibility effects. Figure 4.13 shows that the compressibility effect increases with increasing viscosity.

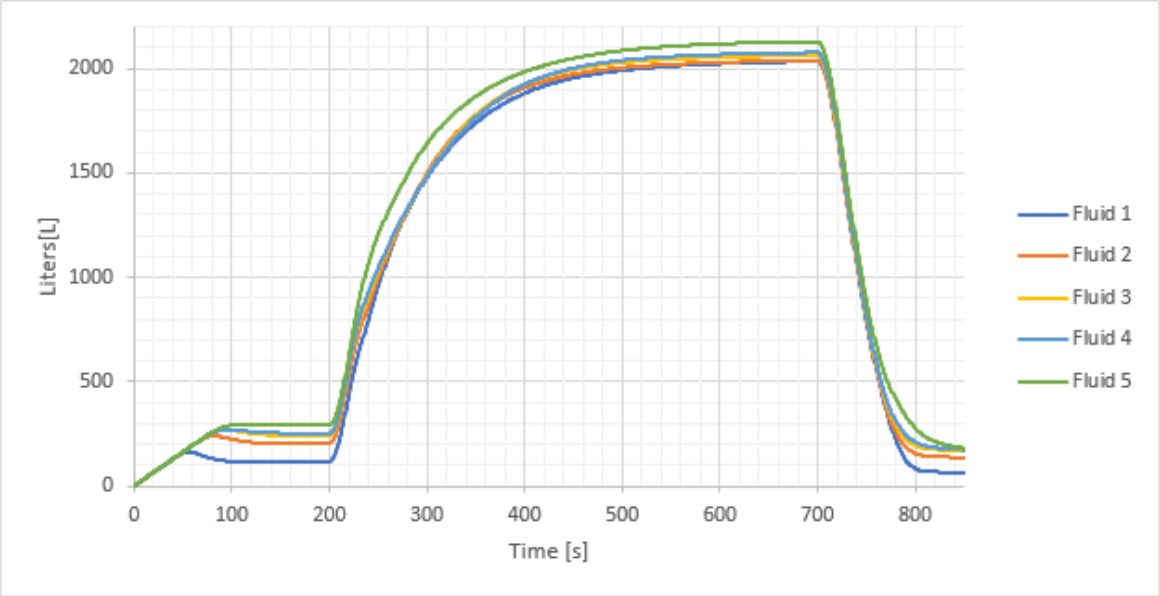

Fig. 4.13 Compressibility effect from various fluids

The pressure drop in the circulation system is a function of viscosity. The moody chart in figure 3.9 shows how the friction factor increases with increasing viscosity. The general equation for pressure drop, equation 3.4, shows how the pressure drop increases with increasing friction factor. This results in an increase in pressure throughout the well when the viscosity increases, and the increase in pressure causes an increase in the compressibility effects.

The transient time period for pump starts and pumps stops for the different fluids are shown in figure 4.14.

The results for pump starts shows small variance in the transient time period, with no specific trend. The simulation results from the pump stops indicates an increasing transient time period for fluids with higher viscosity.

4.2.6 Drilling Different Hole Sections

When drilling well sections that has varying open hole diameters, the compressibility effects changes. The simulations are done with different drilling fluids, drill string, bit depth and flow-rate for each hole section. This is done to make the scenarios realistic. Note that the open hole diameter decreases with increasing depths.

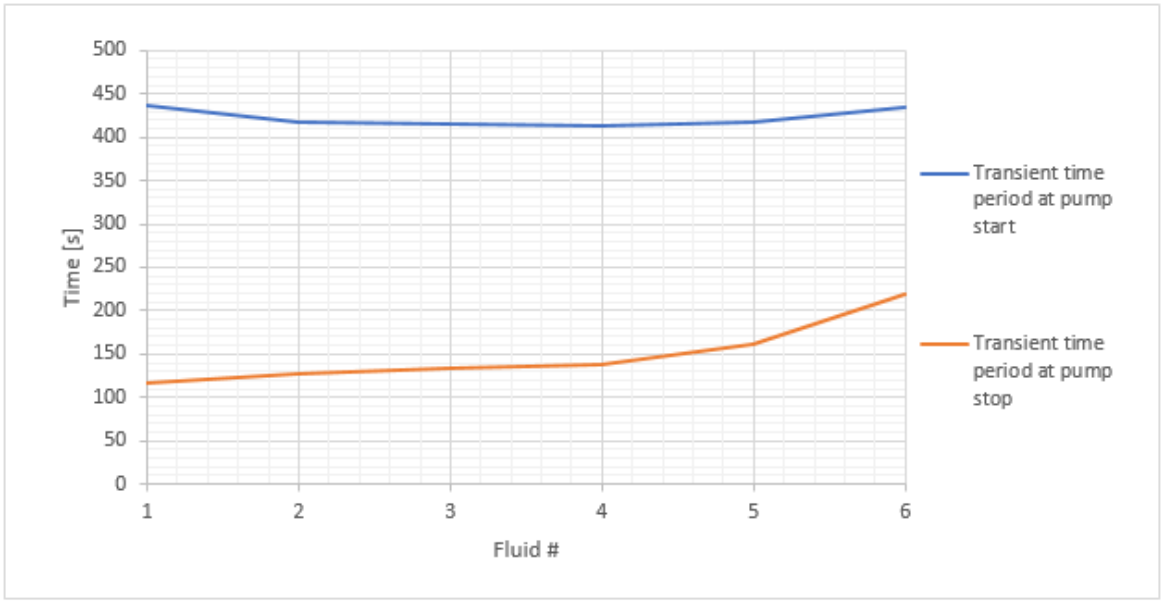

Fig. 4.14 Transient time period changing with different rheology

The compressibility effects in the different hole sections are illustrated in figure 4.15.

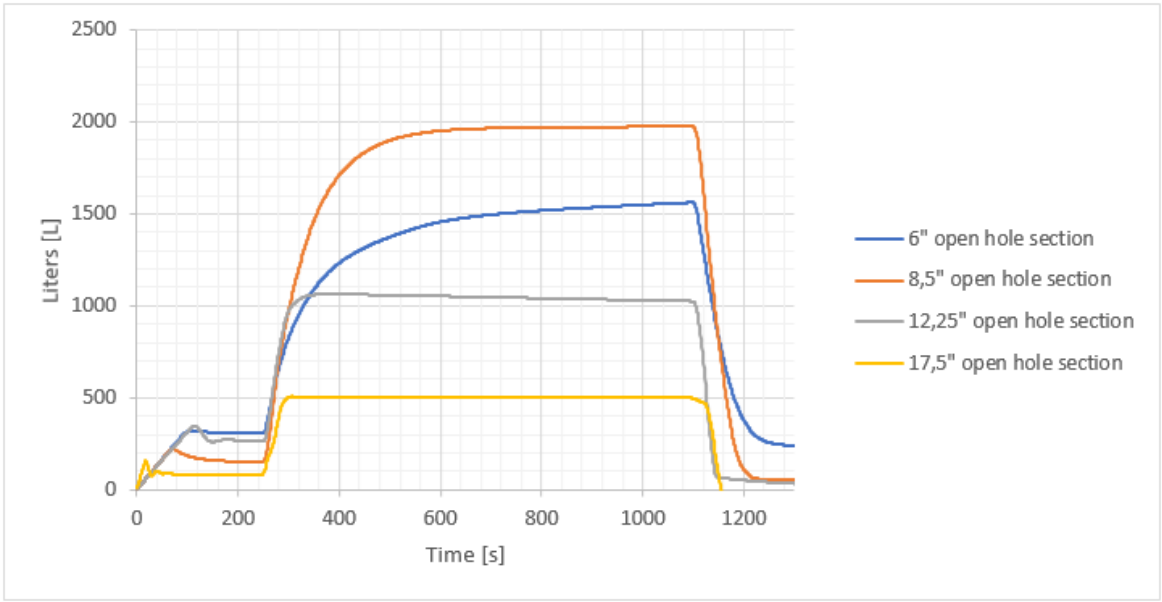

Fig. 4.15 Compressibility effect when drilling different hole sections

In figure 4.15 the compressibility effect increases with reducing open hole sections except for the 6" open hole section. It is intuitive that the compressibility effect should have increased when adding another section to the well, but due to the large reduction in q_{in} when drilling the 6" section the compressibility effect was overwhelmed.

The 6" open hole section is only 300 meters and the pump rate is reduced from 2000 lpm to 850 lpm when drilling it. The increase of compressibility effect from reducing the open hole was overpowered by the reduction in compressibility because of the reduction in flow-rate in.

However, the compressibility effects are not only influenced by the larger volume of mud inside the well. The pressure drop inside the well increases with decreasing well diameter. This is transparent in equation 3.4. The increase in pressure, increases the effect of compressibility.

Note that the time until flow-rate out is equal to flow-rate in ($q_{out} = q_{in}$) for the 6" section is longer than for the 8.5" section. This is illustrated clearly in figure 4.16 where at pump start the transient time period increases when the hole sections diameters are reduced. No consistent trend can be identified from the pump stops scenarios.

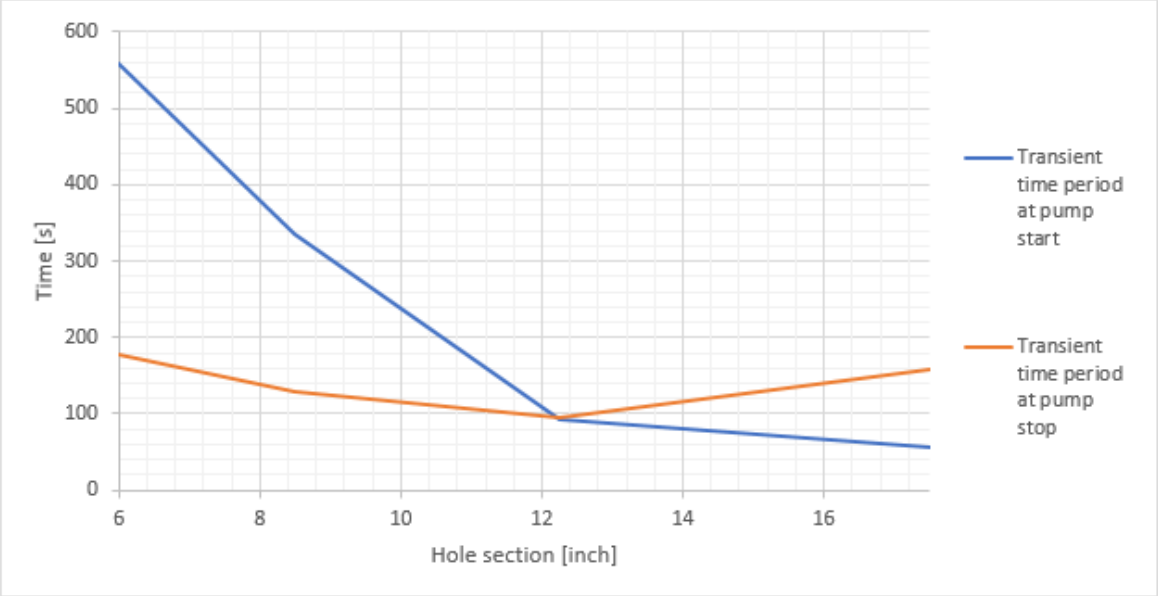

Fig. 4.16 Transient time period as a function of the diameter the open hole section

4.2.7 Gel Strength Variation

At pump start the normal routine is to start pumping with a low flow-rate to break the gel structure that has been formed during pump stop. When breaking the gel structure the compressibility effect is affected by the gel strength inside the well as seen in figure 4.17

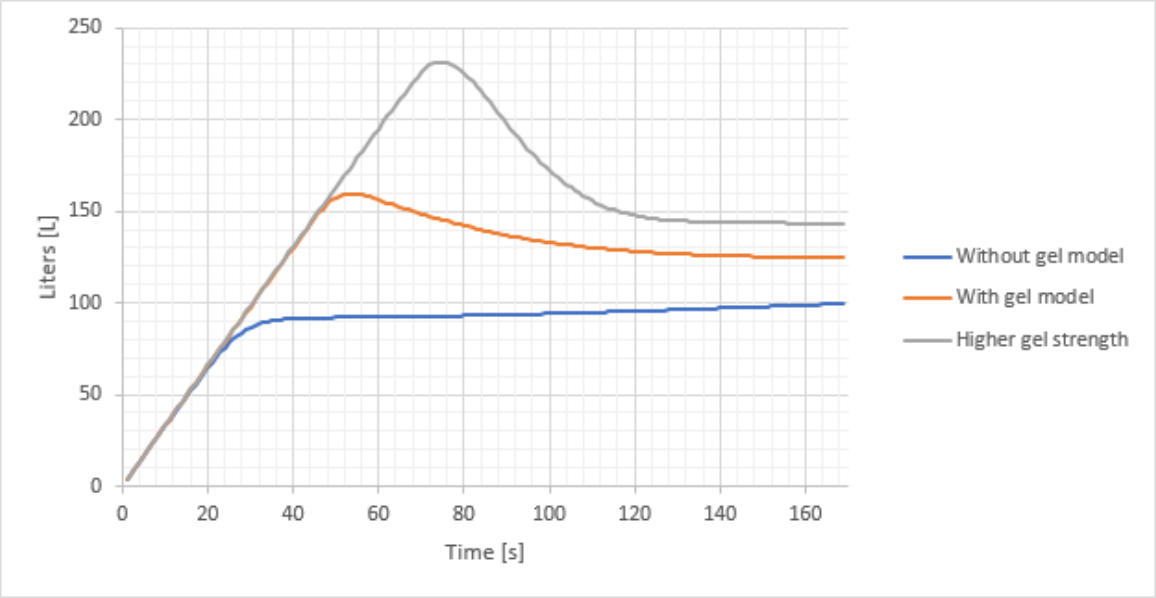

Fig. 4.17 Compressibility effect from gel strength variation

The simulation carried out without gel model, is equivalent to a mud without gel strength. The compressibility effect increases when the gel strength increases. As seen in the figure The compressibility effect has a early peak, when changing the gel strength. This is the nature of gel strength as it has a high initial resistance against flow when it is stationary, as time increases the difference is diminished.

Chapter 5

The Experimental Flow Loop

This chapter will explain the flow loop used for the experimental part of the thesis. Firstly, the flow loop will be introduced and calculations on the pressure drop in the system will be calculated in order to estimate range of flow-rates the "new flow sensor" can be tested for.

The estimated maximum flow-rates is then compared to measured values, which are acquired experimentally.

5.1 Test Equipment

In this section the testing facility is introduced, and the components it consists of is explained. An illustration of the flow loop is given in figure 5.1. Note that various pressure drop that are considered later is also illustrated in figure 5.1; namely $\Delta P_1, \Delta P_2$ and ΔP_3. The various components in the system is described in table 5.1.

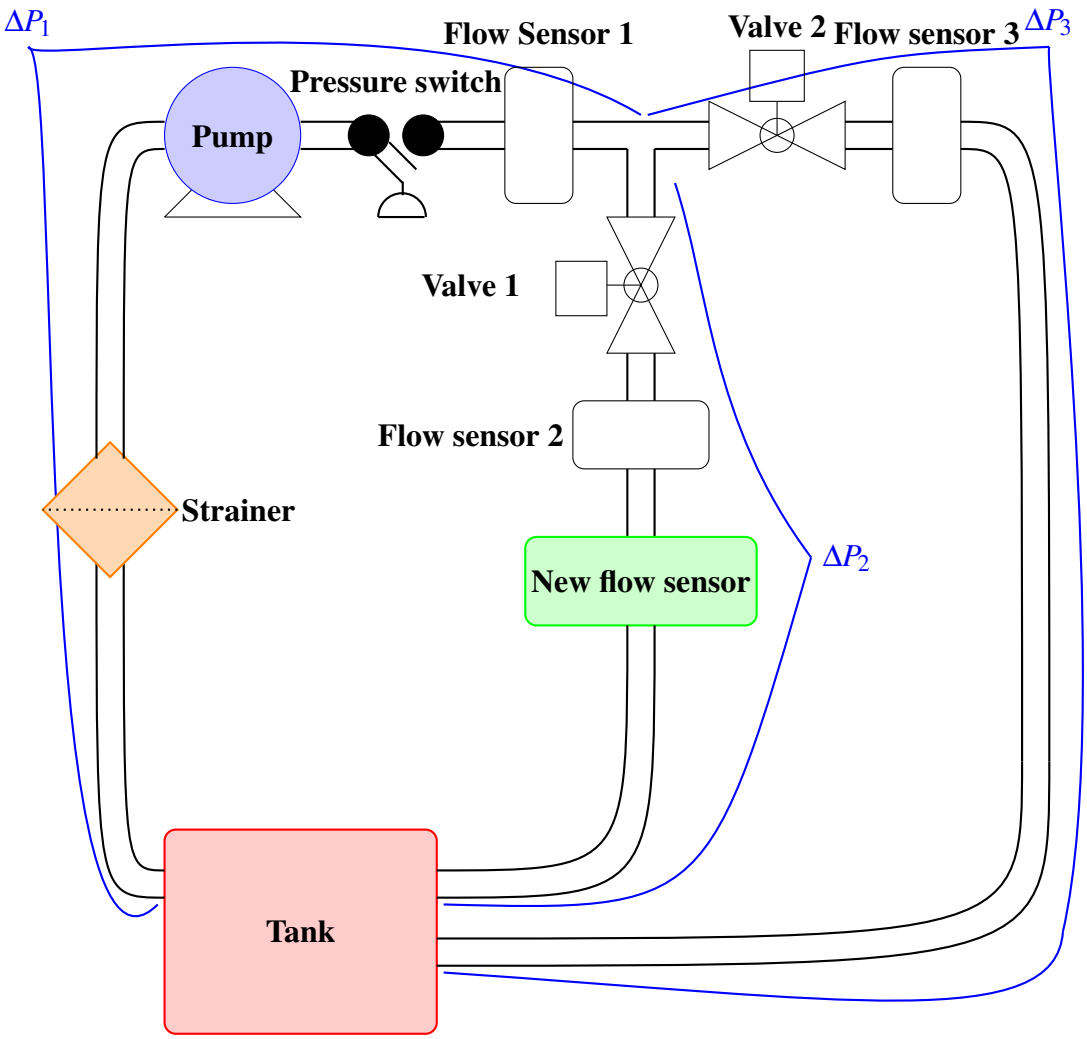

Fig. 5.1 The flow sensor setup

The circulation system is pictured in figure 5.2 with a top view of the flow loop and a side view of the circulation system.

5.1.1 Pump

The pump used has a capacity of ∼29 lpm (2m pressure height) and can provide up to 1.0 bar pressure. The flow-rate from the pump is a function of the pressure loss in the circulation loop (ΔP):

$$Q = f(\Delta P) \tag{5.1}$$

Table 5.1 Flow loop components with description

Flow loop component	Description
Tank	The tank is where the circulated fluid is kept when not circulating.
Strainer	A pump inlet strainer with a 40 mesh (fine) stainless steel filter screen is used to prevent unnecessary pump breakdowns, caused by particles in the fluid.
Pump	The pump is used to circulate the fluid.
Pressure switch	A pressure switch is installed to stop the pump during a pressure build-up, to prevent harm to the equipment.
Flow sensor	Flow sensors are used to measure and control the volumetric flow in the system.
Valve	Valves are used to control the volumetric flow in the system.
New flow sensor	The "new flow sensor" is the flow sensor that will be tested.

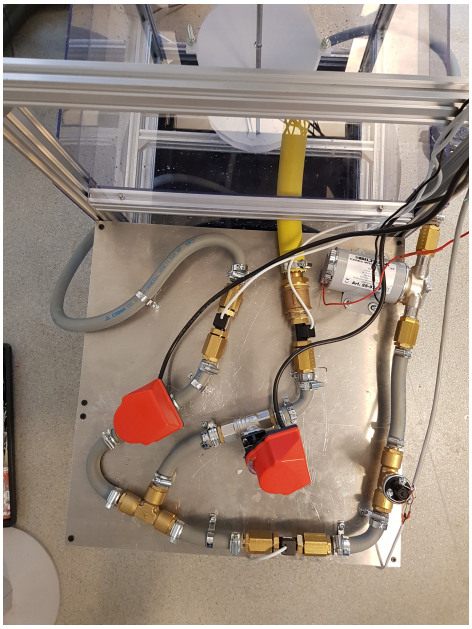

(a) Top view of flow loop

(b) Side view of the circulation system

Fig. 5.2 Different views of the circulation system

The pump used in the flow loop was provided with a flow diagram, as shown in figure 5.3. The flow diagram shows the relationship between Q [lpm] and ΔP[bar]. A polynomial trendline for the curve in the flow diagram, with $R^2 = 1$, is equation 5.2:

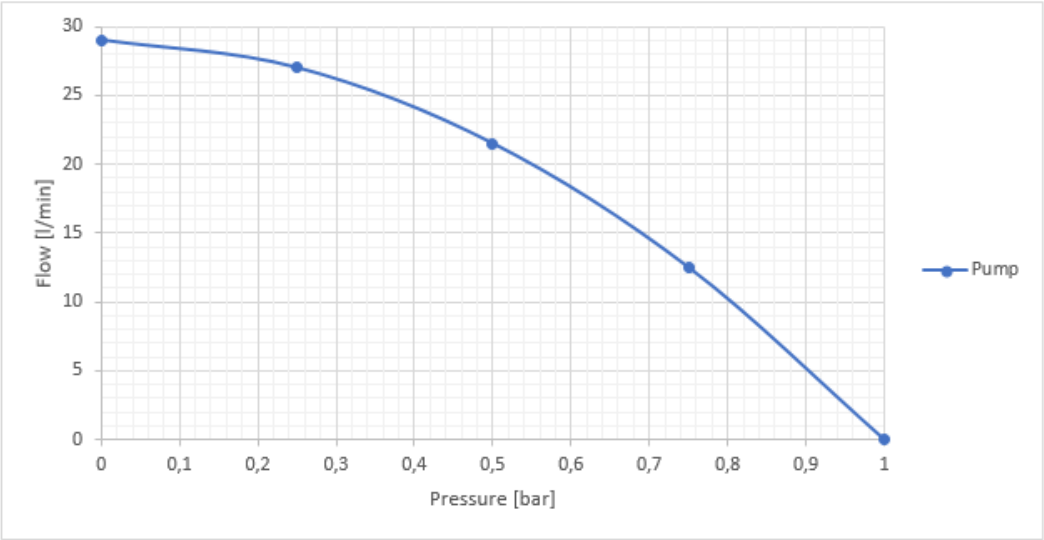

Fig. 5.3 flow diagram for pump

$$Q = -28(\Delta P_{tot})^2 - 1(\Delta P_{tot}) + 29 \tag{5.2}$$

The pressure drop, ΔP, in the flow loop has to be determined to calculate the flow-rates that can be expected in the system.

5.1.2 Flow Sensors

The new flow sensor has to be compared to already working flow sensor to determine how effective and precise it is. Flow sensor 1, 2 and 3 is individually capable of measuring flow-rates between 0.13 GPM to 7.9 GPM (0.5 lpm -30 lpm). When valve 1 and 2 is open the flow sensors will provide the computer with 3 measured values. Going forward in the thesis, the measurements from the different flow sensors will be named:

- Measurement from flow sensor 1: Q_{tot}
- Measurement from flow sensor 2: Q_1
- Measurement from flow sensor 3: Q_2

The flow loop setup illustrated in figure 5.1 indicates that the relationship between the flow sensor measurements is:

$$Q_{tot} = Q_1 + Q_2 \tag{5.3}$$

The objective of this specific setup is to be able to measure flow-rates from 0 to the maximum flow-rate. The individual flow sensors can only measure flow-rates as low as 0.5 lpm, but by having the sensors installed in this way it is possible to estimate very low flow-rates. To estimate very low flow-rates, equation 5.3 is used in combination with the measurements from the 3 flow sensors. E.g. if Q_{tot} is measured to be 25 lpm, Q_1 is too low to measure and Q_2 is measured to be 24.7 lpm. Q_1 is calculated by using equation 5.3 to be 0.3 lpm.

The flow sensors was delivered with a flow diagram which illustrates how the pressure drop across it varies as a function of flow-rate as seen in figure 5.4.

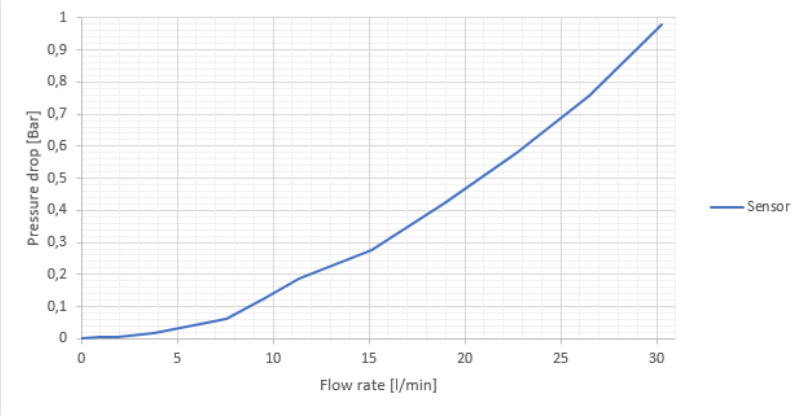

Fig. 5.4 flow diagram for sensor

Polynomial trendline for the curve, with $R^2 = 0.99$, is shown in equation 5.4:

$$\Delta P_{Sensor} = 9.34 \cdot 10^{-4} Q^2 + 4.12 \cdot 10^{-3} Q \tag{5.4}$$

where ΔP [bar] is the pressure drop and Q [lpm] is the flow-rate across the sensor.

5.2 Valves

Valves are used to regulate the flow to the new flow sensor. The valves regulate the pressure drop and the flow-rate across the valves by adjusting the cross-sectional area.

A flow diagram showing the relationship between pressure drop and flow-rate across a fully open valve is shown in figure 5.5, and a polynomial trendline for the curve, with $R^2 = 0.99$, is given in equation 5.5:

$$\Delta P_{Valve} = 1.46 \cdot 10^{-5} Q^2 - 5.66 \cdot 10^{-5} Q \tag{5.5}$$

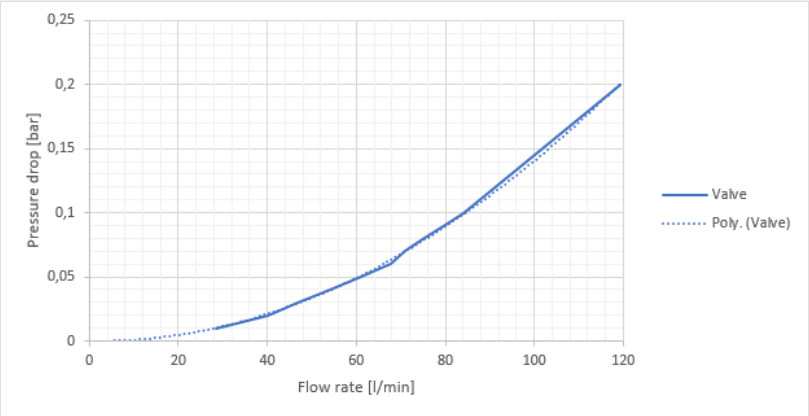

Fig. 5.5 flow diagram for fully open valve

where ΔP [bar] is the pressure drop across the valve when it is fully open and Q [lpm] is the flow-rate across the valve when it is fully open.

5.3 Pressure Drop in the Flow Loop

The pressure drop and its corresponding flow-rates are estimated for 3 scenarios:

1. Valve 1 open and valve 2 closed
2. Valve 1 closed and valve 2 open
3. Valve 1 open and valve 2 open

Firstly, general information concerning the flow loop is considered as well as defining various pressure drop terms to describe the system.

5.3.1 General Information

To estimate the flow-rate for the three scenarios, the pressure drop in the scenarios must be calculated. The total pressure drop consists of pressure drops from several different components. These components are explained in table 5.2.

The total pressure drop in the flow loop is given in equation 5.6. Note that ΔP_1, ΔP_2 and ΔP_3 is defined in figure 5.1 and they are first analyzed separately.

$$\Delta P_{tot} = \Delta P_1 + \Delta P_2 + \Delta P_3 \tag{5.6}$$

Table 5.2 Pressure drop terms with description

Pressure drop term	Description
$\Delta P_{Flow\ lines}$	Pressure drop in the rubber hoses that the drilling fluid is circulated through.
ΔP_{Steel}	Indicates the pressure drop through all the installed components that are made of metal. Metal has a different surface roughness than rubber. Metal components are: pump, pressure switch, T-intersection and valves.
ΔP_{Bends}	Signifies the pressure drop in all the turns and bends in the flow loop.
ΔP_{Valve}	Accounts for the pressure drop across the valves.
$\Delta P_{Flow\ sensor}$	Expresses the pressure drop across the flow sensor.
$\Delta P_{Height\ difference}$	Pressure loss due to height difference between the tank and the pump.

ΔP_1 is equal to the pressure drop from the tank to the T-intersection:

$$\Delta P_1 = \Delta P_{Flow\ lines} + \Delta P_{Steel} + \Delta P_{Flow\ Sensor1} + \Delta P_{Bends} + \Delta P_{Height\ difference} \tag{5.7}$$

ΔP_2 is the pressure drop from the T-intersection to the "New flow sensor":

$$\Delta P_2 = \Delta P_{Flow\ lines} + \Delta P_{Steel} + \Delta P_{Valve1} + \Delta P_{Flow\ Sensor2} + \Delta P_{Bends} \tag{5.8}$$

The final pressure drop, ΔP_3, is the pressure drop from the T-intersection and back to the tank:

$$\Delta P_3 = \Delta P_{Flow\ lines} + \Delta P_{Steel} + \Delta P_{Valve2} + \Delta P_{Flow\ Sensor3} + \Delta P_{Bends} + \Delta P_{Height\ difference} \tag{5.9}$$

General information concerning the flow loop is given in table 5.3. Water is selected as circulation fluid and surface rougnesses are selected from table 3.1.

5.3.2 Estimating Pressure Drop 1, 2 and 3

Firstly, the pressure drops ΔP_1, ΔP_2 and ΔP_3 are analyzed separately. The pressure drop in flow lines, $\Delta P_{Flow\ lines}$ and ΔP_{Steel}, are calculated with equation 3.4 and the pressure drop in flow lines with bends are given by equation 3.12:

Table 5.3 General information concerning the flow loop

Flow loop	Values
Fluid density	1000 kg/m^3
Viscosity	1.0016 at 20 °C
Flow line diameter	0.0127 m
Surface roughness [rubber]	0.07 mm
Surface roughness [steel]	0.05 mm

Note that the first term in equation 3.12, $\frac{1}{2} f_s \rho u^2 \frac{\pi R_b}{D} \frac{\theta}{180^\circ}$, is equivalent to the pressure drop in a straight line given by equation 3.4. The second term, $\frac{1}{2} k_b \rho u^2$, is the pressure drop due to bending. Therefore the first term is included in $\Delta P_{Flow\ lines}$ in order to isolate the pressure loss caused by the bends. The second term is the ΔP_{Bends} where k_b is estimated from figure 3.11

Furthermore, the pressure drop across the flow sensors, $\Delta P_{Flow\ sensor}$, are given by equation 5.4. pressure drop across the valve, ΔP_{Valve}, when fully open is given by equation 5.5. The estimated pressure drop from bends (ΔP_{Bends}) is estimated for bends varying from 40° - 150°

5.3.2.1 Pressure Drop: ΔP_1

Required information to determine the pressure drop, ΔP_1, is listed in table 5.4:

Table 5.4 Information concerning ΔP_1

Parameters concerning ΔP_1	Values
Flow line length	1.835 m
Steel length	0.315 m
Height difference	0.88 m

The pressure drop, ΔP_1, is shown as a function of flow-rate in figure 5.6. Polynomial trendline for the curve gives equation 5.10.

$$\Delta P_1 = 1.42 \cdot 10^{-3} Q_{tot}^2 + 4.71 \cdot 10^{-3} Q_{tot} + 8.63 \cdot 10^{-2} \tag{5.10}$$

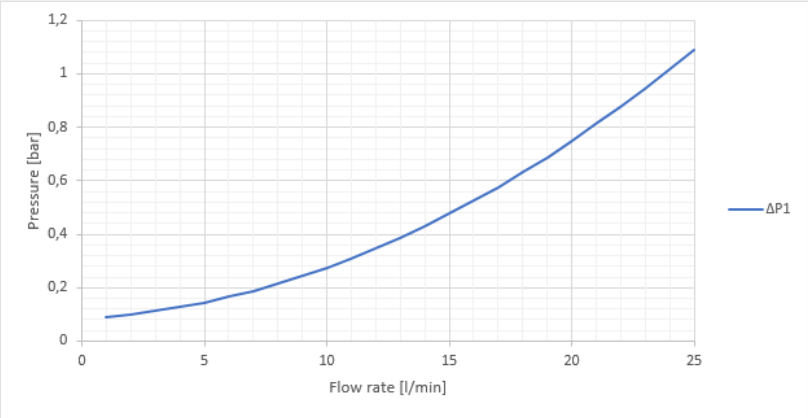

Fig. 5.6 ΔP_1 as a function of flow-rate

Further analysis of the pressure drop is investigated in figure 5.7. The figure shows how the percentage contributions from the various terms changes with increasing flow-rate.

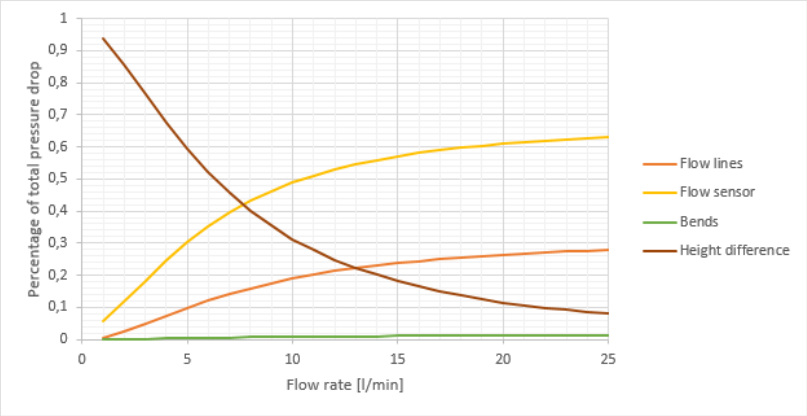

Fig. 5.7 Percentage contribution to ΔP_1 from various terms

At low flow-rates the height difference contributes to most of the pressure difference, but as flow-rate increases the pressure drop from the flow sensor and flow lines becomes larger than the height difference. This is expected as the pressure difference due to variation of height is constant. The flow sensor becomes the largest pressure drop when $Q \approx 7.7$ lpm. Note that the pressure drop from bends is very low relative to the other pressure drops.

5.3.2.2 Pressure Drop: ΔP_2

Additional information concerning ΔP_2 is found in table 5.5.

Table 5.5 Information concerning ΔP_1

Parameters concerning ΔP_2	Values
Flow line length, d=0.0127 m	0.18 m
Flow line length, d=0.025 m	0.25 m

The pressure drop, ΔP_2, is shown as a function of flow-rate in figure 5.8.

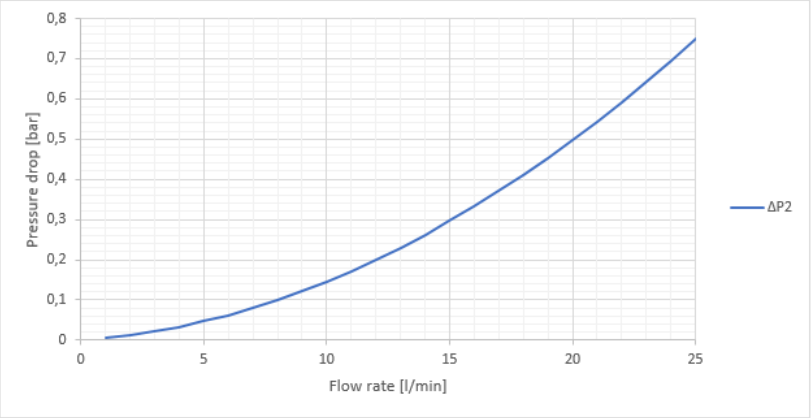

Fig. 5.8 ΔP_2 as a function of flow-rate

A polynomial trendline for the curve is given equation 5.11

$$\Delta P_2 = 1.03 \cdot 10^{-3} Q_1^2 + 4.19 \cdot 10^{-3} Q_1 \tag{5.11}$$

The percentage contributions to ΔP_2 is analyzed and shown in figure 5.9. For ΔP_2 the flow lines have short lengths and the flow line consists of a section with a larger diameter. Thus the pressure drop from flow lines are relatively low. The majority of the pressure drop is from the flow sensor.

5.3.2.3 Pressure Drop: ΔP_3

Information needed for ΔP_3 calculations are found in table 5.6:

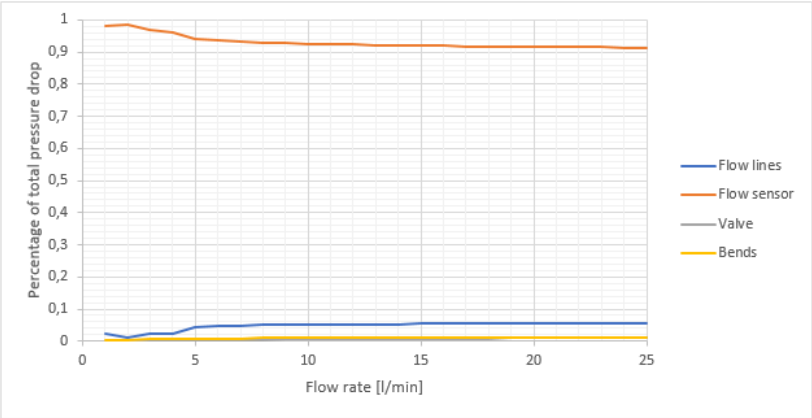

Fig. 5.9 ΔP_2 contribution from the various terms

Table 5.6 Information concerning ΔP_3

Parameters concerning ΔP_3	Values
Flow line length, d=0.0127 m	0.18 m
Height difference	0.88 m

The pressure drop, ΔP_3, is shown as a function of flow-rate in figure 5.10.

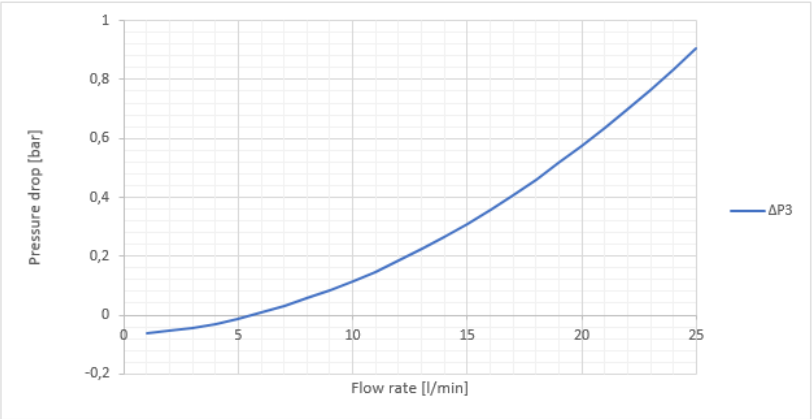

Fig. 5.10 ΔP_3 as a function of flow-rate

Polynomial trendline for the curves gives equation 5.12.

$$\Delta P_3 = 1.38 \cdot 10^{-3} Q_2^2 + 4.55 \cdot 10^{-3} Q_2 - 8.63 \cdot 10^{-2} \tag{5.12}$$

The pressure difference contributions from the various terms are shown in figure 5.11. Notice that the flow sensor and flow lines contributes to the majority of the pressure loss.

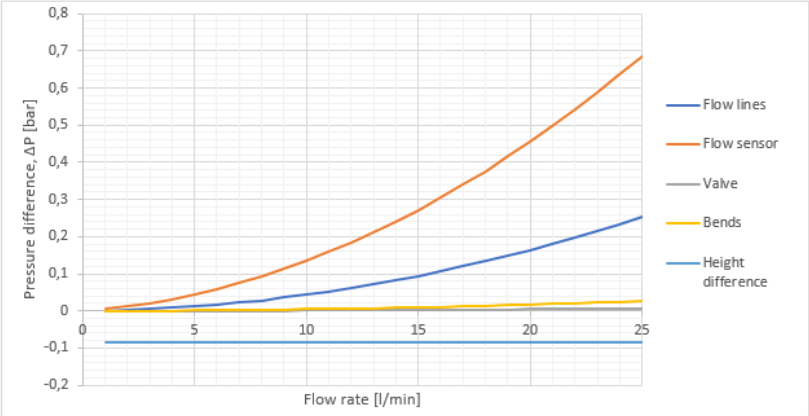

Fig. 5.11 ΔP_3 contribution from the various terms

5.4 Estimating the Flow-Rates for Different Scenarios

5.4.1 Valve 1 open and valve 2 closed

When valve 1 is open and valve 2 is closed we get the maximum flow-rate directed to the "New flow sensor". During this scenario $Q_1 = Q_{tot}$. Note that when valve 2 is closed the pressure drop, ΔP_3, is equal to zero. The total pressure drop in the system is then diminished to:

$$\Delta P_{tot} = \Delta P_1 + \Delta P_2 \tag{5.13}$$

Putting in for ΔP_1 and ΔP_2 gives:

$$\Delta P_1 + \Delta P_2 = 2.45 \cdot 10^{-3} Q_{tot}^2 + 8.9 \cdot 10^{-3} Q_{tot} + 8.63 \cdot 10^{-2} \tag{5.14}$$

Equation 5.14 is plotted with equation 5.2 in figure 5.12. The estimated maximum flow-rate to the "new flow sensor" is determined graphically: $Q_{max} \approx 14.1$ lpm.

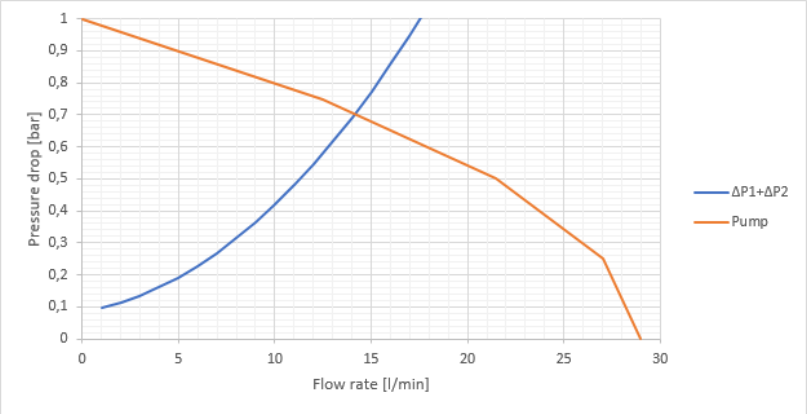

Fig. 5.12 Maximum flow-rate to the "New flow sensor"

5.4.2 Valve 1 closed and valve 2 open

The pressure drop, ΔP_2, is zero when valve 1 is closed and valve 2 is open. The maximum flow-rate through the diverter line is estimated in this case, and $Q_2 = Q_{tot}$. The total pressure drop in the system is diminished to:

$$\Delta P_{tot} = \Delta P_1 + \Delta P_3 \tag{5.15}$$

Inserting for ΔP_1 and ΔP_3 results in equation 5.16.

$$\Delta P_1 + \Delta P_3 = 2.80 \cdot 10^{-3} Q_{tot}^2 + 9.26 \cdot 10^{-2} Q_{tot} \tag{5.16}$$

A graphical comparison between equation 5.2 and equation 5.16 gives figure 5.13. The estimated maximum flow-rate through the diverter line is determined graphically: $Q_{max} \approx$ 14.15 lpm.

5.4.3 Valve 1 fully open and valve 2 fully open

When both valves are open the flow will split into two flow lines. The challenge with this scenario is that $Q_{tot} \neq Q_1 \neq Q_2$. To estimate the three flow-rates a relationship between Q_1 and Q_2 needs to be derived.

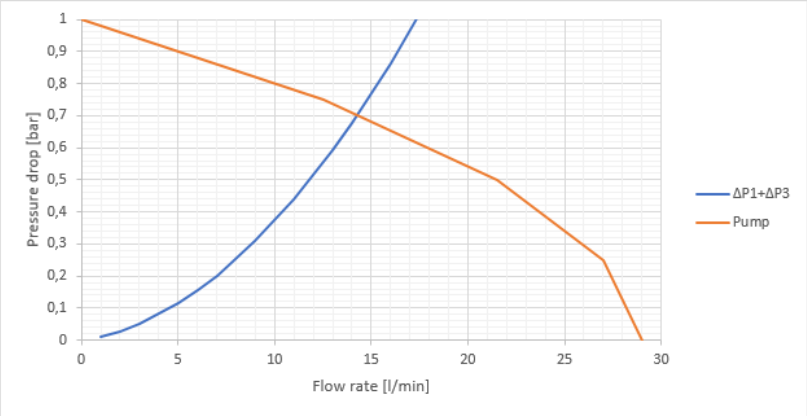

Fig. 5.13 Maximum flow-rate in the diverter line

Fluid will flow in the path of least resistance, and thus ΔP_2 must be equal to ΔP_3.

$$\Delta P_2 = \Delta P_3 \tag{5.17}$$

$$\Delta P_2 - \Delta P_3 = 0 \tag{5.18}$$

By plotting equation 5.18 for various values of Q_1 and Q_2 figure 5.14 is aquired:

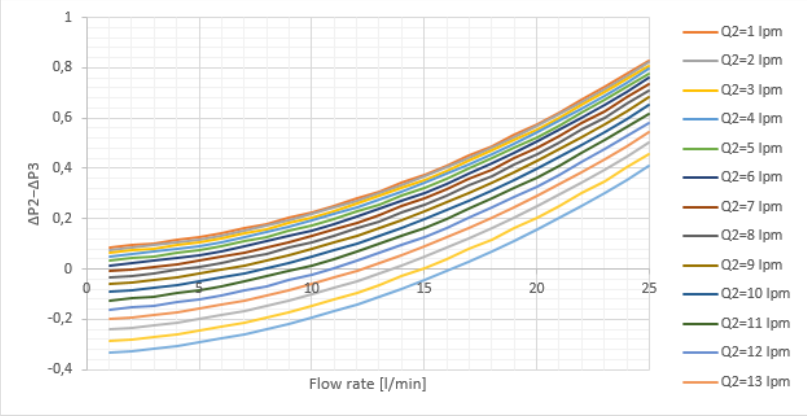

Fig. 5.14 Maximum flow-rate in the diverter line

From plotting the values for Q_2 and Q_1 when $\Delta P_2 - \Delta P_3 = 0$ a relationship between Q_1 and Q_2 can be derived, the relationship is plotted in figure 5.15. Polynomial trendline result in a relationship as shown in equation 5.19.

$$Q_1 = -4.31 \cdot 10^{-2} Q_2^2 + 2.44 Q_2 - 11.4, \quad Q_2 \in [7, 16] \tag{5.19}$$

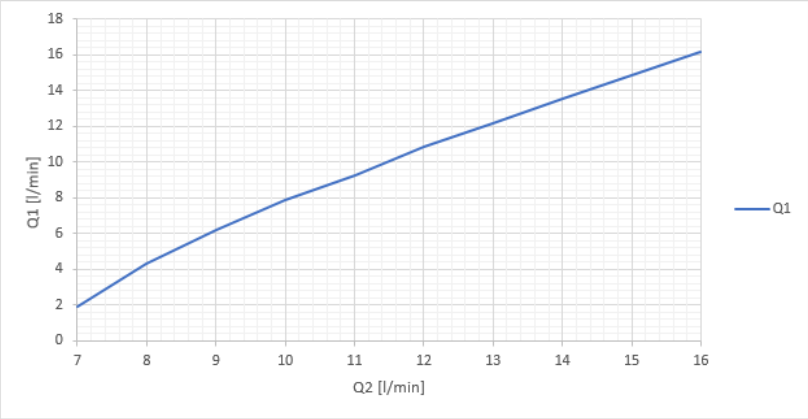

Fig. 5.15 Relationship between Q_1 and Q_2 when $\Delta P_2 - \Delta P_3 = 0$, $Q_2 \in [7 \text{ lpm}, 16 \text{ lpm}]$

Expression for Q_{tot} is calculated from equation 5.3:

$$Q_{tot} = -4.31 \cdot 10^{-2} Q_2^2 + 3.44 Q_2 - 11.4, \quad Q_2 \in [7, 16] \tag{5.20}$$

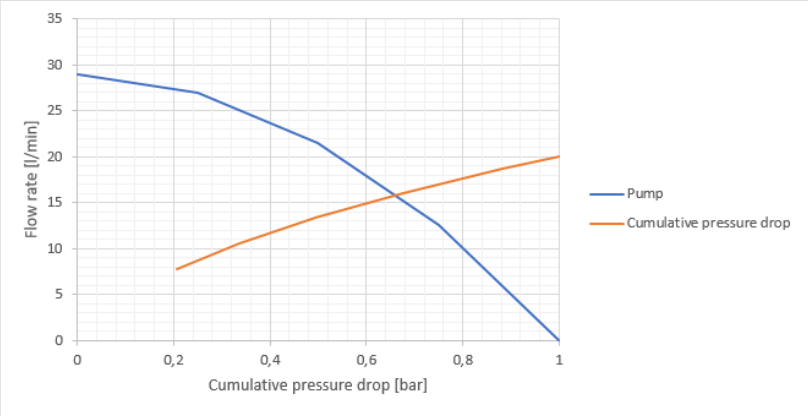

Fig. 5.16 Cumulative pressure drop vs pump flow diagram

The intersection in figure 5.16 between equation 5.2 and equation 5.20 shows a $Q_{tot} \approx 15.8$ lpm, which equals to:

$$Q_1 = 6.9 \text{ lpm} \tag{5.21}$$

$$Q_2 = 8.9 \text{ lpm} \tag{5.22}$$

5.5 Estimated Flow-Rates Versus Experimental flow-Rates

In this section the estimated flow-rates is compared to the experimentally tested flow-rates. The estimated flow-rates would develop as shown as in figure 5.17:

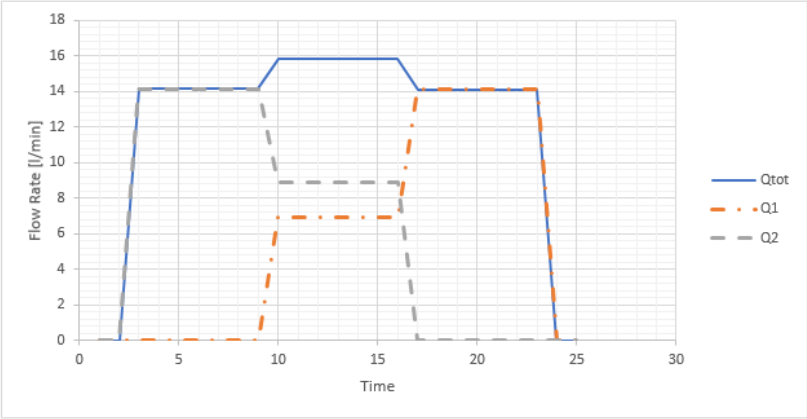

Fig. 5.17 Estimated flow-rates developed

The results from the measured values is shown in figure 5.18.

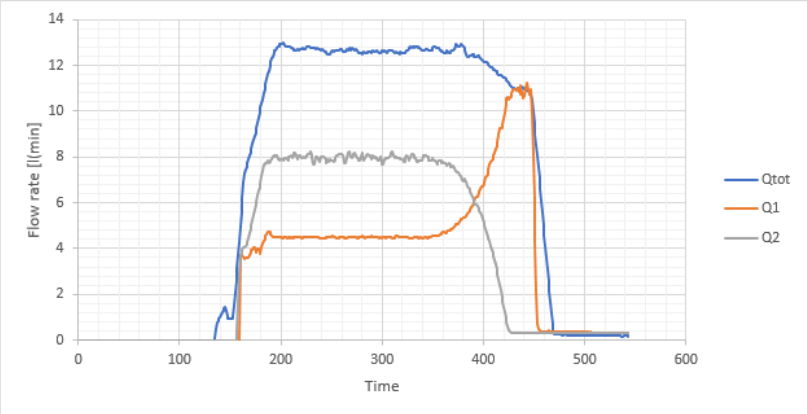

Fig. 5.18 Experimentally flow-rates developed

By analyzing the two graphs it is clear that the estimated flow-rates were over estimated. This can have been caused by inaccuracies in the pressure drop calculations or by uncertainties with the equipment not working as stated in the equipment data.

The first option is that the estimated pressure drop is too low. During the analysis of the pressure drop it was clear that the bends created a very low pressure drop. From visual inspection of the flow loop there are certain bends that are at such an high angle with low bend radius that the cross sectional area to the hoses is reduced. The equation used to calculate

the pressure drop in bends, does not take this into account. This would result in a under estimated pressure loss from bends.

The second option is that there are uncertainties related to the equipment data to the pump, flow sensors and the valves. This could mean that the pump delivers a smaller pressure than stated in the flow diagram or that the flow-rate sensors/valves creates a larger pressure drop than the data sheets suggests. This would result in a over estimated flow-rates.

5.6 Controller

A PI-controller is used to operate the electrical valves to either increase, or decrease the flow-rate to achieve the desired flow-rate to the "new flow sensor". The controller makes sure that one valve is always fully open, this is done to prevent pressure build-ups.

5.6.1 PI-Controller

Using the general equation for PI-controller

$$u(t) = K_p e(t) + K_i \int_0^t e(\tau) d\tau \tag{5.23}$$

To transform the PID-controller to a discrete version the following procedure is done. First, take the derivative on both sides of equation 5.23:

$$\frac{du(t)}{dt} = K_p \frac{de(t)}{dt} + K_i e(t)$$

Using Euler's method to define:

$$\frac{du(t)}{dt} = \frac{u(t) - u(t-1)}{\Delta t}$$

$$\frac{de(t)}{dt} = \frac{e(t) - e(t-1)}{\Delta t}$$

Inserting terms from Euler's method into equation 5.23:

$$\frac{u(t)-u(t-1)}{\Delta t} = K_p \frac{e(t)-e(t-1)}{\Delta t} + K_i e(t)$$

Discrete version can be derived:

$$u(t) = u(t-1) + K_p\left[e(t)-e(t-1)\right] + K_i \Delta t e(t) \tag{5.24}$$

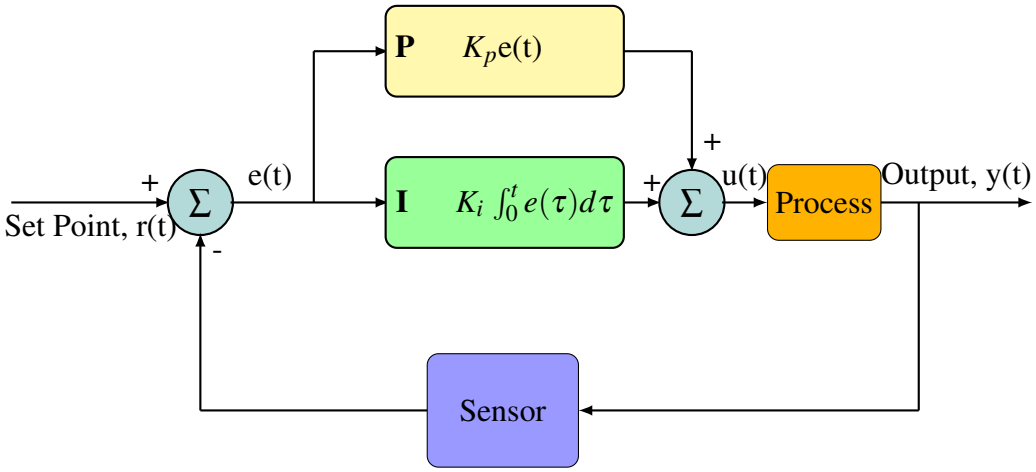

Fig. 5.19 PI-Controller Flow Diagram

Figure 5.19 is used to explain equation 5.24. The sensor is measuring the flow-rate y(t) and feeding the information to the controller. The controller calculates an error e (e = r(t)-y(t)), where y(t) is the desired flow-rate put into the controller. The controller gives an output u(t) to the valve telling it either to increase or decrease the valve opening.

Unfortunately, the originally planned PI-controller was proven to be insufficient during testing of the valves. The electrical controllers for the valve did not work as intended, so an modified controller had to be developed.

5.6.2 Modified Controller

The electrical valves that is used for controlling the flow-rate had schematics showing that the valves would open/close by two different signal wires. During testing this seen to not be the case. The valves opened/closed randomly when they received a signal, but unless the signal was broken the valves would open until it was fully open, or close until it was fully closed. Unfortunately, this rendered the PI-controller insufficient to control the flow.

Instead, a new controller was developed to control the flow. It was programmed in such a way that it will start with valve 1 closed and valve 2 open. This way the initial conditions are $Q_1 = 0$ and all the flow will go through the diverter line. Then valves 1 will open until both valves are fully open and then valve 2 will begin to close to maximize the flow-rate towards the "new flow sensor". During this procedure, if the desired flow-rate is met at any point the controller will stop controlling the valves. By following this procedure one valve is always fully open.

5.7 Electrical Schematics

Electrical schematics is found in appendix A. This includes a electrical schematic to the flow-rate controller and one electrical schematic to the spinning wheel controller.

Chapter 6

New Flow Meter: Measuring Principle

This chapter is divided into the two following sections:

- Introducing the new flow sensor and explaining its various components, as well as their purpose.
- The measuring principle of the new flow sensor.

6.1 The New Flow Sensor

The new flow sensor consists of three critical components:

- Spinning wheel
- Servo motor
- Load cells

In this section they are introduced separately and their relationship to each other is explained.

6.1.1 Spinning Wheel

The spinning wheel is the main component of the new flow sensor. The spinning wheel is visualized in figure 6.1 with a top view and side view.

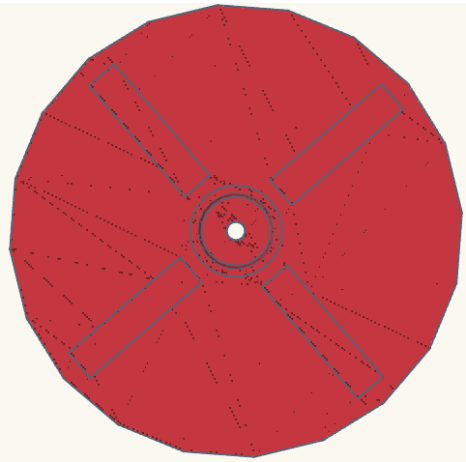

(a) Top view of the spinning wheel

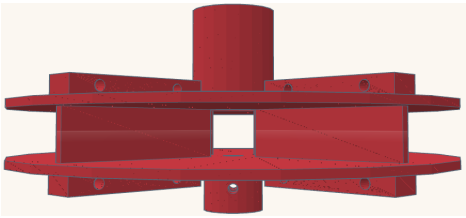

(b) Side view of the spinning wheel

Fig. 6.1 Different views of spinning wheel

The spinning wheel is designed in tinkercad and is 3-D printed. 3-D printing allows for customization and control of the proportions. The tested prototype has a diameter of 19 cm.

As seen in figure 6.1 the spinning wheel is essentially two spherical plates with four walls between them. The upper plate, lower plate and the walls are printed separately, and the pieces are connected with bolts. This way, the walls may be exchanged by walls of various heights, and if there is damage to one component it can be reprinted quickly.

6.1.2 Servo Motor

The servo motor is a rotary actuator that allows for precise control of angular position, velocity and acceleration. The motor is used to rotate the spinning wheel. The spinning wheel is connected to the motor by a steel rod as seen in figure 6.2.

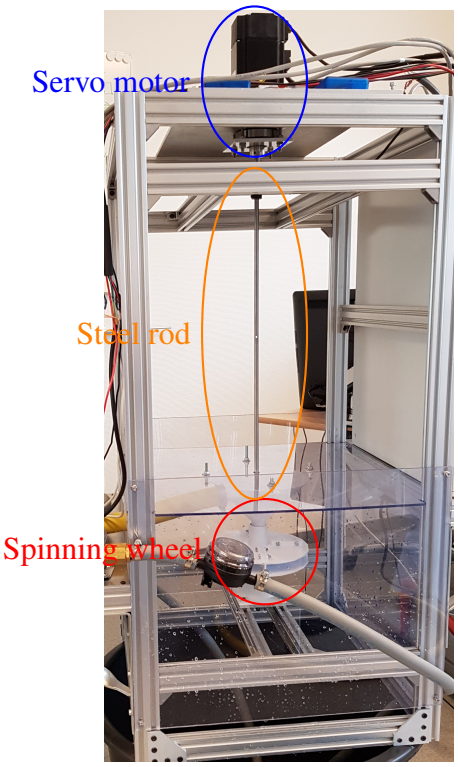

Fig. 6.2 Side view of test setup

6.1.3 Load Cells

The servo motor that is rotating the spinning wheel is mounted on the flow loop in such a way that it will rotate slightly when the motor experiences a torque. The load cells are placed in a position that will measure this torque, as shown in figure 6.3.

The measured torque will be equal to

$$\tau = Fr \tag{6.1}$$

Where F [N] is the force illustrated in figure 6.3 and r [m] is the distance the force is measured from the rotational axis. As seen in the figure there are two load cells. Two load cells are used to verify the measurements as well as increase the precision of the measurements.

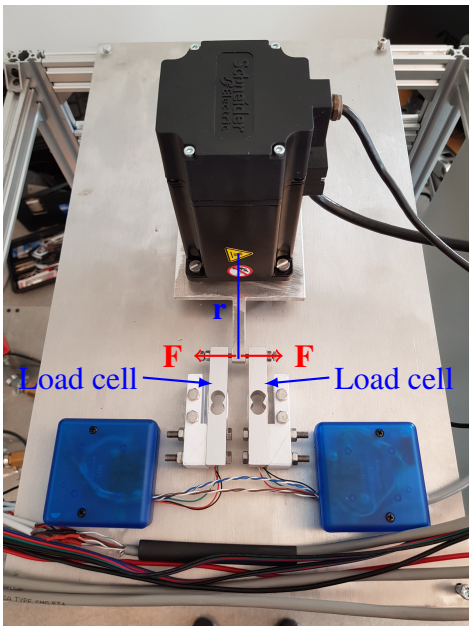

Fig. 6.3 Load cells

6.2 Measuring Principle

The method to determine flow-rate is divided into two parts. The first part explains how the mass flow-rate is derived, and the second part describes how the density is estimated.

6.2.1 Mass Flow-Fate

Firstly, the generated Coriolis force that is measured is introduced. This section will explain how the Coriolis force is generated and how it is measured.

To explain the generation of the Coriolis force, a cross section of the spinning wheel is analyzed. This is needed to see how the circulated fluid affect the spinning wheel. The analyzed cross sectional area is illustrated in figure 6.4.

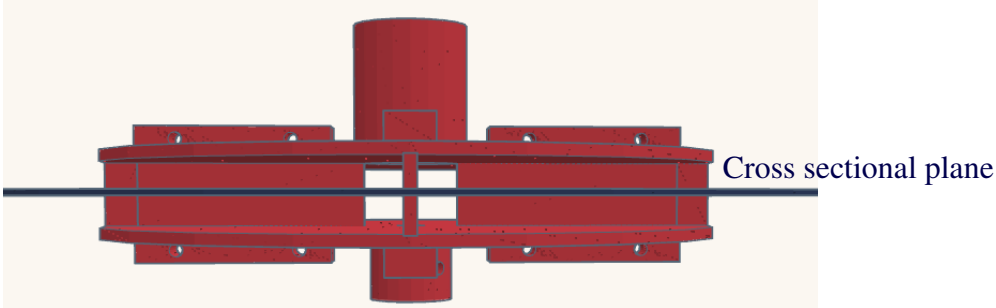

Fig. 6.4 Cross sectional plane on the spinning wheel

The cross sectional area is seen from above in figure 6.5.

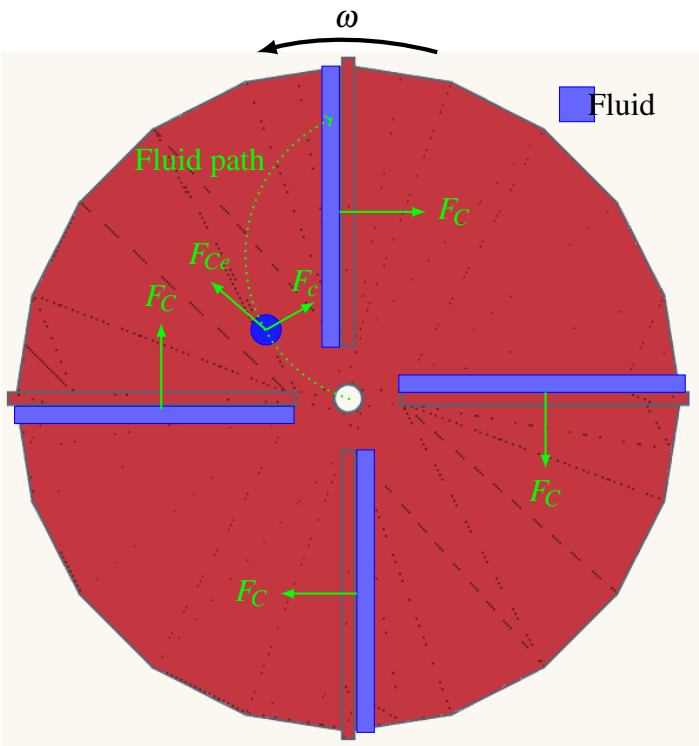

Fig. 6.5 Spinning wheel cross section seen from above

In this figure the fluid's behaviour is illustrated, when the spinning wheel is rotating at a speed ω. When the spinning wheel is rotating the fluid will be pushed outwards by a centrifugal force (F_{Ce}) and to the side by a Coriolis force (F_C). When the fluid hits the wall, the fluid will impose a Coriolis force (F_c) on the spinning wheel, which will increase the torque on the motor.

The hypothesis for the measurements, is that the additional torque will be proportional to mass flow-rate, as expressed in equation 6.2:

$$\tau \propto \dot{m} \tag{6.2}$$

6.2.2 Density Estimation

To estimate the density of the fluid that is being circulated through the flow sensor, a different aspect of controller must be discussed.

The controller that controls the RPM is able to vary the rotation of the spinning wheel in step changes as shown by the blue line in figure 6.6. The torque will increase when the RPM increases, and decrease when the RPM decreases. Furthermore, the torque will oscillate when the RPM is increased or decreased, as shown in figure 6.6. The second part of the hypothesis is that the oscillations will have a time period, T, that will be proportional to the moment of inertia to the circulated fluid:

$$\rho \propto I \tag{6.3}$$

The relationship between density and the measured torque needs to be investigated and established.

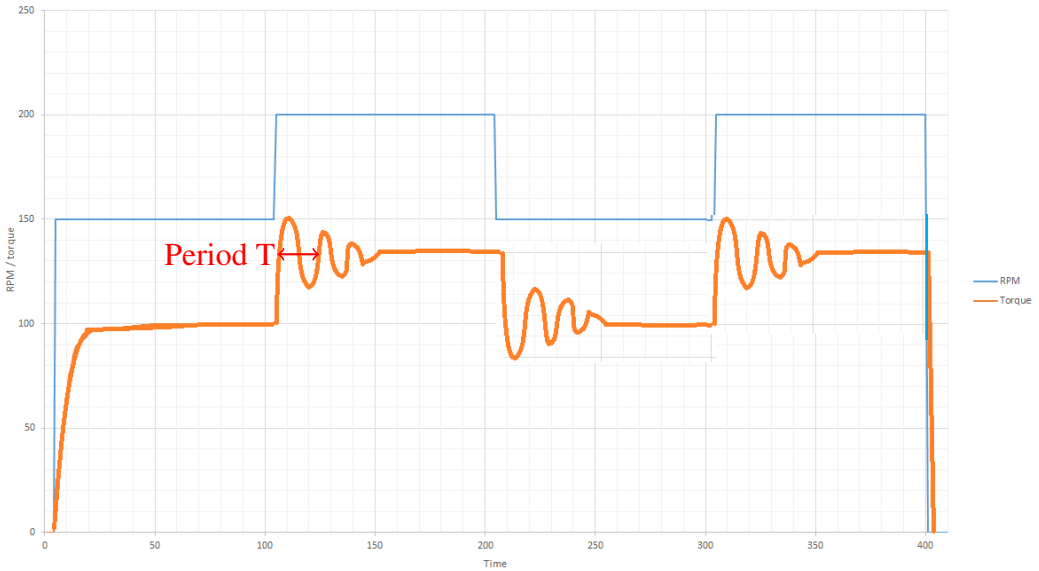

Fig. 6.6 RPM step changing and following torque variance

When the mass flow-rate and the density is estimated, the volumetric flow-rate can be calculated by using equation 6.4:

$$\dot{V} = \frac{\dot{m}}{\rho} \tag{6.4}$$

Chapter 7

Experimental Results

In this chapter the results from the testing will be presented and discussed.

7.1 Available Flow-Rates

During testing the lowest flow-rate that could be obtained was $\sim$2.77 lpm, as The modified controller struggled with lower flow-rates. The maximum flow-rate is restricted to 8.5 lpm by the geometric proportions of the funnel. Higher flow-rates causes overflow.

The funnel is mounted over the spinning wheel to direct flow into the middle of the spinning wheel as shown in figure 7.1.

7.2 Torque Measurements

Torque measurements has to be very precise with minimal amount of noise to verify the measuring principle to the new flow sensor. The load cells that were originally planned to use for the torque measurements proved insufficient. A alternate methods used was by using the servo motor itself. The servo motor uses different amount of power, for different amount of torque. An indirect torque measurement can be obtained by converting the amount of power to torque.

Both methods for measuring torque was tested and compared, as shown in figure 7.2. Note that the measurements are performed without flow-rate.

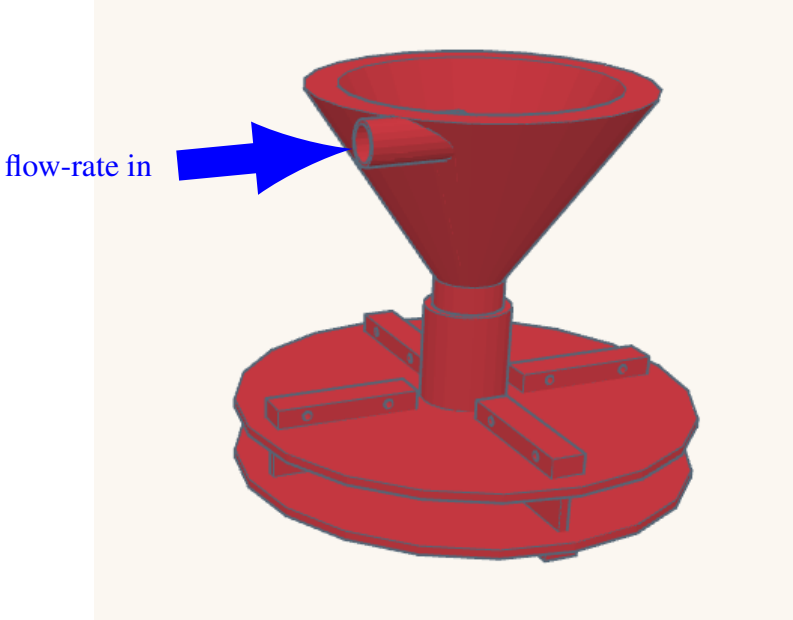

Fig. 7.1 Funnel over spinning wheel

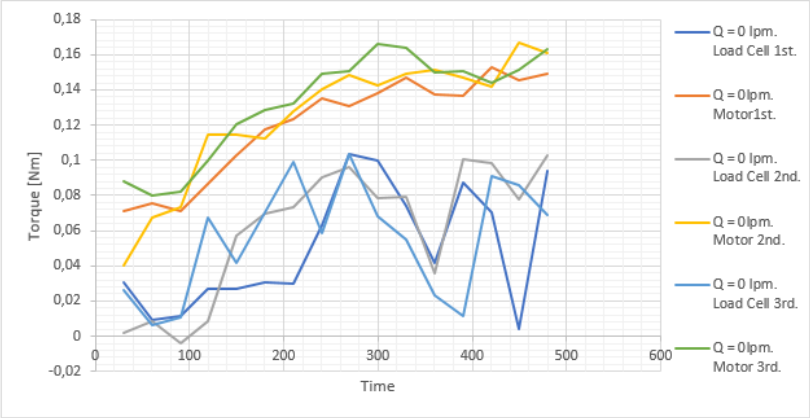

Fig. 7.2 Load cell and servo motor torque measurements

The figure shows that the measurements from the servo motor is more precise and consistent than the measurements from the load cells. The torque measurements from the load cells relies on rotation of the servo motor. This rotation may have been influenced by too large amounts of static friction in the roller bearings that allows the motor to rotate slightly.

7.3 Analyzing the Relationship Between Torque, RPM and Mass Flow-Rate

The objective of the flow-rate sensor is that it will be used to estimate flow-rate from torque measurements. Thus it is critical that the relationship between torque, RPM and mass flow-rate is investigated.

This chapter will investigate the first part of the hypothesis presented in the previous chapter, that said the additional torque measured should be proportional to the mass flow-rate. Note that graphs in this section show volumetric flow-rates instead of mass flow-rates. These values are identical, as clean water is used during testing where 1 lpm is equal to 1 kg/min.

7.3.1 Additional Torque

Additional torque needs to be defined. When a specific RPM is set, the additional torque is the torque experienced at a given flow-rate minus the torque measured at 0 lpm. This is shown in figure 7.3.

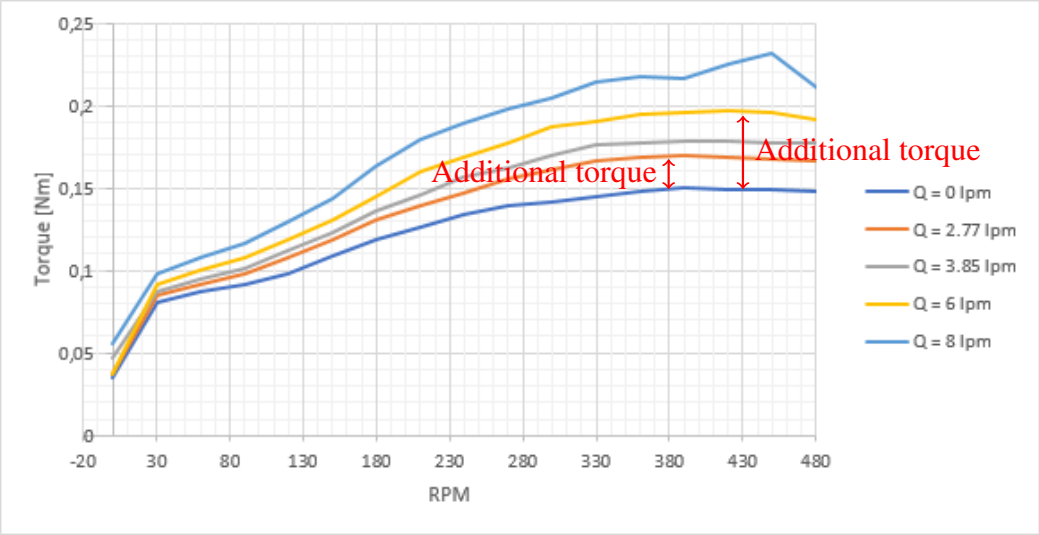

Fig. 7.3 Defining additional torque

7.3.2 Intermediate Screening

The first screening done was by doing three seperate measurements at 0 lpm, 2.77 lpm, 3.85 lpm, 6 lpm and 8 lpm for various RPMs ranging between 30 and 480.

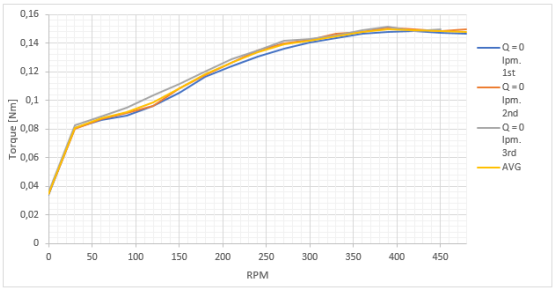

(a) Flow-rate = 0 lpm

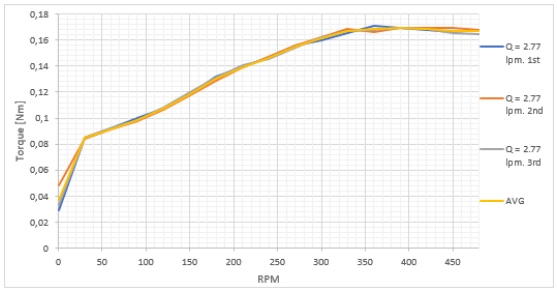

(b) Flow-rate = 2.77 lpm

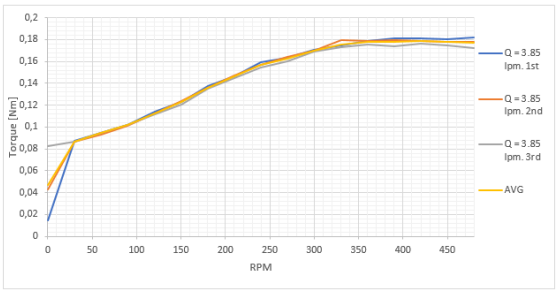

(c) Flow-rate = 3.85 lpm

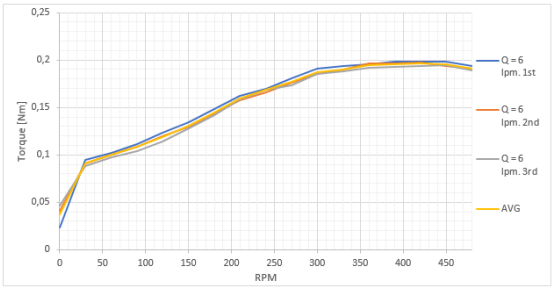

(d) Flow-rate = 6 lpm

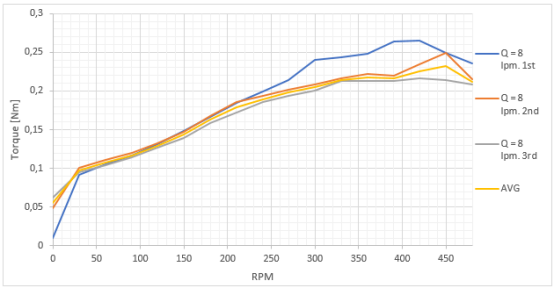

(e) Flow-rate = 8 lpm

Fig. 7.4 Intermediate screening results from various flow-rates

The three series of measurements, for various flow-rates, with their average is plotted in figure 7.4. Most of the measurements are overlapping each other fairly well, implying that the amount of noise in the measurements is fairly low.

The average of the measurements are used in the continued calculations. There is one anomaly in figure 7.4e when the flow-rate was equal to 8 lpm that is excluded from the continued calculations.

The investigated relationship that is of importance to the hypothesis is the relationship between flow-rate and additional torque, for different RPMs.This relationship is shown in figure 7.5

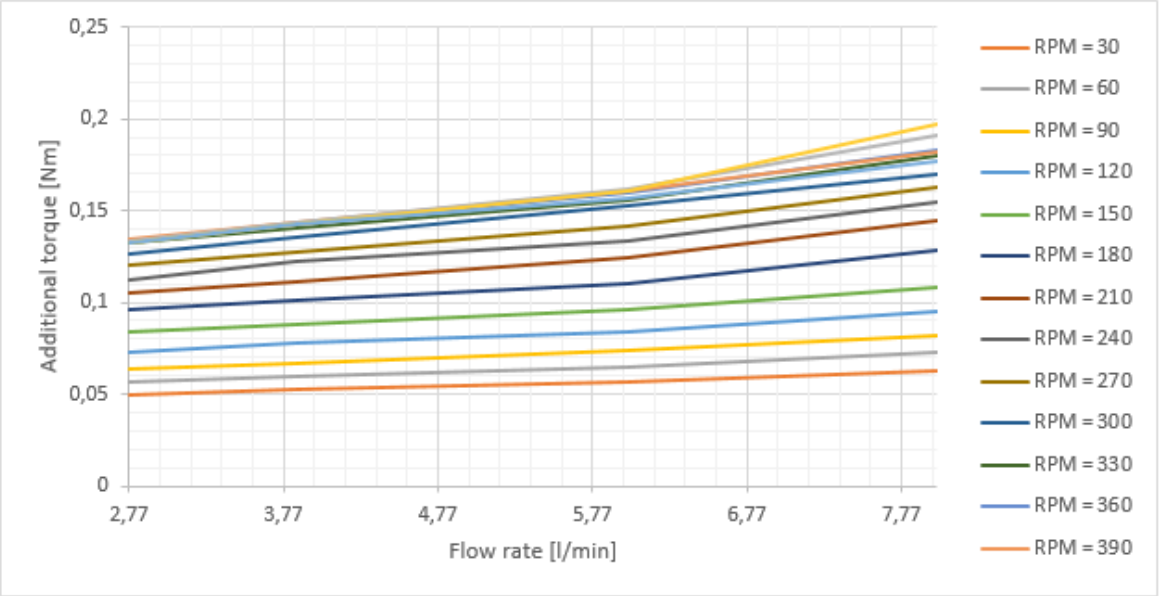

Fig. 7.5 Additional torque as a function of flow-rate - intermediate screen

In figure 7.5 the torque increases with both RPM and flow-rates. The relationship between flow-rate and additional torque seem linear for lower flow-rates, but there is a slight bend towards 8 lpm. This screening shows that there is a trend between additional torque and flow-rate, but a more comprehensive screening, with measurements at intervals of $\sim$0.5 lpm as to be conducted

7.3.3 Comprehensive Screening

The final screening was carried out with three separate measurements for flow-rates between 2.77 lpm and 8 lpm. All of the measurements can be found in appendix B. Additional torque is plotted as a function of flow-rate in figure 7.6.

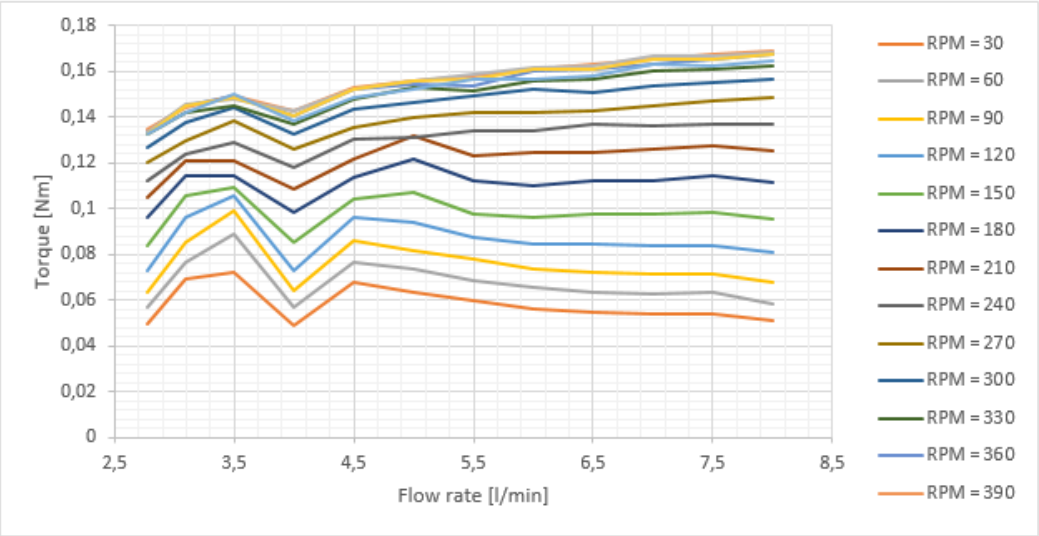

Fig. 7.6 Additional torque as a function of flow-rate - full screen

Unfortunately, no definite relationship can be concluded from the measurements. The amount of noise in the measurements is too high, causing unwanted variations in torque measurements. The torque measurements are relatively low, and to achieve conclusive results, the amount of noise must be very low.

There are two ways to increase the accuracy of the measurements:

- By increasing the overall amount of torque that is measured. Larger torque measurements would be less susceptible to noise and this can be achieved by increasing the diameter of the spinning wheel.
- Reduce the amount of noise in the measurements, by doing the following:
  1. Making sure the spinning wheel is stabilized better around the steel rod to avoid unnecessary oscillations
  2. The spinning wheel, steel rod and servo has issues with alignment. This can cause unnecessary noise
  3. Reduce the amount of vibrations from the flow-rate
  4. The torque measurements are currently measured by the amount of power the servo motor uses. This is a potential inaccurate measurement, where as a direct torque measurement could be more precise

7.4 Density Estimation

The principle behind the density estimation is described in chapter 6. It is vital that it is possible to estimate the density in order to estimate the volumetric flow-rate. This section analyses the oscillations that occur when changing the RPM step-wise. The step changes that are investigates is 100 RPM to 150 RPM, 150 RPM to 200 RPM and 200 RPM to 250 RPM. Note that the flow-rate is constant at 8 lpm.

7.4.1 Analysis of Oscillations During Step Changes in RPM

Firstly, a step change from 100 RPM to 150 RPM is analyzed as shown in figure 7.7:

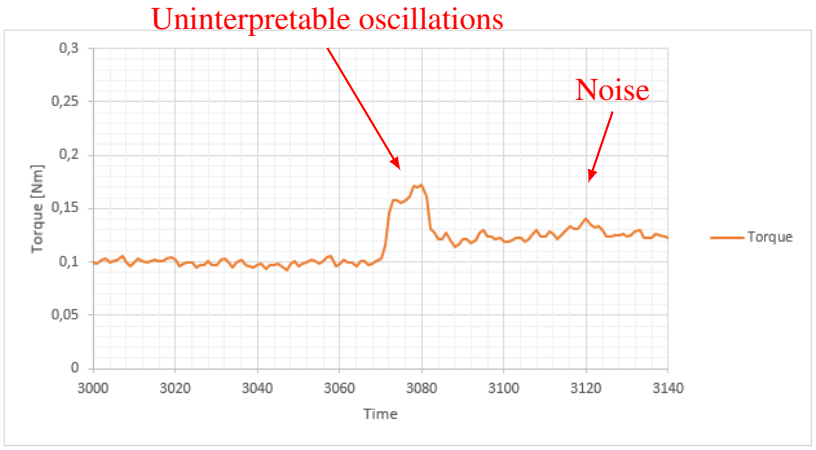

Fig. 7.7 Torque variance with step change from 100 RPM to 150 RPM

The result shows that there are significant amounts of noise in the measurements, and the oscillations are uninterpretable. Thus a relationship between the time period T of the oscillations and the density can not be derived from this measurement.

Secondly, a step change from 150 RPM to 200 RPM is analyzed as shown in figure 7.8:

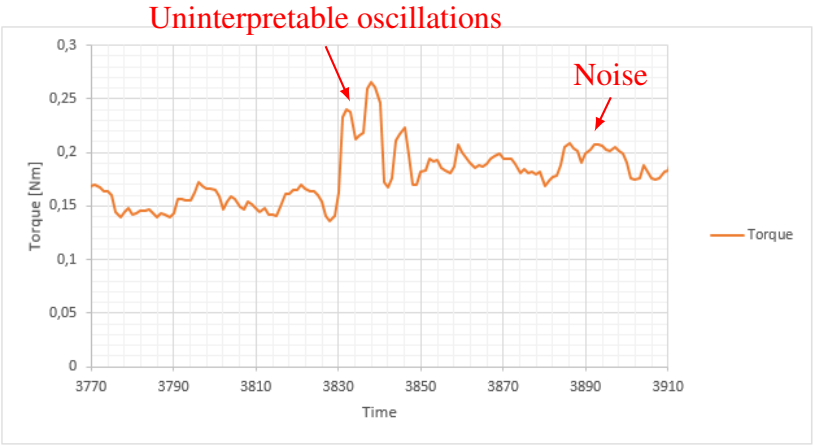

Fig. 7.8 Torque variance with step change from 150 RPM to 200 RPM

Figure 7.7 shows the same issues with noise and uninterpretable oscillations.

Finally, a step change in RPM from 200 to 250 is evaluated in figure 7.9:

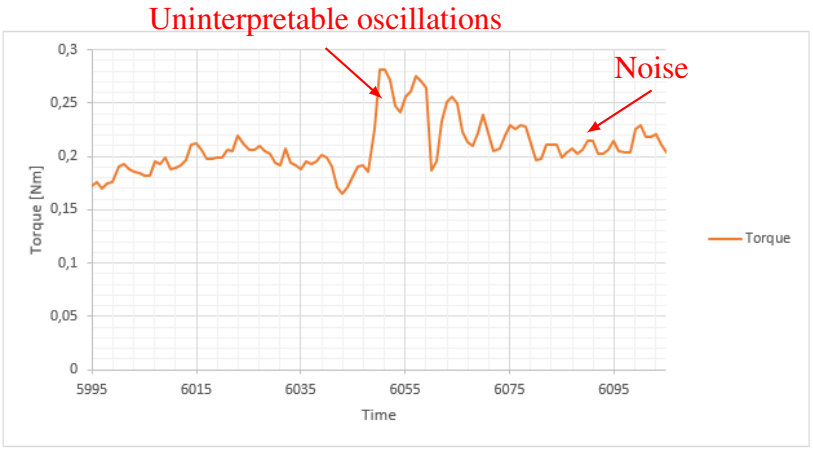

Fig. 7.9 Torque variance with step change from 200 RPM to 250 RPM

The results are uninterpretable because of relatively large amounts of noise that is highlighted in the figures, rendering the results non-conclusive.

Chapter 8

Conclusion

The first objective of the thesis was to investigate the challenge of transient time periods, which in turn is created by compressibility effects. Several parameters were altered during simulations to estimate how compressibility effects varied with different parameters.

The second objective was to test the flow-rate sensor that has been developed at IRIS. Unfortunately, the measurements were affected by too large amounts of noise to estimate mass flow-rates or volumetric flow-rates. Still, various conclusive remarks can drawn from the testing.

Thus this thesis' conclusion is divided into two parts:

- flow-rate out measurements analysis
- Conclusive remarks from the experimental testing

8.1 Flow-Rate Out Measurements Analysis

Compressibility effects are unavoidable during drilling and circulation, and therefore transient time periods are unavoidable as well. Based on the simulations performed to estimate compressibility effects, the following conclusions can be drawn:

- Compressibility effects increases with increasing flow-rates because of the larger ECD that is generated when circulating at higher flow-rates. The increase in pressure compresses the fluid, and allows for an additional mud to enter the well
- Effects from compressibility increases with increasing bit depth. This happens because there are a larger volume of fluid to compress

- A decreasing effect of compressibility is observed when the density increases. This is a consequence of higher density fluids having a larger percentage of particles, and thus a lower percentage of fluid to compress
- Compressibility effects increase with increasing OWR, as oil is more compressible than water
- A trend of increasing compressibility effects is noticed for more viscous fluids, compared to less viscous fluids.
- When drilling a real well, the hole size decreases with increasing depth. As investigated earlier, compressibility effects increase with depth, but the compressibility effect increases with reducing hole sizes as well. This occurs because the flow-rate increases in smaller hole sections, and thus the increased friction generated will additionally compress the fluid

8.2 Conclusive Remarks From the Experimental Testing

During testing of the the flow sensor the results showed a large amount of noise, which rendered the measurements insufficient to determine a definitive relationship additional torque and mass flow-rate or volumetric flow-rate. At least, a trend was observed between the additional torque and flow-rate from an intermediate screening. Furthermore, the following conclusions can be drawn from the experimental testing:

- The tolerance to noise should be increased. This can be done by increasing the diameter of the spinning wheel, which would result in a larger torque measurements
- Noise should be reduced before further testing. This can be done in several ways.
    1. Stabilizing the spinning wheel around the steel rod to avoid unnecessary noise and oscillations. The spinning wheel is experiencing small amount of tilt, due to a small gap between the spinning wheel and steel rod
    2. Perfecting the alignment between the spinning wheel, funnel and motor to avoid reduce noise
    3. Reducing the amount of vibration from the pump and the flow-rate
    4. Optimizing the measurement of torque. The torque measurements should be measured directly, and not indirectly through the motor. This would allow for more precise measurements

Chapter 9

Future Work

This section will go over potential future work connected to the flow sensor. Future work includes optimizing the current flow sensor to verify the measuring principle.

9.1 The Spinning Wheel

The spinning wheel can be designed in various ways. Three aspects of the spinning wheel will be discussing in this section:

- Spinning wheel diameter
- Shorter walls
- Additional walls

9.1.1 Spinning Wheel Diameter

The results gained through the experimental part is influenced by too much noise. Through increasing the diameter of the spinning wheel, the overall torque measurements would increase and the noise tolerance would increase.

9.1.2 Shorter Walls

Lower walls should be tested to see if the density estimate would have more stable oscillations during step changes in the RPM.

9.1.3 Additional Walls

The current spinning wheel has 4 walls between the lower and upper plate, but the effect of increasing the number of walls should be investigated. This would reduce the travel time before the fluid hits a wall and exerts a Coriolis force on the wall. Increasing the number of walls could yield more stable oscillations to determine the density.

9.2 Viscosity and Density

Investigate the effects the density and viscosity variations has on the new flow sensor. Conduct experiments to establish a relationship between the measured torque and density and viscosity.

9.3 Determine the Quality of the Flow Sensor

The achievable precision of the new flow-rate needs to be determined, in order to compare it to existing flow-rate sensors. The size of a full-size flow sensor has to be investigated.

References

[1] D. Reitsma *et al.*, "A simplified and highly effective method to identify influx and losses during managed pressure drilling without the use of a coriolis flow meter." in *SPE/IADC Managed Pressure Drilling and Underbalanced Operations Conference and Exhibition*. Society of Petroleum Engineers, 2010.

[2] J. Brakel, B. Tarr, W. Cox, F. Jorgensen, H. V. Straume *et al.*, "Smart kick detection: First step on the well-control automation journey," *SPE Drilling & Completion*, 2015.

[3] E. Cayeux, B. Daireaux *et al.*, "Insights into the physical phenomena that influence automatic gain/loss detection during drilling operations," *SPE Drilling & Completion*, 2016.

[4] A. E. Products, *Navigating Narrow Drilling Margins*, 2015 (Accessed: 3/02/2016, 2017). [Online]. Available: http://axonep.com/navigating-narrow-drilling-margins

[5] E. Cayeux, B. Daireaux *et al.*, "Precise gain and loss detection using a transient hydraulic model of the return flow to the pit." Society of Petroleum Engineers, 2013.

[6] S. International, *Kicks*, 2015 (Accessed: 20/04/2016, 2017). [Online]. Available: http://petrowiki.org/Kicks

[7] D. Hargreaves, S. Jardine, B. Jeffryes *et al.*, "Early kick detection for deepwater drilling: New probabilistic methods applied in the field," in *SPE Annual Technical Conference and Exhibition*. Society of Petroleum Engineers, 2001.

[8] G. M. Ritchie, R. Hutin, W. D. Aldred, J. Luppens *et al.*, "Development and testing of a rig-based quick event detection system to mitigate drilling risks," in *IADC/SPE Drilling Conference*. Society of Petroleum Engineers, 2008.

[9] B. Tarr, D. W. Ladendorf, D. Sanchez, G. M. Milner *et al.*, "Next-generation kick detection during connections: Influx detection at pumps stop (idaps) software," *SPE Drilling & Completion*, 2016.

[10] F. Le Blay, E. Villard, S. C. Hilliard, T. Gronas *et al.*, "A new generation of well surveillance for early detection of gains and losses when drilling very high profile ultradeepwater wells, improving safety, and optimizing operating procedures," in *SPETT 2012 Energy Conference and Exhibition*. Society of Petroleum Engineers, 2012.

[11] D. Reitsma *et al.*, "Development of an automated system for the rapid detection of drilling anomalies using standpipe and discharge pressure," in *SPE/IADC Drilling Conference and Exhibition*. Society of Petroleum Engineers, 2011.

[12] Y. A. Cengel, R. H. Turner, and J. M. Cimbala, *Fundamentals of thermal-fluid sciences fourth edition*. McGraw-Hill New York, NY, 2012.

[13] Y. UK, *Coriolis Flow Meter (Principle of Operation)*, 13. aug- 2011 (Accessed: 14/02/2016, 2017). [Online]. Available: https://www.youtube.com/watch?v=PvXgaDoZr1E

[14] J. Orban, K. Zanker *et al.*, "Accurate flow-out measurements for kick detection, actual response to controlled gas influxes," in *SPE/IADC Drilling Conference*. Society of Petroleum Engineers, 1988.

[15] *Øvinger i Bore- og Brønnvæsker (PET210)*. Universitetet i Stavanger, 2014.

[16] O. Skjeggestad, *Boreslamteknologi*. Alma Mater Forlag AS, 1989.

[17] *PRESSURE LOSS IN PIPE*, April 29, 2012 (Accessed: 15/05/2017). [Online]. Available: https://neutrium.net/fluid_flow/pressure-loss-in-pipe/

[18] S. Jayanti, *Bends, Flow and Pressure Drop in*, 2. February 2011 (Accessed: 15/05/2017). [Online]. Available: http://www.thermopedia.com/content/577/

[19] A. Persson, "How do we understand the coriolis force?" *Bulletin of the American Meteorological Society*, vol. 79, no. 7, pp. 1373–1385, 1998.

[20] ——, "The coriolis effect—a conflict between common sense and mathematics," *Italian Meteorological Society*, pp. 20–31, 2005.

[21] K. Ogata and Y. Yang, "Modern control engineering," 1970.

[22] J. Smuts, *PID Controllers Explained*, March 7, 2011 (Accessed: 20/05/2017). [Online]. Available: http://blog.opticontrols.com/archives/344

[23] K. J. Aström and R. M. Murray, *Feedback systems: an introduction for scientists and engineers*. Princeton university press, 2010.

Appendix A

Electrical Schematics

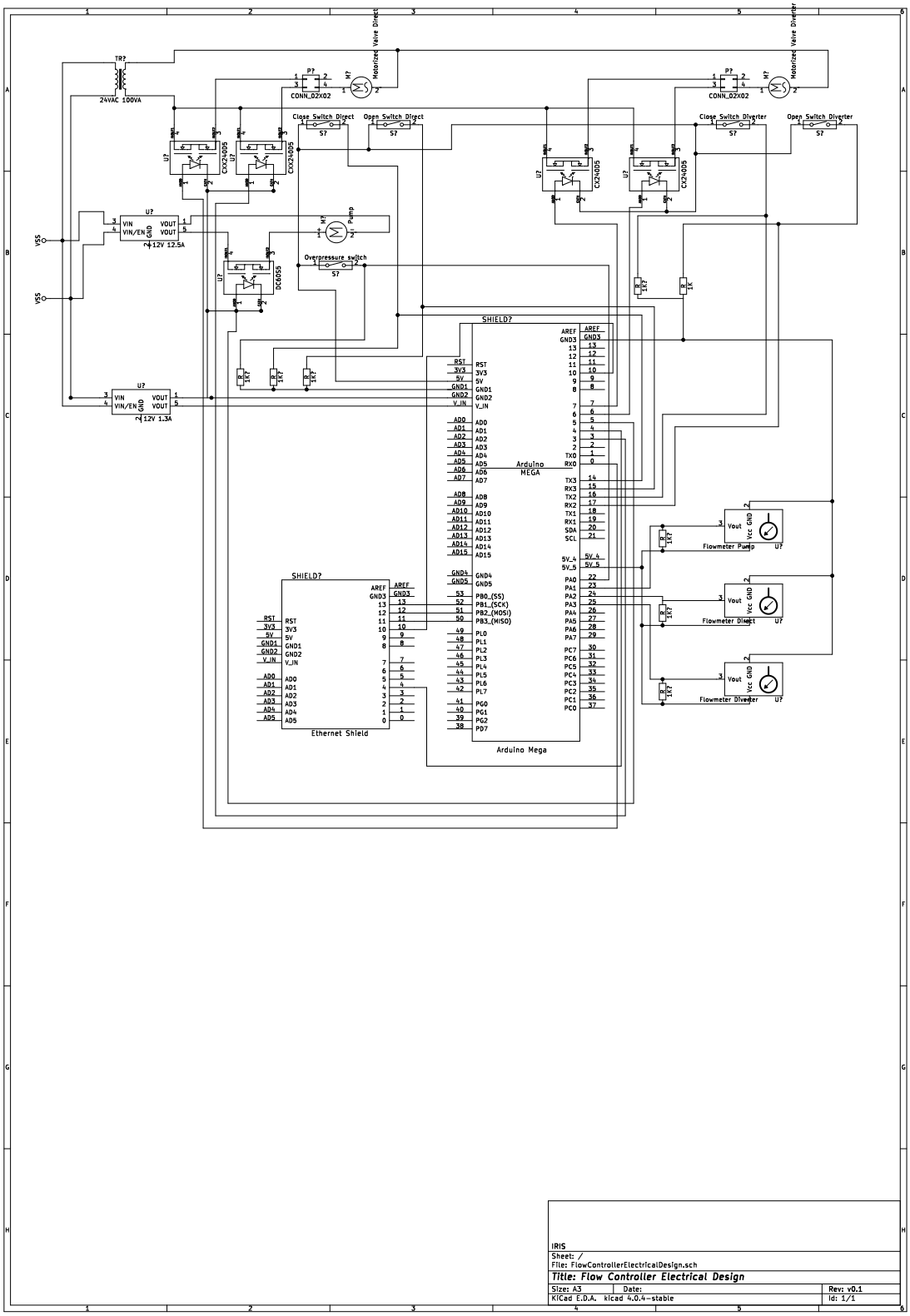
TR?
24VAC 100VA
Motorized Valve Direct
Motorized Valve Diverter
CONN_02X02
Close Switch Direct
Open Switch Direct
Close Switch Diverter
Open Switch Diverter
CX24005
Pump
Overpressure switch
VSS
U?
VIN
VIN/EN
GND
VOUT
+12V 12.5A
+12V 1.3A
SHIELD?
Ardulno MEGA
Ethernet Shield
Ardulno Mega
Flowmeter Pump
Flowmeter Direct
Flowmeter Diverter
Vout
Vcc
GND
IRIS
Sheet: /
File: FlowControllerElectricalDesign.sch
Title: Flow Controller Electrical Design
Size: A3
Date:
Rev: v0.1
KiCad E.D.A. kicad 4.0.4-stable
Id: 1/1

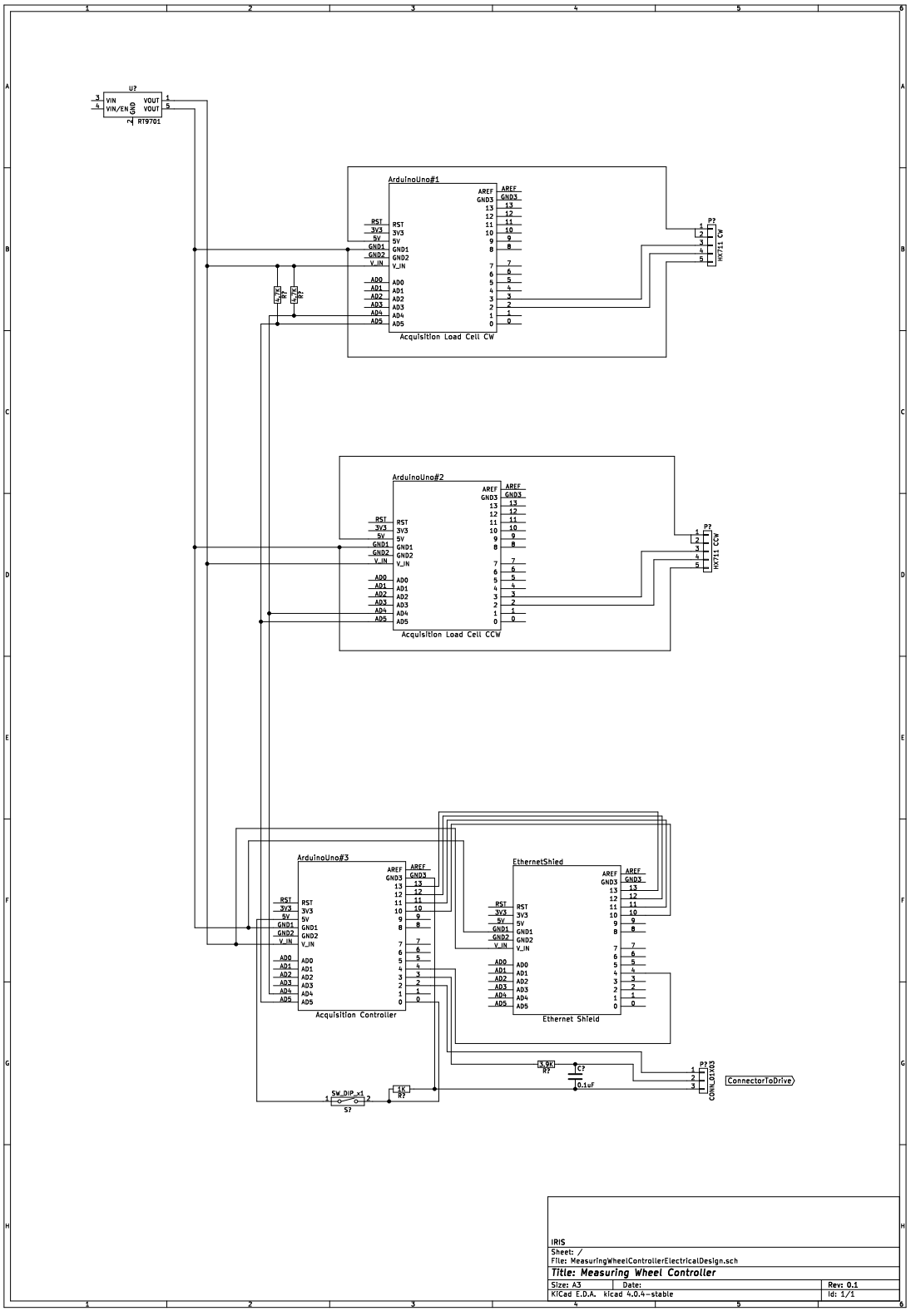
U?
VIN
VIN/EN
GND
VOUT
VOUT
RT9701
ArduinoUno#1
Acquisition Load Cell CW
P?
HX711 CW
ArduinoUno#2
Acquisition Load Cell CCW
P?
HX711 CCW
ArduinoUno#3
Acquisition Controller
EthernetShield
Ethernet Shield
4.99K
R?
C?
0.1uF
P?
CONN_01X03
ConnectorToDrive
SW_DIP_x1
S?
1K
R?
IRIS
Sheet: /
File: MeasuringWheelControllerElectricalDesign.sch
Title: Measuring Wheel Controller
Size: A3
Date:
Rev: 0.1
KiCad E.D.A. kicad 4.0.4-stable
Id: 1/1

Appendix B

Measurements From Final Screening

This appendix contains the measurements connected full screening of the new flow sensor.

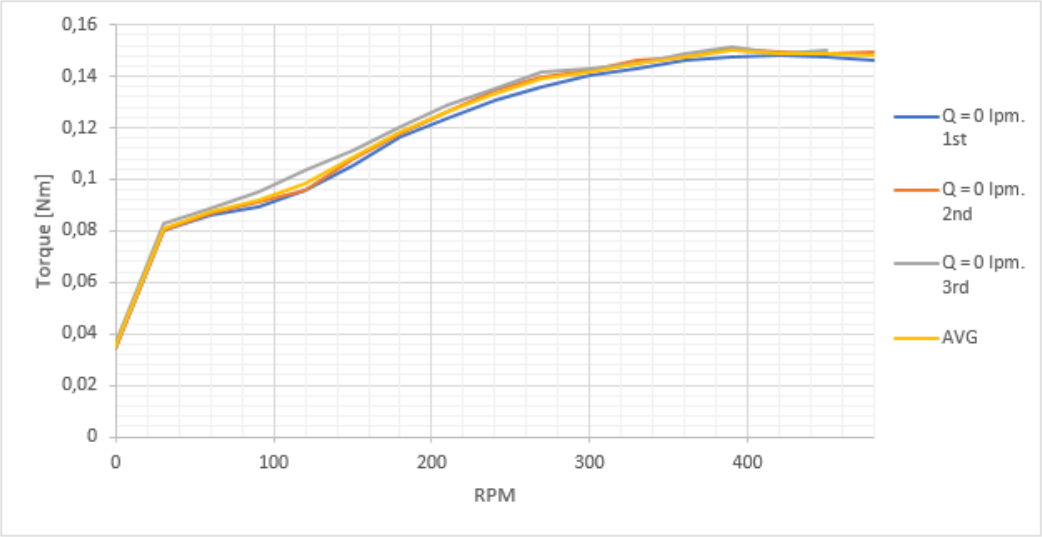

Fig. B.1 Flow rate = 0 lpm

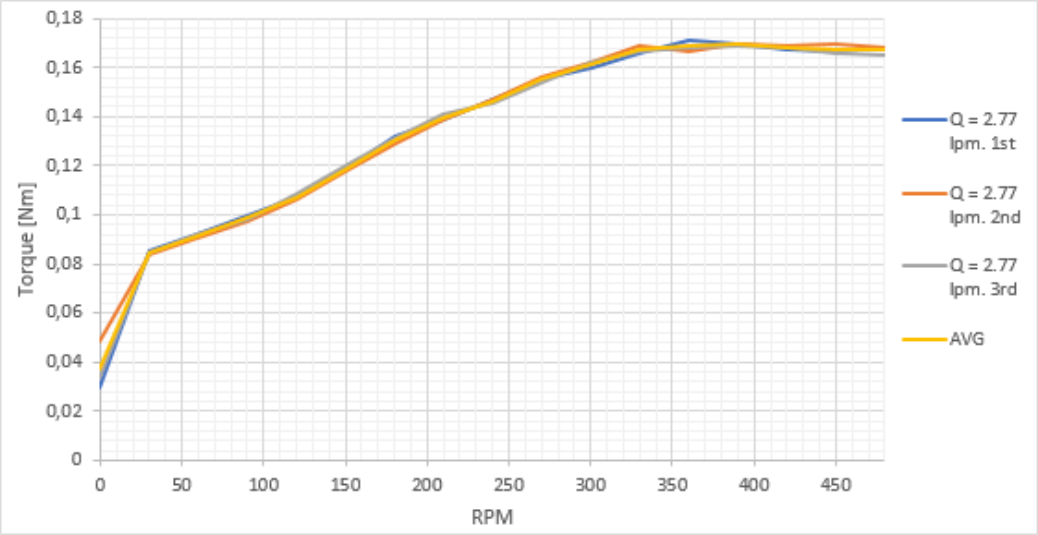

Fig. B.2 Flow rate = 2.77 lpm

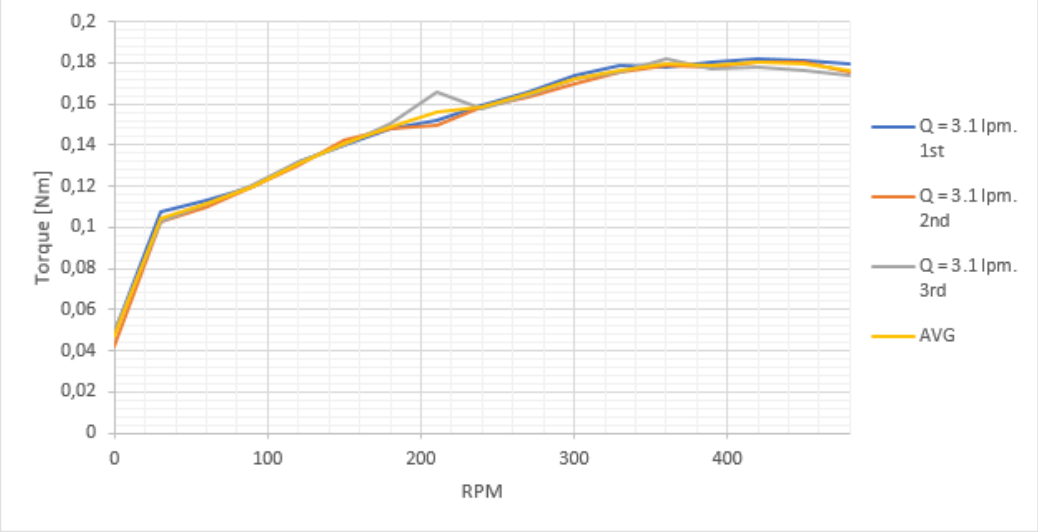

Fig. B.3 Flow rate = 3.1 lpm

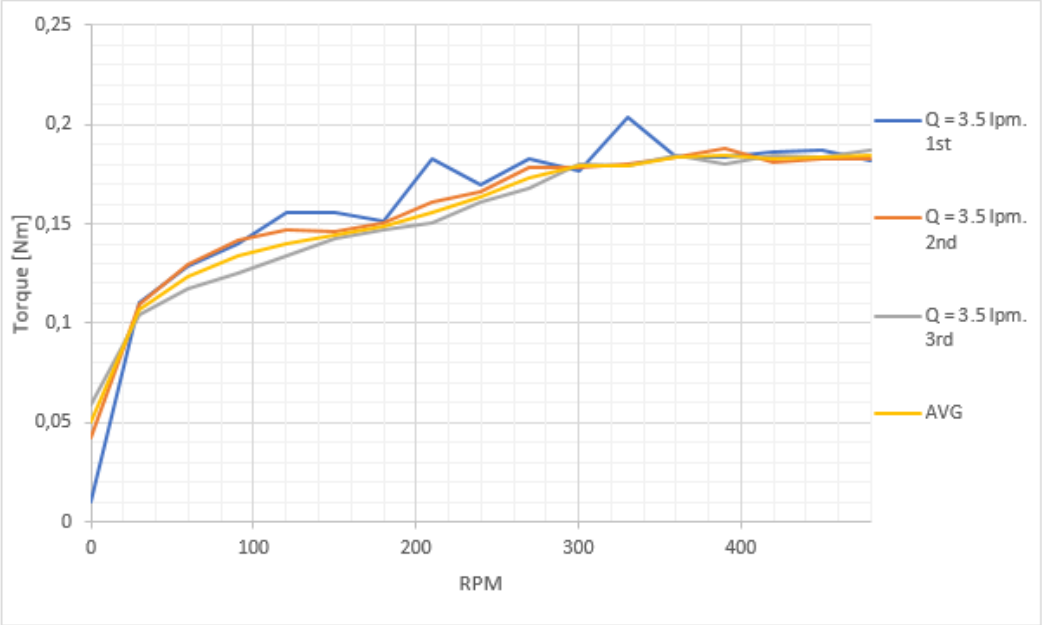

Fig. B.4 Flow rate = 3.5 lpm

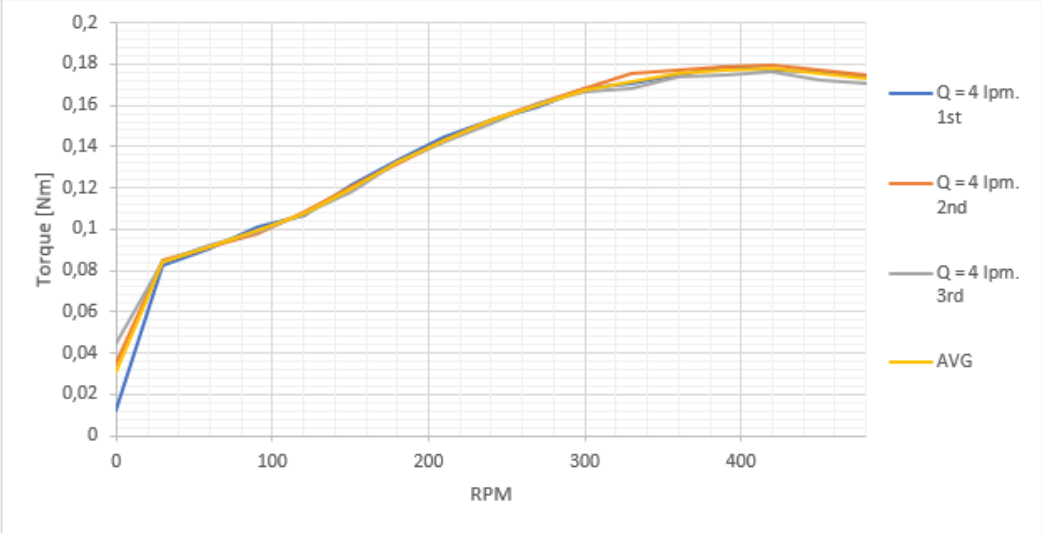

Fig. B.5 Flow rate = 4 lpm

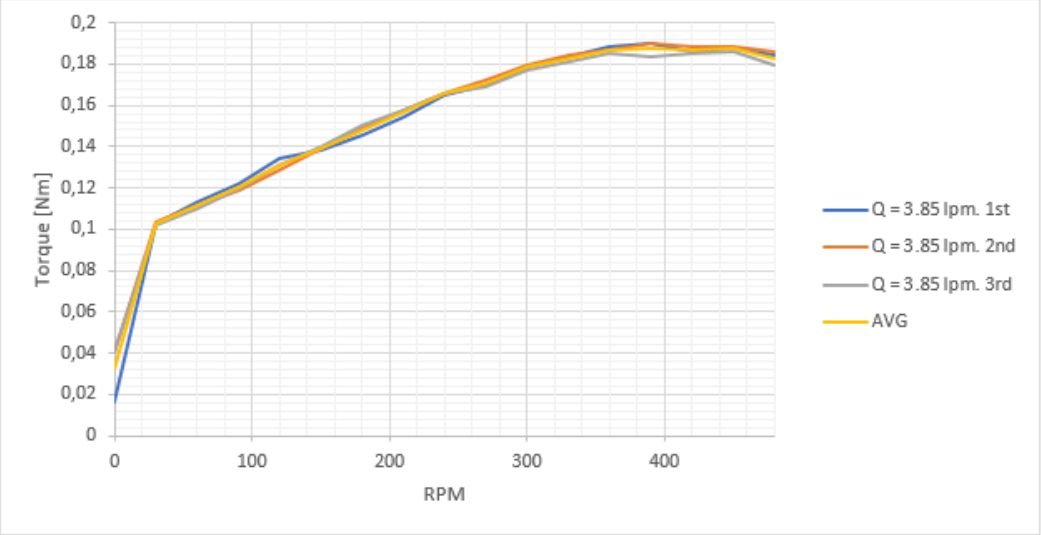

Fig. B.6 Flow rate = 4.5 lpm

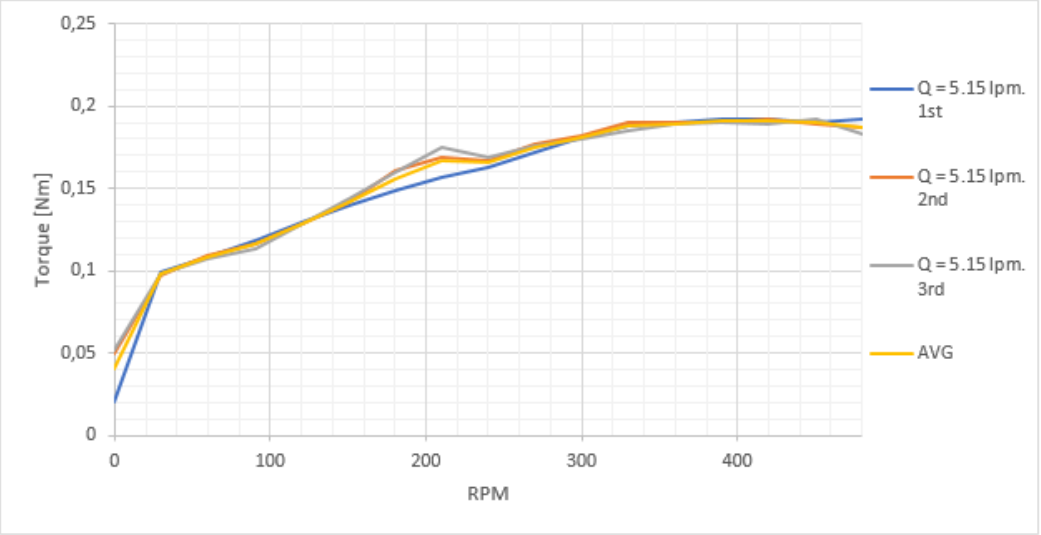

Fig. B.7 Flow rate = 5.15 lpm

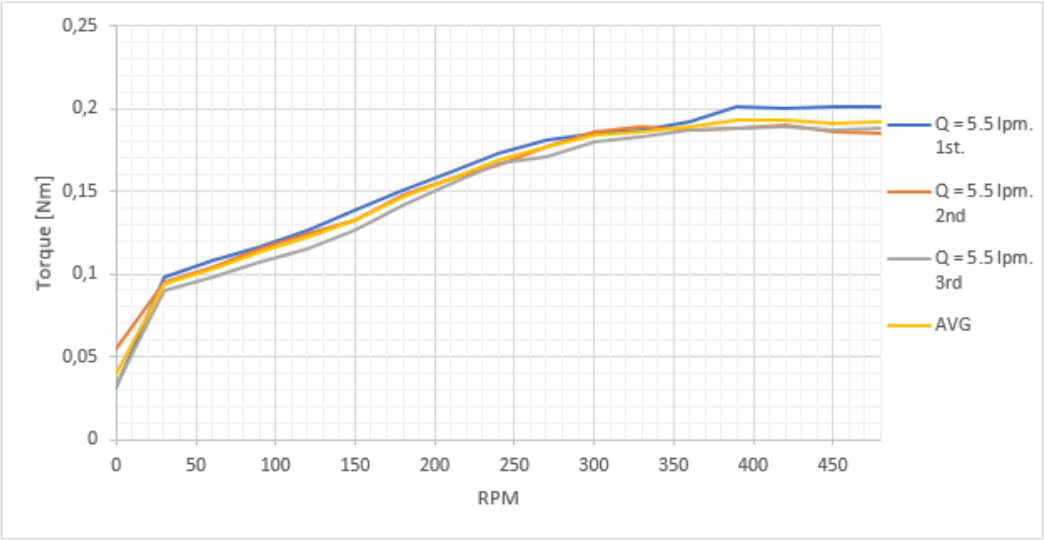

Fig. B.8 Flow rate = 5.5 lpm

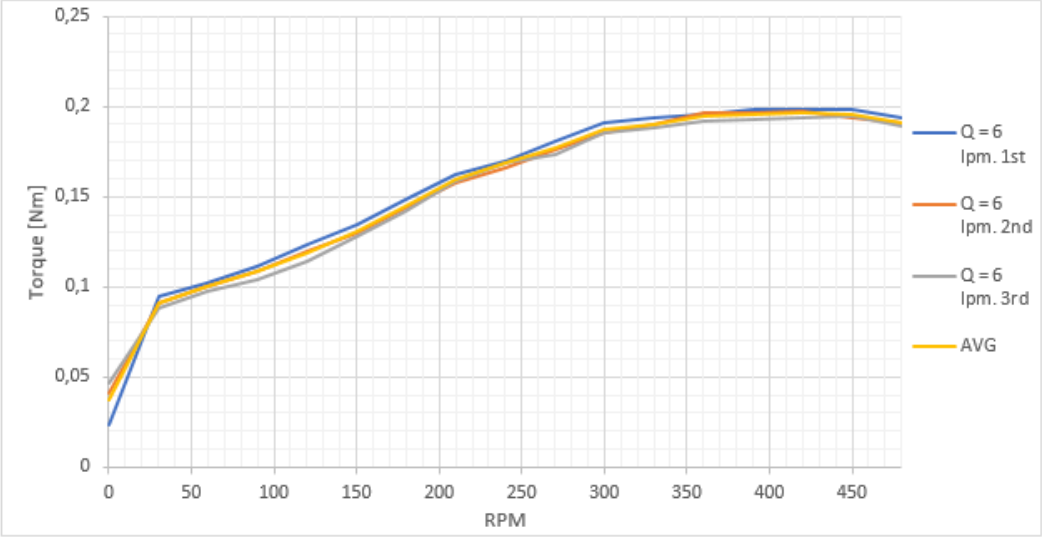

Fig. B.9 Flow rate = 6 lpm

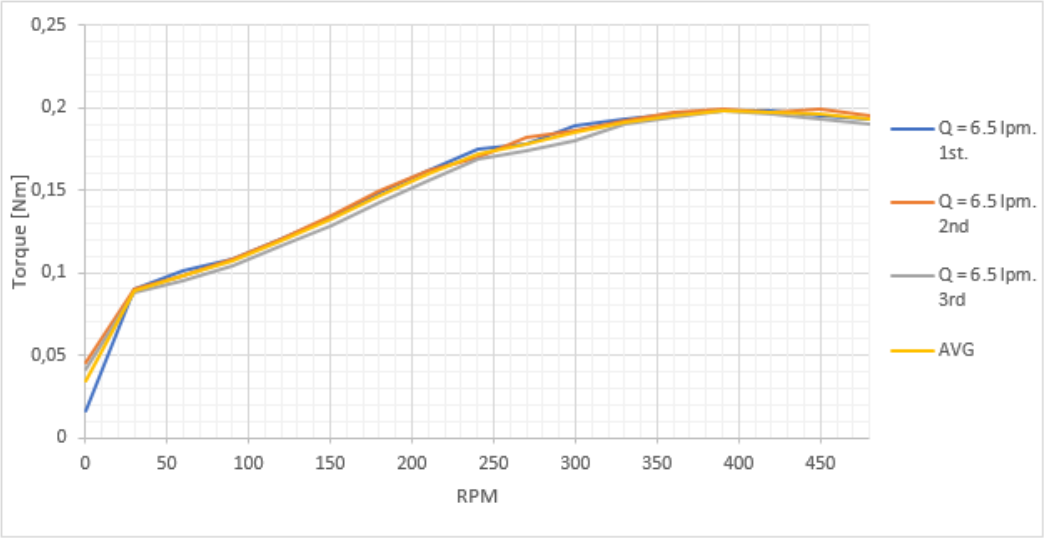

Fig. B.10 Flow rate = 6.5 lpm

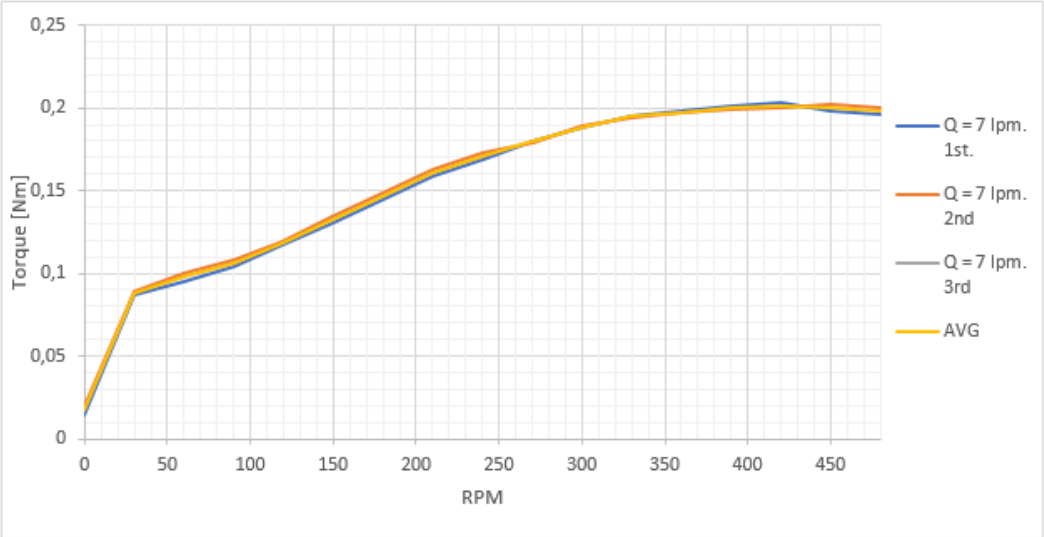

Fig. B.11 Flow rate = 7 lpm

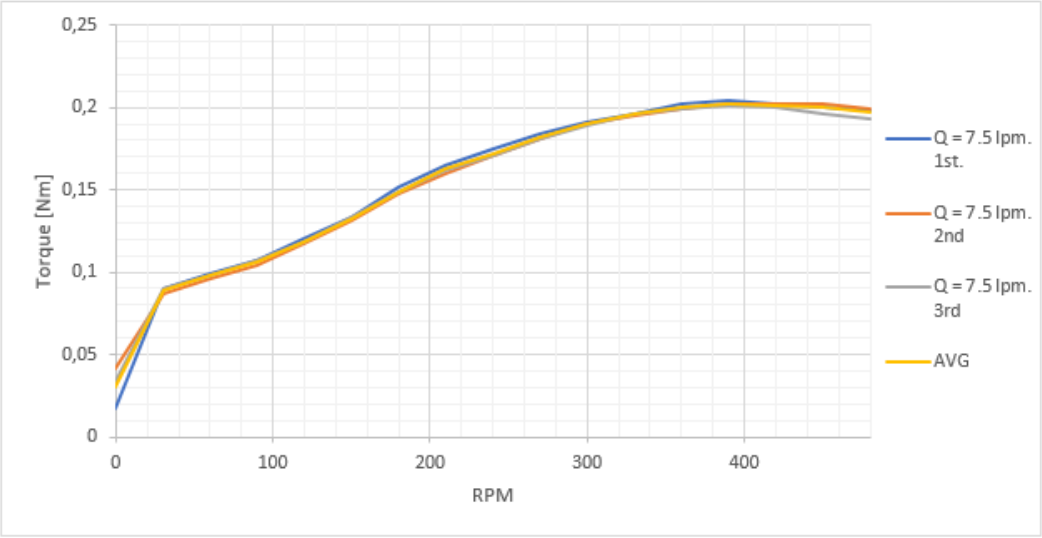

Fig. B.12 Flow rate = 7.5 lpm

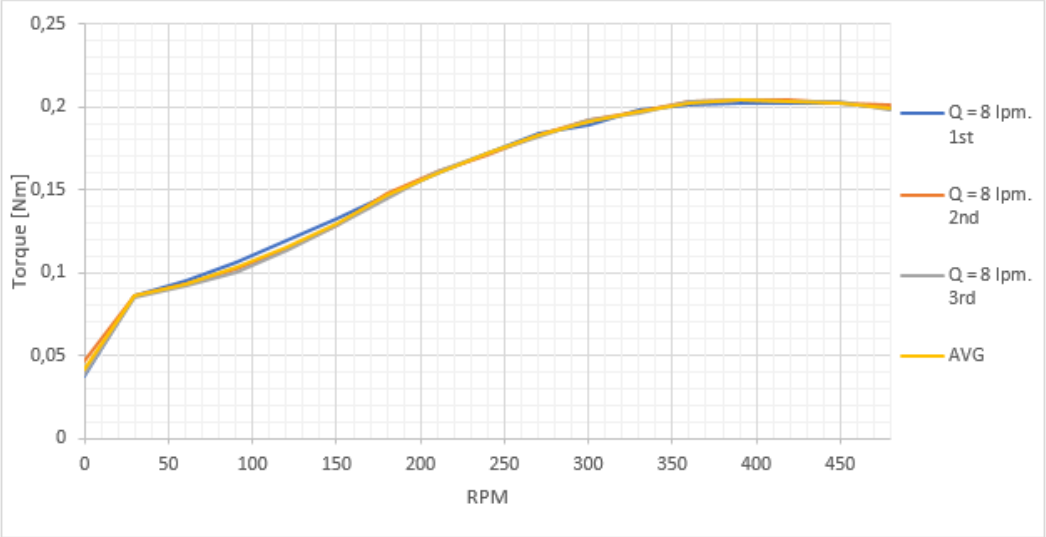

Fig. B.13 Flow rate = 8 lpm